

THESIS

SIMULATION AND ANALYSIS OF AN 18L NATURAL-GAS ENGINE WITH A FOCUS ON
CYLINDER DEACTIVATION AND EXHAUST PRESSURE DYNAMICS

Submitted By

Christopher Barry Page

Department of Mechanical Engineering

In partial fulfillment of the requirements

For the Degree of Master of Science

Colorado State University

Fort Collins, Colorado

Summer 2016

Master's Committee:

Advisor: Daniel Olsen

Anthony Marchese
Michael De Miranda

Copyright by Christopher Barry Page 2016

All Rights Reserved

ABSTRACT

SIMULATION AND ANALYSIS OF AN 18L NATURAL-GAS ENGINE WITH A FOCUS ON CYLINDER DEACTIVATION AND EXHAUST PRESSURE DYNAMICS

A GT-Power model of a Waukesha VGF-18 engine was created to investigate engine performance and pressure wave dynamics in the exhaust system of an 18L natural-gas engine. Exhaust pressure plays a large role in engine dynamics as it affects in-cylinder temperature, pressure, power output, emissions, air exchange and exhaust gas recirculation. The model was also evaluated to predict performance differences between cylinder deactivation and nominal six-cylinder operation. Cylinder deactivation allows for experimental modifications to be made on a small number of cylinders while still being able to extrapolate the data to fit the fully operational engine. Experimental cylinder deactivation results in a decrease in cost, time spent on labor, and propagation of uncertainty during experimental modification. An analysis was made on the effects of cylinder deactivation on engine operation and exhaust pressure dynamics.

The flow solver was verified analytically and the combustion solver was verified with Chemkin. The results were validated with experimental data and the general engine parameters and fuel flow were found to have a predictive confidence level over 95%, the combustion, temperatures, and manifold pressures calculated by the model were found to have a predictive confidence level just above 90%. Following validation there were several geometric modifications done to the exhaust manifold and exhaust runners of the model to determine the pressure wave dynamics at the exhaust port of cylinder 1 as well as the engine performance. The tests found that modifying the exhaust runner length parameter had the greatest effect on engine performance and that modifying the exhaust manifold aspect ratio (cross-sectional area over length) had the greatest effect on average exhaust pressure.

Five of the six cylinders were deactivated in the model by replacing the combustion chambers with purely mechanical piston-cylinders full of non-combustible air. It was found that cylinder deactivation resulted in a increase in the frictional affects as a percentage of brake power, but the difference was significantly less for the cylinder deactivation method where the pistons are removed from the inactive cylinders.

TABLE OF CONTENTS

ABSTRACT.....	ii
LIST OF TABLES.....	vii
LIST OF FIGURES.....	x
LIST OF SYMBOLS.....	xii
Chapter 1- Background and Introduction.....	1
1.1 Motivation and Application.....	1
1.2 Review of Literature.....	2
1.2.1 Exhaust Pressure Importance.....	2
1.2.2 Cylinder Deactivation.....	3
1.2.3 GT-Power.....	4
1.3 Overview.....	5
Chapter 2- Methods and Materials.....	6
2.1 Models and Development.....	6
2.1.1 Flow Modeling.....	6
2.1.2 Combustion Modeling.....	8
2.1.3 Mechanical Modeling.....	10
2.1.4 Heat Transfer Modeling.....	11
2.1.5 Calculating Volumetric Efficiency.....	13
2.1.6 Calculating Engine Performance Parameters.....	13

Chapter 3- Multi-Cylinder Model Development.....	15
3.1 Single-Cylinder Model Development	15
3.1.1 Combustion Verification.....	16
3.1.2 Flow Verification	19
3.2 Six-Cylinder Model Development	22
3.3 Defining Individual Components.....	24
3.3.1 Defining the Inlet and Exhaust ‘EndEnvironment’ Components.....	24
3.3.2 Defining the Various ‘OrificeConn’ Components	25
3.3.3 Defining the Fuel and Air Injection Components (InjConn)	26
3.3.4 Defining the Inlet Pipe Flow Components.....	27
3.3.5 Defining the Cylinder and Valve Components	33
3.3.6 Defining the Exhaust Pipe Flow Components	33
3.3.7 Defining the Engine and Crank Components.....	38
3.4 Sub-Models.....	39
3.5 Six-Cylinder Validation	45
Chapter 4- Pressure Analysis and Mitigation Techniques	49
4.1 Objective	49
4.2 Design and Parametric Variations.....	49
4.2.1 Manifold Volume Variation.....	49
4.2.2 Exhaust Runner Modification	50
4.3 Results of Exhaust Manifold and Runner Variations.....	51

4.3.1 Results of Exhaust Manifold Variation.....	51
4.3.2 Results of Exhaust Runner Variation.....	55
Chapter 5- Cylinder Deactivation	65
5.1 Six-cylinder Deactivation Techniques	65
5.2 The Deactivated-Cylinder Model Method 1: Pressure-Spring Cylinders	66
5.3 The Deactivated-Cylinder Model Method 2: Removed Pistons	69
5.4 Effects of Cylinder Deactivation on the Exhaust Traveling Pressure Waves	70
5.5 Effects of Cylinder Deactivation on Engine Performance	75
5.6 Effects of Pressure Mitigation Techniques on the Deactivated-Cylinder Models	76
Chapter 6- Summary and Conclusion	83
6.1 Summary	83
6.2 Conclusions.....	83
6.3 Future Research Ideas	85
References.....	86
Appendix A- Waukesha VGF-18 Engine Experimental Data	89
Appendix B- Pressure-Spring Verification Raw Data	99
Appendix C- Validation Graphs	101

LIST OF TABLES

Table 1. Input values for Chemkin piston-cylinder combustion solver.	17
Table 2. Combustion Verification with Chemkin.....	18
Table 3. Pressure-Spring Verification Example.....	19
Table 4. Inlet and Exhaust ‘EndEnvironment’ Attributes.....	24
Table 5. Entrance Bellmouth (OrificeConn) Component Attributes	25
Table 6. Back Pressure (OrificeConn) Component Attribute	26
Table 7. Fuel and Air Injection (InjConn) Component Attributes	27
Table 8. Ziptube (PipeRound) Component Attributes	28
Table 9. Material Roughness Pre-Defined Values for Various Materials.....	29
Table 10. InletManifold (PipeRound) Component Attributes	29
Table 11. Inlet Manifold Flow Split (Man-fs) Component Attributes.....	30
Table 12. Inlet Runner Component Attributes and Values	32
Table 13. Inlet Valve Component Attributes and Values	32
Table 14. Cylinder (EngCylinder) Component Attributes	33
Table 15. Exhaust Port (PipeRound) Component Attributes	34
Table 16. Exhaust Runner (PipeRectangle) Component Attributes.....	34
Table 17. RunnerMix (FlowSplitGeneral) Component Attributes	35
Table 18. Exhaust Manifold Runner (PipeRectangle) Component Attributes.....	36
Table 19. Exhaust Manifold Flow Split (FlowSplitTRight) Component Attributes.....	37
Table 20. Exhaust Manifold (PipeRound) Component Attributes.....	38
Table 21. Engine (EngineCrankTrain) Component Attributes	39
Table 22. Combustion Sub-Model Attributes	40
Table 23. Engine Cylinder Geometry Sub-Model Attributes	40

Table 24. Engine Friction Sub-Model Attributes.....	41
Table 25. In-Cylinder Heat Transfer Sub-Model Attributes.....	41
Table 26. Cylinder Wall Temperature Sub-Model	42
Table 27. Flow Pipe Heat Transfer Sub-Model Attributes	42
Table 28. Methane Sub-Model Attributes.....	43
Table 29. Air Injection Sub-Model Attributes	43
Table 30. Oxygen Molecular Properties Sub-Model Attributes	44
Table 31. Nitrogen Sub-Model Attributes	44
Table 32. Initial Fluid State Sub-Model Attributes.....	45
Table 33. Six-Cylinder Model Validation at 60% Load with T-Test Values	45
Table 34. Six-Cylinder Model Validation at 70% Load with T-Test Values	46
Table 35. Six-Cylinder Model Validation at 80% Load with T-Test Values	46
Table 36. Six-Cylinder Model Validation at 90% Load with T-Test Values	47
Table 37. Six-Cylinder Model Validation at 100% Load with T-Test Values and Total T-Test Value for All Loads.....	47
Table 38. Exhaust manifold variation input values.....	50
Table 39. Exhaust runner variation input values.....	51
Table 40. Engine Performance Affected by Exhaust Manifold Variation	53
Table 41. Exhaust Runner Length Effect on Engine Performance	58
Table 42. Exhaust Runner Cross-Sectional Area Effects on Engine Performance	60
Table 43. 100x Runner Volume Effects on Engine Performance	63
Table 44. Deactivated Cylinder Component Attributes.....	68
Table 45. Deactivated Cylinders Initial Condition Sub-Model Attributes.....	68
Table 46. Engine Performance Comparison between Six-Cylinder and Deactivated Cylinder GT-Power Models.	75
Table 47. Exhaust manifold variation input values.....	76

Table 48. Exhaust runner variation input values.....	76
Table 49. Engine Performance Response to Exhaust Runner Length Variation in a Deactivated-Cylinder Engine Model with Removed Pistons.....	79
Table 50. Engine Performance Response to Exhaust Runner Cross-Sectional Area Modification in a Deactivated-Cylinder Engine Model with Removed Pistons.....	80
Table 51 Engine Performance Response to Exhaust Manifold Volume Modification in a Deactivated-Cylinder Engine Model with Removed Pistons.....	81

LIST OF FIGURES

Figure 1 Effect of exhaust backpressure (BP) on in-cylinder pressure during air-exchange processes.[6]..3

Figure 2 Demonstration of Constructive/ Destructive interference[12]..... 4

Figure 3 Schematics of staggered grid approach with scalars calculated at centroid and vector quantities at boundaries.[17] 6

Figure 4. Relationship between Indicated, Crank Pin, Shaft, and Brake Quantities [16] 14

Figure 5. Simplified Single-Cylinder model for a Waukesha VGF..... 16

Figure 6. Initial Six-Cylinder model 22

Figure 7. The final six-cylinder model with four ports per cylinder and an air injector..... 23

Figure 8. 3D Representation of Man-fs Flow Split..... 31

Figure 9. 3D Representation of RunnerMix (FlowSplitGeneral) Component 35

Figure 10. 3D Representation of Exhaust Manifold flow Split 37

Figure 11. Traveling Pressure Waves in the Exhaust Port of Cylinder 1 for the Original Manifold Design
..... 52

Figure 12. Brake Torque Affected by Exhaust Manifold Geometric Variation..... 53

Figure 13. Traveling Pressure Waves in the Exhaust Port with an Exhaust Manifold 8 Times the Original
Volume..... 54

Figure 14. . Traveling Pressure Waves in the Exhaust Port of Cylinder 1 for an Exhaust Manifold with a
Small Aspect Ratio (Length to C.S. Area)..... 55

Figure 15. Traveling Pressure Waves in Exhaust Port 1 for the Original Model (OG) 56

Figure 16. Traveling pressure waves in the exhaust port with varying exhaust runner lengths. 57

Figure 17. Traveling pressure waves in the exhaust port with an exhaust runner 10x the original length. 59

Figure 18. Traveling pressure waves in the exhaust port with an exhaust runner with varying cross
sectional areas. 60

Figure 19. Traveling pressure waves in the exhaust port with an exhaust runner with 10x the original cross-sectional area.	61
Figure 20. Traveling pressure waves in the exhaust port with an exhaust runner with 10x the original cross-sectional area and 10x the original length.	62
Figure 21. Traveling Pressure Waves in Exhaust Port 1 for an Exhaust Runner 20X the Original Length	64
Figure 22. Decommissioned Cylinder GT-Power Model	67
Figure 23. Cylinder Deactivation by Removing Cylinders in GT-Power.....	69
Figure 24. In-Cylinder Pressure vs. Crank Angle for Activated (Cylinder 1) and Deactivated (Cylinders 3 and 5) Cylinders	70
Figure 25. Exhaust Port Pressure Vs. Crank Angle for Deactivated Cylinder Model	71
Figure 26. Diagram of Pressure Waves Traveling through the Exhaust Manifold	72
Figure 27. Traveling Pressure Waves in the Five Exhaust Manifold Segments with Five Deactivated Cylinders	73
Figure 28. Forwards, Backwards, and Total Traveling Pressure Waves in Exhaust Manifold Segment 5 of the Deactivated Cylinder GT-Power Model	74
Figure 29. Forwards, Backwards, and Total Traveling Pressure Waves in Exhaust Manifold Segment 1 of the Deactivated Cylinder GT-Power Model	74
Figure 30. Traveling Pressure Waves in Exhaust Port 1 for Different Exhaust Manifold and Runner Designs.....	78
Figure 31. Traveling Pressure Waves in the Exhaust Port of Cylinder 1 with Varying Exhaust runner Length	78

LIST OF SYMBOLS

\dot{m}	Boundary mass flux, $\dot{m} = \rho Au$
m	Mass of volume
V	Volume
V_{disp}	Displacement Volume
P	Pressure (static), Cylinder pressure
ρ	density
A	Flow area (cross-sectional)
A_s	Heat transfer surface area
e	Total internal energy (internal plus kinetic) per unit mass
H	Total enthalpy, $H = e + \frac{P}{\rho}$
h	Heat transfer coefficient
T_{fluid}	Fluid temperature
T_{wall}	Wall temperature
$T_b(t)$	Instantaneous brake torque
$T_s(t)$	Instantaneous shaft torque
I_{ct}	Cranktrain inertia
$\dot{\omega}_{ct}(t)$	Instantaneous cranktrain acceleration
N	Instantaneous engine speed
n_r	Revolutions per cycle (1 for 2-stroke, 2 for 4-stroke)
u	Velocity at the boundary
C_f	Skin friction loss coefficient, Fanning friction factor
C_p	Pressure loss coefficient
C_v	Specific Heat
D	Equivalent diameter, pipe diameter
dx	Length of mass element in the flow direction (discretization length)
dp	Pressure differential across dx
P_0	Total (stagnation) pressure
M	Mach number
γ	Specific heat ratio
Δx	Minimum discretized element length
Δt	Time step
c	Speed of sound
A_{eff}	Effective area for flow
Pr	Prandtl number
Nu	Nusselt number

Re_D	Reynolds number based on pipe diameter
k	Thermal conductivity
t	time
ε	Emissivity, pipe wall sand roughness
σ	Stefan-Boltzmann constant
m_u	Unburned zone mass
m_f	Fuel mass
m_a	Air mass
$m_{f,i}$	Injected fuel mass
e_u	Unburned zone energy
V_u	Unburned zone volume
Q_u	Unburned zone heat transfer rate
h_f	Enthalpy of fuel mass
h_a	Enthalpy of air mass
$h_{f,i}$	Enthalpy of injected fuel mass
m_b	Burned zone mass
V_b	Burned zone volume
Q_b	Burned zone heat transfer rate
AA	Anchor Angle
D	Duration
E	Wiebe Exponent
CE	Fraction of fuel burned (combustion efficiency)
BM	Burned fuel percentage at anchor angle
BS	Burned fuel percentage at duration start
BE	Burned fuel percentage at duration end
BMC	Burned midpoint constant
BSC	Burned start constant
BEC	Burned end constant
WC	Wiebe constant
SOC	Start of combustion
BP	Back Pressure
$IMEP$	Indicated Mean Effective Pressure
$BMEP$	Brake Mean Effective Pressure
BKW	Brake Power
BTQ	Brake Torque
$GIMEP$	Gross Indicated Mean Effective Pressure
$GISFC$	Gross Indicated Specific Fuel Consumption
θ	Instantaneous crank angle

Chapter 1- Background and Introduction

1.1 Motivation and Application

Exhaust pressure dynamics play a significant role in engine performance. Exhaust pressure has a direct correlation to volumetric efficiency, in-cylinder temperature, and emissions.[1][2] There are two important applications for cylinder deactivation. One is dynamic deactivation of cylinders on a multi-cylinder engine to improve part load efficiency.[3] The second is to convert a multi-cylinder engine to a single cylinder research engine. In research, deactivating cylinders allows for researchers to make experimental modifications to a small number of cylinders while still being able to extrapolate the data to fit the fully operational engine. Deactivating cylinders allows researchers to decrease cost, time spent on labor, and lower the propagation of uncertainty during experimental modification.

There is a distinct lack of research performed on the effects of cylinder deactivation on research engines. It has been hypothesized that cylinder deactivation can cause increased vibrations, higher amplitude pressure pulsations in the exhaust and intake manifolds, and potentially higher stresses on the driveshaft.[4] This thesis will be focusing on the traveling pressure waves in the exhaust manifold of a Waukesha VGF-18 and the engines response to the deactivation of five of its six cylinders. An analysis of pressure wave mitigation through geometric modification is also performed.

In order to extrapolate data from a deactivated cylinder engine to a fully functioning engine there are certain precautions that need to be taken. The engine needs to run in a similar fashion to when it was fully operational and be able to produce consistent results. When the exhaust valve opens, a compression wave is sent downstream and reflects back as a rarefaction wave when an opening in the exhaust system is encountered.[5] In a six-cylinder engine, when one valve is closing another one is opening. This results in pressure waves combining, canceling out, and ultimately averaging to result in a low average pulsation amplitude in the exhaust manifold.

It is the purpose of this work to determine how cylinder deactivation affects the pressure seen directly outside the exhaust valves immediately prior to opening and in the exhaust manifold during the entire cycle, as well as look into different methods of decreasing the pressure pulsation amplitudes to acceptable levels for research.

1.2 Review of Literature

1.2.1 Exhaust Pressure Importance

Exhaust pressure plays a large role in engine dynamics and affects in-cylinder temperature, pressure, power output, emissions, air exchange and exhaust gas recirculation.[6] Back pressure (BP) refers to the pressure resisting the flow of exhaust gas out of the cylinder. Back pressure is often caused by bends and obstructions in the exhaust runners leading to the manifold; BP is often different than the average exhaust manifold pressure.[7] Figure 1 demonstrates the effect BP has on in-cylinder pressure during the air-exchange processes. It is shown that higher BP results in higher in-cylinder pressures. Conversely, when BP increases there is a distinct decrease in the volumetric efficiency of the engine that can be attributed to the increase of residual gas scavenged by the engine when there is a high pressure on the outside of the exhaust valve during the exhaust stroke.[6][8] Exhaust pressure has no discernable effect on gross indicated mean effective pressure (e.g. GIMEP) or gross indicated specific fuel consumption (e.g. GISFC) but does show an inverse relationship with the indicated mean effective pressure (IMEP) for all four strokes due to the extra work required to expel the exhaust gas.[6]

Pressure waves in the inlet and exhaust pipes of internal combustion engines are a well-known phenomenon caused by the opening and closing of the inlet and exhaust valves of a cylinder. These pressure waves, or pressure pulsations, can be large in amplitude and can play a major role in engine performance. Traveling pressure waves are useful for increasing the performance of an engine in two primary ways. One way is improving cylinder scavenging by creating a low pressure event at the exhaust valve in the case of the exhaust pipe.[9] The second way is by creating a high boost pressure at inlet

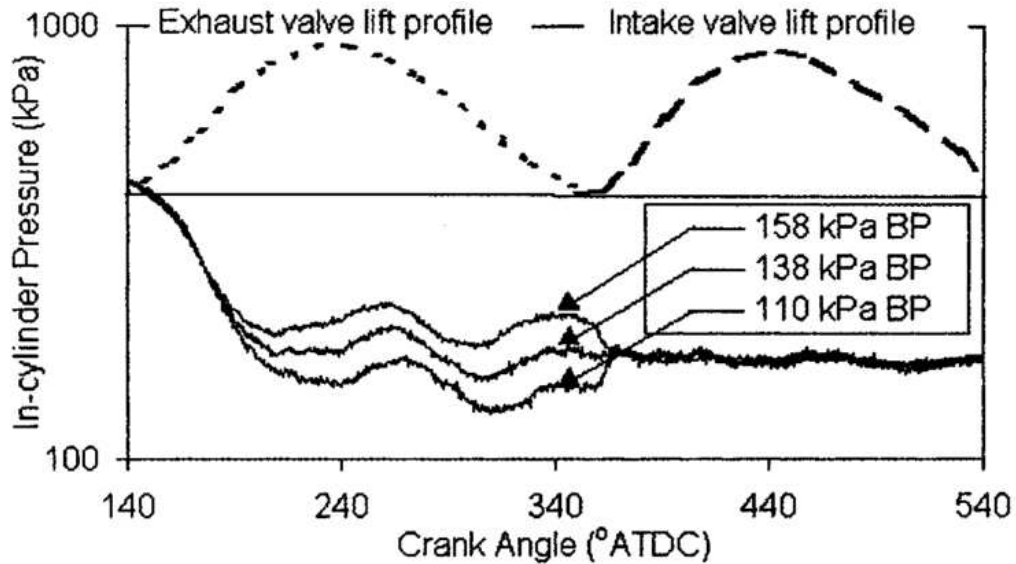


Figure 1 Effect of exhaust backpressure (BP) on in-cylinder pressure during air-exchange processes.[6] valve opening for the case of the inlet pipe.[10][11] The pressure in the exhaust system of an engine is periodically interrupted by the opening of the exhaust valve. When this happens an incident pressure wave travels through the exhaust pipe and into the exhaust manifold but a portion of the wave is reflected back towards the exhaust valve.[12] As demonstrated in Figure 2, this reflected wave can constructively interfere with other pressure waves to create large pulsation amplitudes or destructively interfere with other waves to decrease amplitudes.[8][9] By using destructive interference a constant pressure can be seen by the exhaust valve and by using well-timed constructive interference the exhaust valve can experience extremely low pressures during the exhaust phase resulting in increased scavenging and a better volumetric efficiency.

1.2.2 Cylinder Deactivation

Cylinder deactivation can offer a means of reducing fuel consumption of multi cylinder engines when operating under part loads. It is most effective on spark ignition engines that use throttle valves at part load to restrict intake flow, reducing intake manifold pressure. Older, less efficient engines that are converted to offer deactivated-cylinder-operation showed fuel consumption reduction of as much as 20%.[4] Pumping losses are significantly reduced when an engine is operating in a

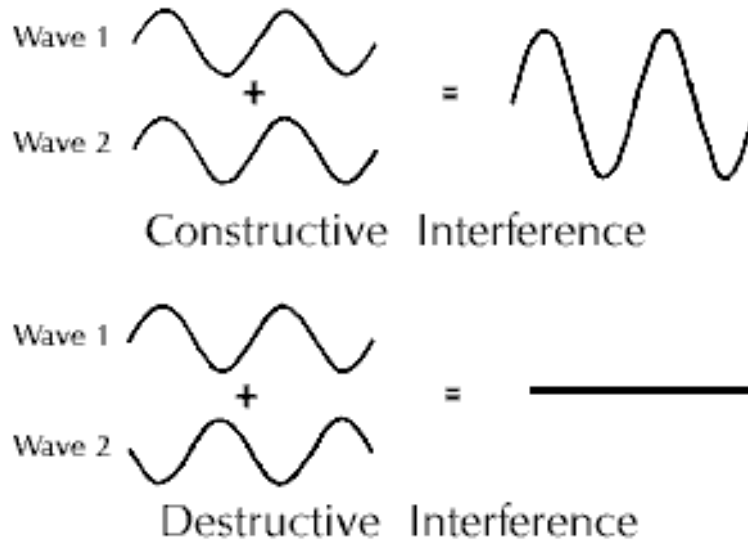


Figure 2 Demonstration of Constructive/ Destructive interference[12]

deactivated-cylinder mode. In typical light load use the throttle valve is nearly closed so the engine works harder to draw air, causing high losses. If cylinder deactivation is used the throttle valve can be left open, decreasing pumping losses for the same power output.[3] Three methods used for deactivating cylinders are shutting the inlet valves so that no charge can get into the cylinder, disabling the ignition source in the cylinder, and decoupling the motion of the piston from the rotation of the crankshaft.[3] Cylinder deactivation can cause an extra torsional load on the drive-shaft. It is recommended that a torsional analyses be performed prior to deactivation to identify safe and high risk operational ranges.[4]

For research, cylinder deactivation is used to minimize the level of effort and cost required to conduct engine combustion research. If the engine has only one operational cylinder then only one cylinder needs to be modified and the data can be extrapolated to find the approximate effects that the changes would have on a fully operational engine, saving time, money, and decreasing the variability in the experiment.[13]

1.2.3 GT-Power

GT-Power is a 1-D engine simulation program that uses various methods for modeling fluid, mechanical, and combustion components of an engine. GT-Power is used extensively in industry by

engine manufacturers and is an important engine research and development tool. The program has been used in research to solve a wide range of problems. For example, it was used to model a two stroke diesel engine with the goal of reducing CO2 emissions[14] and to optimize the turbine/compressor impeller diameters of a turbocharger. [15]

1.3 Overview

The pressure just downstream of the exhaust valve during the exhaust and intake strokes of a 4-stroke internal combustion engine can affect an engines volumetric efficiency, power output, thermal efficiency, and emissions. As deactivated-cylinder engines become more and more prevalent in industry and research it becomes important to understand the effects cylinder-deactivation have on the exhaust dynamics of an engine. This is especially important for research purposes since the engine needs to run consistently and predictably in order to mitigate the propagation of uncertainties.

The focus of this thesis is on the simulation of a natural-gas, medium-bore, Waukesha engine and analysis of the exhaust pressure dynamics when fully-operational and with deactivated cylinders. The software used is a one-dimensional fluids-based engine program called GT-Power. First a model was created to simulate the fully-operational Waukesha engine and was correlated to experimental data. Next the model was converted into a single-cylinder version of the Waukesha. Finally, an analysis was performed on the exhaust dynamics of both simulations and the effects of various modifications on engine performance using GT-Post.

Chapter 2- Methods and Materials

2.1 Models and Development

GT-Power is a one-dimensional engine solver that includes friction, flow, combustion, mechanical, and heat-transfer solvers.[16] The solutions found in the program are based on one-dimensional fluid dynamics that represent heat transfer and flow in the piping and other engine components.[16] Models are constructed with a mix of supplied templates and user-defined reusable compound objects.

2.1.1 Flow Modeling

The flow models solve of the Navier-Stoked equations, which are equations for the conservation of mass, momentum, and energy. All quantities are averaged across the flow direction and can be solved with explicit or implicit time integrators. The simulations described in this thesis use an explicit time integration method. Explicit time integration method provides a higher accuracy solution for mass flow rate, density, and internal energy than an implicit solver.[17] The solver uses a “staggered grid” discretization method where scalar variables are assumed to be uniform over each volume, shown in Figure 3.

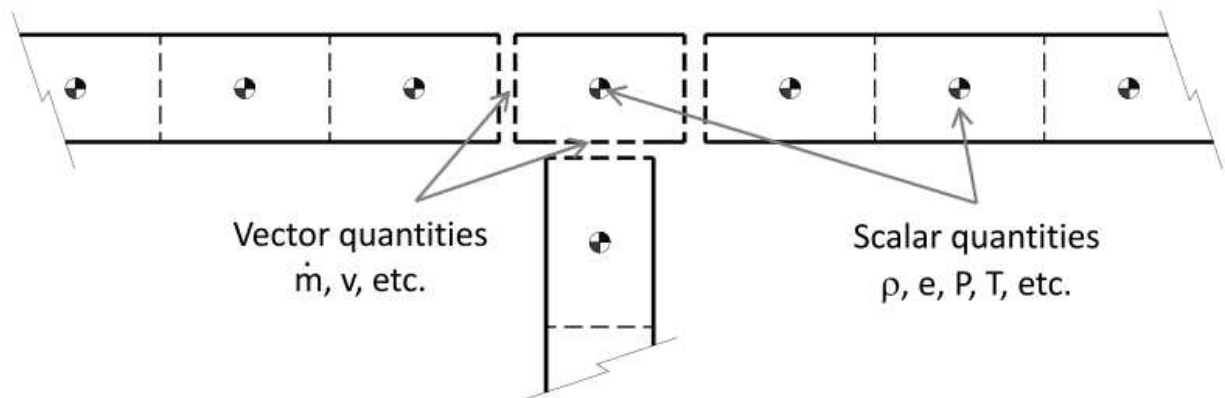


Figure 3 Schematics of staggered grid approach with scalars calculated at centroid and vector quantities at boundaries.[17]

The conservation equations solved by GT-Power are shown:

$$\mathbf{Continuity:} \frac{dm}{dt} = \sum_{boundaries} \dot{m}$$

$$\mathbf{Energy (Explicit Solver):} \frac{d(me)}{dt} = -p \frac{dv}{dt} + \sum_{boundaries} (\dot{m}H) - hA_s(T_{fluid} - T_{wall})$$

$$\mathbf{Enthalpy (Implicit Solver):} \frac{d(\rho HV)}{dt} = \sum_{boundaries} (\dot{m}H) + V \frac{dp}{dt} - hA_s(T_{fluid} - T_{wall})$$

$$\mathbf{Momentum:} \frac{d\dot{m}}{dt} = \frac{dpA + \sum_{boundaries}(mu) - 4C_f \frac{\rho u |u|}{2} \frac{dxA}{D} - C_p \left(\frac{1}{2} \rho u |u|\right) A}{dx}$$

The left hand side of the equations represent the derivatives of the primary variables. Secondary variables are solved in a slightly different way. Total pressure is calculated using a compressible definition and is always calculated as absolute (not gauge). Total Pressure is found using the following equation:

$$P_0 = P + \frac{\rho u^2}{2} \left(1 + \frac{M^2}{4} + (2 - \gamma) \frac{M^4}{24}\right)$$

The explicit solver, as mentioned above, primarily solves mass flow rate, density, and internal energy. The values of these variables at the next time step are calculated based on the conservation equations. In the explicit method the right hand values are calculated using the values from the previous time step which yields the derivative of the primary variables and allows the value at the new time to be calculated by integration of that derivative over the time step. This method requires small time steps and is therefore suitable for highly unsteady flows where a high degree of resolution is required to capture the extremes of the flow behavior.[17] This method produces the most accurate results for predicting pressure pulsations that occur in engine air and exhaust flow.

Flow losses in pipes due to friction along the walls are calculated automatically via a Fanning friction factor that is a function of Reynolds number and the wall surface roughness. The Fanning friction factor, C_f , is then plugged into the momentum equation above. An explicit Colebrook equation is used to

mathematically define a Moody Diagram, which describes the relationship between Reynolds number, wall roughness, and the resulting friction factor. For pipes in the laminar flow regime, defined as having an $Re_d < 2000$, the friction is calculated using the following equation:

$$C_f = \frac{16}{Re_d}$$

For a pipe with a wall sand roughness greater than zero that is in the turbulent regime, the friction factor is given by the Nikuradse formula:

$$C_{f,rough} = \frac{0.25}{(2 * \log\left(\frac{D}{2 * \varepsilon}\right) + 1.74)^2}$$

The pressure and temperature of an environment can be modeled by using an ‘EndEnvironment’ component. This component allows the user to define the ambient environment by temperature, pressure, humidity, and even the velocity of the ambient air relative to the intake system to take into account the effects of air “ramming”.[17]

2.1.2 Combustion Modeling

GT-Power defines combustion as the transfer of a defined amount of unburned fuel mass and air along with the associated enthalpy from an unburned zone to a burned zone in the cylinder, including the release of chemical energy in the fuel-air mixture and the calculation of species and concentrations that result.[16] The solver utilizes a two-zone combustion methodology for the combustion processes in an engine. In GT-Power, combustion occurs in the following manner:

1. At the start of combustion (the spark in the SI engine, or the start of injection in the DI engine) the cylinder is divided into two zones: an unburned zone and a burned zone. All of the contents of the cylinder at that time start in the unburned zone, including residual gases from the previous cycle and EGR. [16]
2. At each time step, a mixture of fuel and air is transferred from the unburned zone to the burned zone. The amount of fuel-air mixture that is transferred to the burned zone is defined by the burn rate. This burn rate is prescribed (or calculated by) the combustion model[16]

3. Once the unburned fuel and associated air has been transferred from the unburned zone to the burned zone in a given time step, a chemical equilibrium calculation is carried out for the entire "lumped" burned zone. This calculation takes into account all of the atoms of each species (C, H, O, N) present in the burned zone at that time, and obtains from these an equilibrium concentration of the 11 products of combustion species (N₂, O₂, H₂O, CO₂, CO, H₂, N, O, H, NO, OH). The equilibrium concentrations of the species depend strongly on the current burned zone temperature and to a lesser degree, the pressure.[16]
4. Once the new composition of the burned zone has been obtained, the internal energy of each species is calculated. Then, the energy of the whole burned zone is obtained by summation over all of the species. Applying the principle that energy is conserved, the new unburned and burned zone temperatures and cylinder pressure are obtained.[16]

The following energy equations are solved separately for each time step in each zone:

$$\textbf{Unburned Zone: } \frac{d(m_u e_u)}{dt} = -P \frac{dV_u}{dt} - Q_u + \left(\frac{dm_f}{dt} h_f + \frac{dm_a}{dt} h_a \right) + \frac{dm_{f,i}}{dt} h_{f,i}$$

$$\textbf{Burned Zone: } \frac{d(m_b e_b)}{dt} = -P \frac{dV_b}{dt} - Q_b - \left(\frac{dm_f}{dt} h_f + \frac{dm_a}{dt} h_a \right)$$

The unburned equation has four terms on the right hand side; these terms account for pressure work, heat transfer, combustion, and addition of enthalpy from injected fuel. The combustion term contains the instantaneous rate of fuel consumption or burn rate. [16][17]

The specific combustion used in for this paper is a spark-ignition Wiebe model. This model imposes a burn rate for a typical spark ignited engine using a Wiebe function. The benefits of using this model is that it provides a convenient means for implementing a burn rate and can be used to run a semi-predictive combustion model.[16] The Wiebe equations are given below:

$$BMC = -\ln(1 - BM) \quad \text{Burned Midpoint Constant}$$

$$BSC = -\ln(1 - BS) \quad \text{Burned Start Constant}$$

$$SOC = AA - \left[\frac{(D)(BMC)^{1/E+1}}{BEC^{1/(E+1)} - BSC^{1/(E+1)}} \right] \quad \text{Start of Combustion}$$

$$WC = \left[\frac{D}{BEC^{1/(E+1)} - BSC^{1/(E+1)}} \right]^{-(E+1)} \quad \text{Wiebe Constant}$$

$$Combustion(\theta) = \left[1 - e^{-(WC)(\theta - SOC)^{(E+1)}} \right] \quad \text{Burn Rate Calculation}$$

The cumulative burn rate is calculated and normalized to 1.0. the combustion starts at 0.0% burned and progresses to a defined value specified by the “Fraction of Fuel Burned” attribute in GT-Power.[18]

2.1.3 Mechanical Modeling

GT-Power uses a dynamic analysis method to solve for large displacements, finite rotation, and small elastic deformations of multibody systems. The semi-discrete equations of flexible-multibody systems are[18]:

$$M_f(\underline{q}) \ddot{\underline{q}} = \underline{F}(t, \underline{q}, \dot{\underline{q}})$$

$$M(\underline{y}) = \begin{bmatrix} I & 0 \\ 0 & M_f(\underline{q}) \end{bmatrix}, \quad \underline{y} = \begin{bmatrix} \underline{q} \\ \dot{\underline{q}} \end{bmatrix}, \quad \underline{g}(t, \underline{y}) = \begin{bmatrix} \dot{\underline{q}} \\ \underline{F}(t, \underline{q}, \dot{\underline{q}}) \end{bmatrix}$$

I is the identity matrix. By inverting the mass matrix, the generic governing equations of motion become:

$$\dot{\underline{y}} = \underline{f}(t, \underline{y}),$$

$$\underline{f}(t, \underline{y}) = M^{-1}(\underline{y}) \underline{g}(t, \underline{y})$$

Where M_f is a 6x6 positive definite mass matrix, \underline{F} is a 6x1 right hand side vector, \underline{q} is a 6x1 matrix representing the linear displacements of a reference point, and $(\dot{\bullet})$ represents the derivative with respect to time.[18] Because there is only one reference point, or node, a rigid body can only be connected to other components at this node. If additional connections are required more connecting nodes can be defined relative to the reference node, and this relative position remains unchanged during

simulation. Adding additional connecting nodes does not increase the degrees of freedom of the system so the number of unknowns for a rigid body in space will always be six regardless of additional nodes.[18]

In order to solve these equations a set of integration schemes, both implicit and explicit, have been developed by Gamma Technologies, Inc. To solve mechanical problems in a general and efficient manner the solution architecture is based on the Finite Element method (FEM).[18] Each component and connection creates one or more elements which in turn point to a set of nodes. Each node contains all of the state information such as position, displacement, velocity, acceleration or a constraint force.[18] GT-Power has a separate computational technique for flexible-body kinematics but is left out as no flexible bodies are modeled in this paper.

2.1.4 Heat Transfer Modeling

There are multiple types of heat transfer calculations used by GT-Power: in-cylinder, flow-to-wall, and wall-to-environment. The heat transfer from fluids inside of pipes to their walls is calculated using a heat transfer coefficient. The heat transfer coefficient is calculated at every timestep from the fluid velocity, the thermos-physical properties, and the wall surface roughness. For smooth pipes, that are laminar, turbulent, or transitional, the Colburn analogy is used to solve for heat transfer:

$$h_g = \left(\frac{1}{2}\right) * C_f * \rho * U_{eff} * C_p * Pr^{(-\frac{2}{3})}$$

Surface roughness has a very strong influence on heat transfer coefficient, especially for very rough surfaces such as cast aluminum. The heat transfer coefficient for rough pipes is calculated by using the same heat transfer coefficient as smooth pipes, then increasing it using the following correlation:

$$h_{g,rough} = h_g * \left(\frac{C_{f,rough}}{C_f}\right)^n$$

$$n = 0.68 * Pr^{0.215}$$

When the friction coefficient of a rough pipe gets four times larger than the friction coefficient for an equivalent smooth pipe, the heat transfer coefficient no longer increases. There is a “heat transfer multiplier” attribute in pipes and flow splits that can be used to scale the calculated heat transfer

coefficient in individual pipes, if necessary. The internal heat transfer coefficient, the predicted fluid temperature, and the internal wall temperature are used to calculate the total heat transfer. The wall temperature input for pipes is used as an initial wall temperature when the heat transfer coefficient is used. The heat transfer from the fluid to the pipe is solved at every timestep and the nodal temperatures are updated once per cycle.

The wall-to-environment heat transfer is calculated using a ‘WallTempSolver’ sub-model. Calculated wall temperatures are solved using the internal heat transfer, external heat transfer, thermal capacitance of the walls, and the initial wall temperature entered by the user. The user enters data describing the forced convection, free convection, and/or radiation for wall temperature calculations. The wall temperature solver uses equations resulting from discretized energy conservation using the finite volume method. Each of the wall layers for a pipe sub volume is used as a control volume for the energy equation. Heat transfer across the radial faces of the volumes are calculated using a resistance to conductive heat transfer as well as radiation between the surfaces on either side of an air gap, and conductive heat transfer at the axial boundaries. [17] The following are the generalized equations used for solving heat transfer in the model:

$$\textit{Conservation of Energy: } \int \frac{\partial(\rho C_v T)}{\partial t} dV = \int (-\nabla \cdot q) dV$$

$$\textit{Heat flux due to conduction: } q_{\textit{conduction}} = -k\nabla T$$

$$\textit{Heat flux due to radiation: } q_{\textit{radiation}} = -\varepsilon\sigma(T_1^4 - T_2^4)$$

$$\textit{Heat flux due to convection: } q_{\textit{convection}} = h(T_g - T_w)$$

$$\textit{External convection coefficient: } h_{\textit{external}} = \max(Nu * \frac{k}{D * h_{\textit{input}}})$$

In-cylinder heat transfer is modeled using the combination of two sub-models, one for heat transfer within the cylinder, and one defining the wall temperatures. A Woschni correlation without swirl was used to calculate the in-cylinder heat transfer coefficient. This model type accounts for differences in the treatment of heat transfer coefficients during the period when valves are open, where heat transfer is

increased by inflow velocities through the intake valve and by backflow through the exhaust valve. This model is recommended by GT-Power when swirl data is not available.[17]

2.1.5 Calculating Volumetric Efficiency

In spark ignited engines the volumetric efficiency (VE), and thus airflow, is the single most influential engine performance datum, the affects brake torque when the fuel-to-air-ratio is fixed.[17] GT-Power calculates cylinder volumetric efficiency and manifold volumetric efficiency for air, fuel, and burned gasses. GT-Power calculates volumetric efficiency using the following equations:

$$V.E. \text{ Cylinder} = \frac{\oint \dot{m}_{nf} dt}{\rho_{ref} V_{disp}}$$

$$V.E. \text{ Manifold} = \frac{\oint \dot{m}_{nf} dt}{\rho_{man} V_{disp}}$$

Volumetric efficiency is the first metric used for calibrating models in GT-Power due to its large effect on engine performance. The most influential factors on volumetric efficiency in Gt-Power are the intake and exhaust valves, the intake ports, the intake runners, intake manifold, and intake wall temperatures. Other less influential factors include the exhaust ports and the exhaust wall temperatures as well as any resonators used in the model.[16]

2.1.6 Calculating Engine Performance Parameters

The primary attributes dictating engine performance that are analyzed in this paper are the brake mean effective pressure (BMEP), brake power (BKW), indicated mean effective pressure (IMEP), and brake torque (BTQ). Figure 4 shows the relationship between the different quantity names, where the rectangular blocks represent losses and the elliptical boxes represent the resulting available energy at some point in the system. Brake mean effective pressure is a measure of an engine's capacity to do work that is independent of engine displacement. Indicated mean effective pressure may be thought of as the average pressure acting on a piston during the different portions of its cycle. Brake power can be simply defined as the useful power that an engine provides at the output shaft. These quantities are calculated in GT-Power using the following equations:

$$bmep = \frac{2\pi n_r * (btq)}{V_{disp}} * [10^{-5}]$$

$$imep = \frac{\sum_{i=1}^{\#Cylinders} \oint \frac{P_i dV_i}{V_{disp,i}}}{\#Cylinders}$$

$$btq = \frac{bkw}{RPM} * \left(\frac{6000}{2 * \pi} \right)$$

$$bkw = \frac{\oint T_b(t) N dt}{\oint dt} \left[\frac{2\pi}{60000} \right] \text{ and } T_b(t) = T_s(t) - I_{ct} \omega_{ct} \dot{(t)}$$

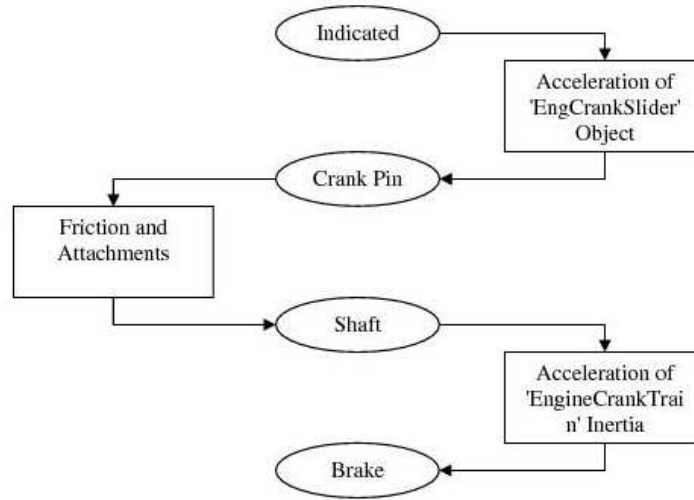


Figure 4. Relationship between Indicated, Crank Pin, Shaft, and Brake Quantities [16]

Chapter 3- Multi-Cylinder Model Development

3.1 Single-Cylinder Model Development

Before the full six-cylinder model was constructed, a simplified single-cylinder model was generated to allow for faster simulation speeds for initial model verification. Figure 5 is a picture of the simplified model and shows that the model contained two end-environments to mimic atmosphere on the intake and exhaust side of the engine, an intake and exhaust system including valves, ports, and runners, a fuel injector, a combustion cylinder, and an engine (driveline). This model does not contain any manifolds because there is only one flow system and therefore cannot be used for full verification of either the exhaust or intake system. This model was developed to verify the combustion solver and a separate model was created to verify the flow/pressure solver used in GT-Power. The cylinder is an independent system so no assumptions need to be made when converting this model to the full six-cylinder model, but since the flow circuit will change significantly during the conversion, certain assumptions need to be made. The first assumption made is that because the components directly before and after the cylinder don't change from model-to-model, the flow solver will not change drastically so the results from the single-cylinder verification can be translated to the six-cylinder model. The second assumption is that the end-environment on the outlet side of the model acts in a very similar way to have a large opening, as would be seen in an exhaust manifold. This assumption is made so that the pressure wave dynamics verification can be translated to the six-cylinder model; this assumption is supported by the calculation methods for end-environments discussed in section 3.3 Defining Individual Components.

In order to maintain as much uniformity as possible between the single-cylinder and six-cylinder model all of the dimensions and geometries used in the single-cylinder model accurately reflect the components of the Waukesha VGF-18 engine that the six-cylinder model is supposed to simulate. Since the single-cylinder model left out the carburetor and inlet manifold, a port injection method was used

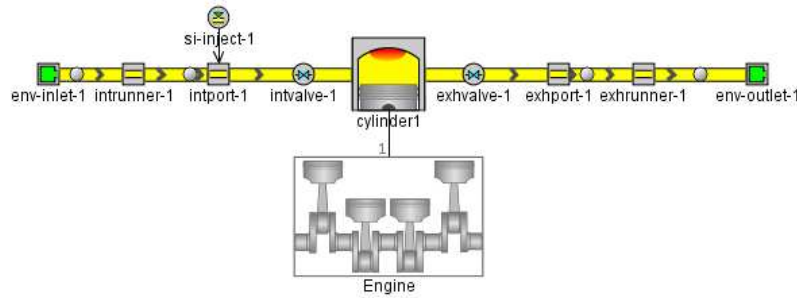


Figure 5. Simplified Single-Cylinder model for a Waukesha VGF.

in the model. The Air-Fuel ratio was held constant and because GT-Power solves combustion as a uniform mixture, this method provides approximately the same results as would be expected in the full six-cylinder model that includes the aforementioned components.

In order to ensure correct dimensions, a real Waukesha VGF-18 engine was taken apart and measured. The ports, valves, and manifolds were all found to be of a cylindrical geometry but the exhaust runners were found to be rectangular with rounded corners. In order to fully-define the model, sub-models were created to define things such as heat-transfer, the combustion objects, wall temperatures, initial states, friction objects, flow control solvers, and fluid mixtures. These models are associated with a number of assumptions and are covered in section 3.4 Sub-Models.

3.1.1 Combustion Verification

In order to verify the combustion process, a conceptual model was created in Chemkin. Chemkin has a base piston-cylinder model that can be used to find chemical species pre and post combustion as well as temperature and pressure at all steps. This simulation used a well-established combustion model known as a Ra-Reitz model to solve for the chemical species at all points during combustion as well as heat release and increase in pressure. The GT-Power model uses a Wiebe function to define combustion, so the two different methods can be compared independently for verification purposes.

The input data used for the Chemkin model was found by a combination of measuring component dimensions and using data found experimentally. Anything geometric was measured or taken from engine

Table 1. Input values for Chemkin piston-cylinder combustion solver.

Chemkin Input Variable	Value	Units
Compression Ratio	11.6	-
Engine Displacement Volume	1095	in ³
Engine Speed	1800	RPM
Starting Pressure	1.2	Atm
Starting Temperature	315	K
CH4 mole fraction in fuel	0.95	fraction
C2H6 mole fraction in fuel	0.05	fraction
N2 mole fraction in oxidizer	0.79	fraction
O2 mole fraction in oxidizer	0.21	fraction
Combustion Solution technique	Ra-Reitz	-
Ignition Temperature for CH4	834	K

specification sheets, the molar fractions for the fuel and oxidizer correlate with the mole fractions used in the GT-Power solver. The input values chosen can be seen in Table 1.

In order to verify that the GT-Power model matched the Chemkin model for the combustion portion of the simulation a comparison of the differences between the two models divided by the averages was made to gain a standardized comparison between the two outputs. The results of this comparison can be seen in Table 2. It is important to note that neither of the models account for pumping or friction losses, heat transfer, valve lash, or any other mechanical affect that would be seen in actual engine operation. Both the Chemkin model and the GT-Power model are idealized to show that in a perfect scenario, GT-Power will produce realistic results. A T-Test and F-Test were used as comparison tools for the two models, with a T-Test comparing the means and an F-Test comparing the variances between the models.[19] Both of the tests resulted in values well above 95%, indicating that the means and variances between the two models are statistically similar.

One more verification method was used on the combustion process, specifically pertaining to the mechanical cylinder-piston solver in GT-Power. A piston-cylinder was created in GT-Power that did not have any fuel and had closed inlet and exhaust valves. The ideal gas relation was then solved

Table 2. Combustion Verification with Chemkin

Measurable	GT-Power	Chemkin	90% Confidence (+/-)	Standard Deviaton
Pressure at beginning of cycle (KPa)	146.5	138.8	21.98	5.46
Pressure at Combustion Start (KPa)	3392	3454	547.1	43.88
Pressure at TDC (KPa)	6967	6840	1083	90.25
Duration (827 KPa to 827 KPa)	137.0	140.0	22.17	2.12
	T-test Score:	0.9941	F-Test Score	0.9803

analytically using measured temperature and volume and solving for pressure at all points in the cycle using the following equation:

$$\frac{P * V}{T} = Constant$$

Using the initial values in GT-Power to calculate the constant to the above equation, the pressure was calculated over two crank train rotations using a calculated value for volume and a recorded value for temperature. The calculated values for pressure were compared to the simulated values of pressure using a two-tailed students T-Test to calculate the confidence in the solution. Table 3 shows example numbers used for during the verification process as well as the maximum pressure values calculated and maximum difference between the recorded and calculated values. The confidence level calculated using the students T-Test was found to be greater than 99%, indicating that the model was extremely accurate to the ideal gas law, successfully verifying the non-combustion piston cylinder pressure solver. These values do not take into account friction or pressure losses that would occur during actual engine operation so the values are expected to be different during the cylinder deactivation simulation, but still accurate.

Table 3. Pressure-Spring Verification Example

Degrees	Temperature [K]	Volume [m ³]	Pressure Recorded [kPa]	Pressure Calculated [kPa]	Max Pressure (GT-Power)	Max Pressure(Calculated)
-74.95	588.2	8.43E-04	187.0	187.0	842.0	840.6
-73.99	584.7	8.56E-04	183.0	183.0	T-Test Confidence Value	Max (difference)
-73.08	580.4	8.73E-04	178.2	178.2	0.992	1.38

3.1.2 Flow Verification

The actual engine models are too unsteady to analyze analytically in order to verify the flow solver. For this reason, a new model was created in order to simplify the flow analysis. This model is a simple pipe flow with a specified air injection rate on one side and an open environment on the other. Figure 6 shows the model created in GT-Power in order to verify the flow solver. The injection component is injecting air into the entrance to the pipe at 1kg/s, as shown in Figure 6. The pipe absolute roughness (ϵ) is an approximation for steel with light rust. Ambient temperatures and pressure were chosen to be averages for sea level. The pipe diameter and length were picked to be reasonable values for steady flow and for approximating pipes in engine flow. The air injection rate was arbitrarily selected to simplify the math involved.

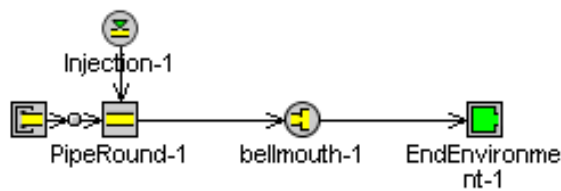


Figure 6. Flow Verification Gt-Power Model

Table 4. Flow Verification GT-Power Inputs

Component Parameters	Value
Pipe Length [in]	12
Pipe Diameter [in]	2
Air Injection Rate [kg/s]	1
Ambient Temperature [k]	298
Ambient Pressure [kPa]	101.3
Absolute Roughness [mm]	0.25

Figure 7 is the conceptual model demonstrating what the GT-Power model is representing. The parameter ‘W’ represents the nodal width used to split the pipe into sub-volumes for numerical analysis. In GT-Power the sub-volumes had a width of 0.1 inches for a high fidelity solution. During analysis, however, values were only recorded every 1.2 inches so that there was only ten data points to analyze. This model represents Fanno flow, i.e. flow in a constant area pipe with adiabatic walls and friction.

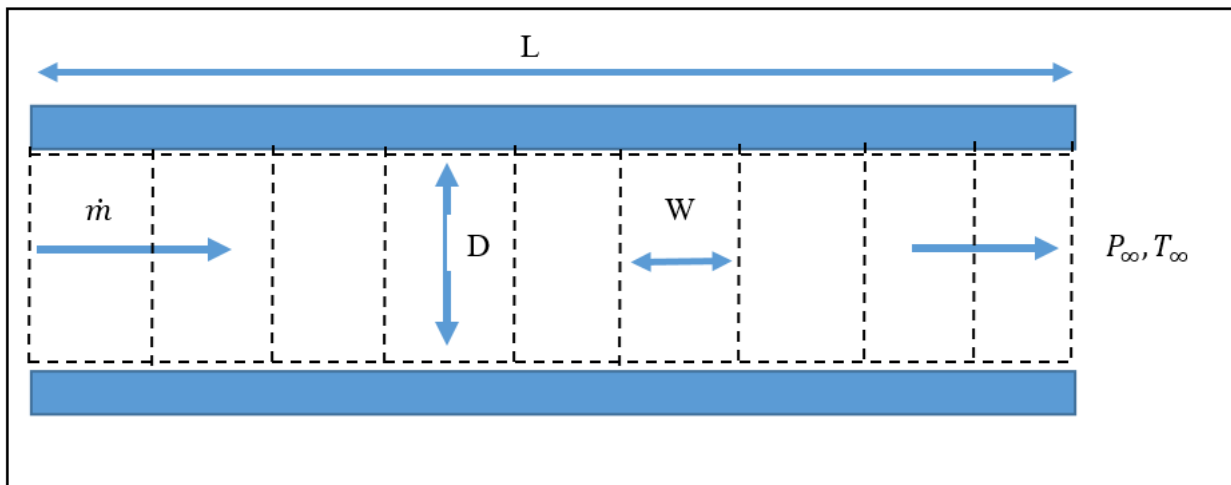


Figure 7. Conceptual Model of Flow Solver in GT-Power

When the GT- Power model was run, the results were analyzed to ensure that the results made sense, i.e. ensuring that the assumptions made were valid. Figure 8 shows the Mach number with respect to pipe location, where a value of ‘0’ is the entrance to the pipe and ‘1’ is the exit of the pipe. As would be expected for Fanno flow, the friction causes entropy to increase, so Mach number in the pipe increases to, but doesn’t pass sonic flow. The following equation relates the change in temperature with Mach and

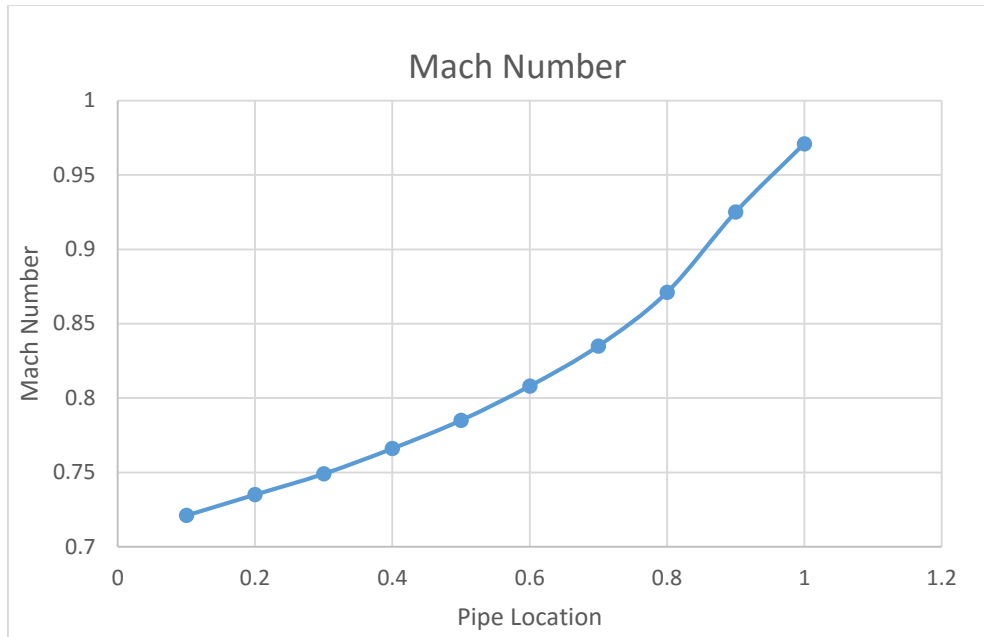


Figure 8 Mach Number Vs. Pipe Location for Flow Verification

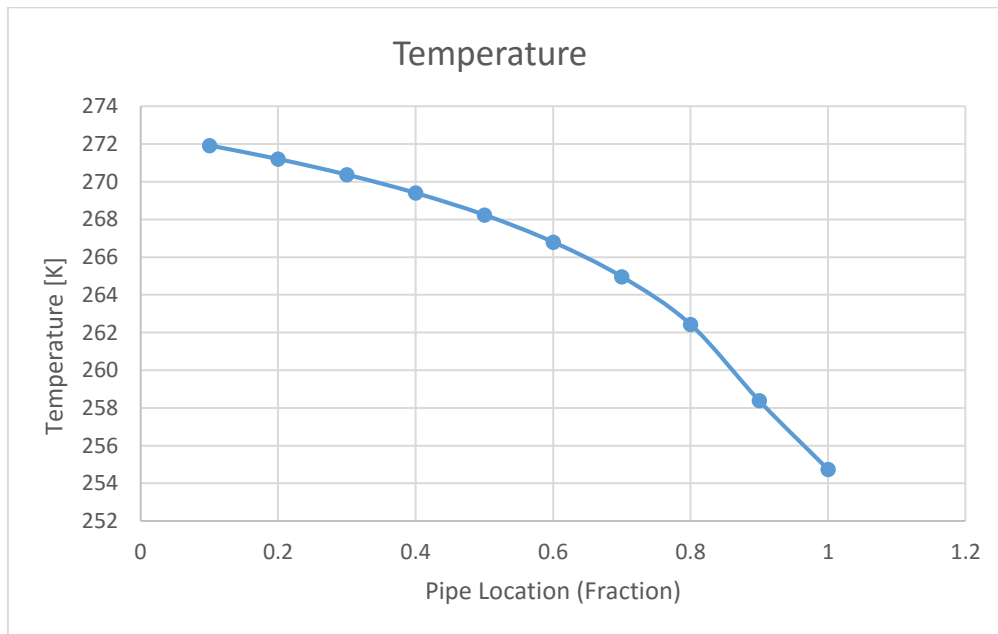


Figure 9. Temperature Vs. Pipe Location for Flow Verification

it can be seen that this will always be a negative number. Figure 9. shows the temperature Vs. pipe location and shows a decrease in pressure with increase in Mach number.

$$\frac{dT}{T} = \frac{-\gamma(\gamma - 1)M^4}{2(1 - M^2)} \frac{f dx}{D}$$

3.2 Six-Cylinder Model Development

After the single-cylinder model was created and the combustion and flow solvers were verified, work was done on modifying the model to work as a full six-cylinder model. In order to do this the single-cylinder model was replicated five times so that the processes verified in section 3.1.1 and 3.1.2 are still verified in the six-cylinder model. The firing order and angles of each cylinder were directly imported from a specification sheet for the Waukesha VGF engine. The dynamic loading of the driveshaft and the main bearings were ignored in the model because of the minimal affects these components play on in-cylinder engine operation. In order to get closer to the actual engine operation manifolds were added on the exhaust and intake side. The fuel injector was moved upstream of the intake manifold, as seen in Figure 10, and a bellmouth was placed upstream of the fuel injection port so that the pressure in the intake system could be controlled to mimic the effects of the turbocharger that is on the Waukesha VGF. This model used simple geometries with a single inlet and exhaust port for each cylinder and only a single gas mixture injector, which is not an entirely accurate representation of the engine. This model was used in initial stages to assess the validity of this model for predictive capabilities and to gauge the computing requirements the model possessed.

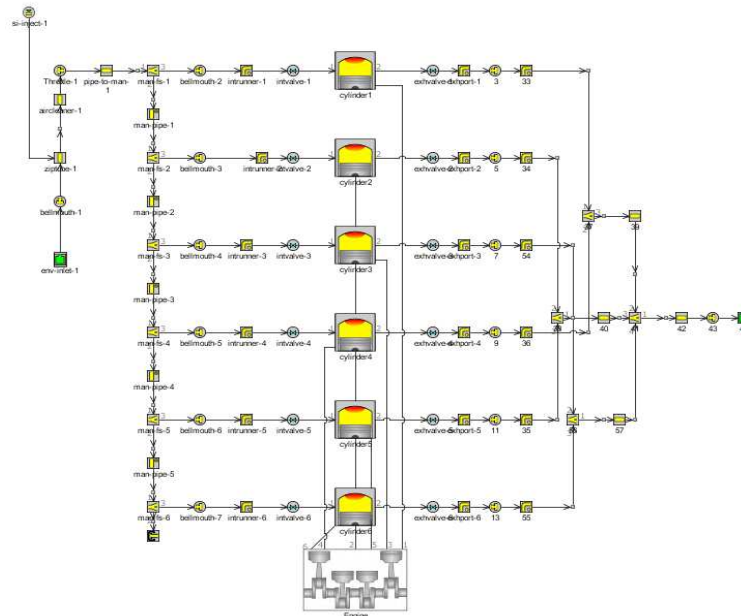


Figure 10 Initial Six-Cylinder model

Figure 11 is the final six-cylinder model used for the simulation of the Waukesha VGF. The final model used an air injector to simulate the turbocharger and had four ports per cylinder to more accurately depict the geometries of the Waukesha engine. Other modifications include wall friction in the piping as well as elevation changes in the exhaust runner and humidity in the ambient environment. There were certain unknowns in the system that needed to be solved iteratively, such as the size of the bellmouth's at the beginning of the inlet system and end of the exhaust system to best simulate the effects of a turbocharger. Other components solved iteratively include surface roughness in the ports entering and exiting the cylinder and certain portions in the sub-models that will be discussed further in section 3.4 Sub-Models. This model was validated by comparing experimental results for engine performance with simulation results, which is discussed further in section 3.5 Cylinder Deactivation.

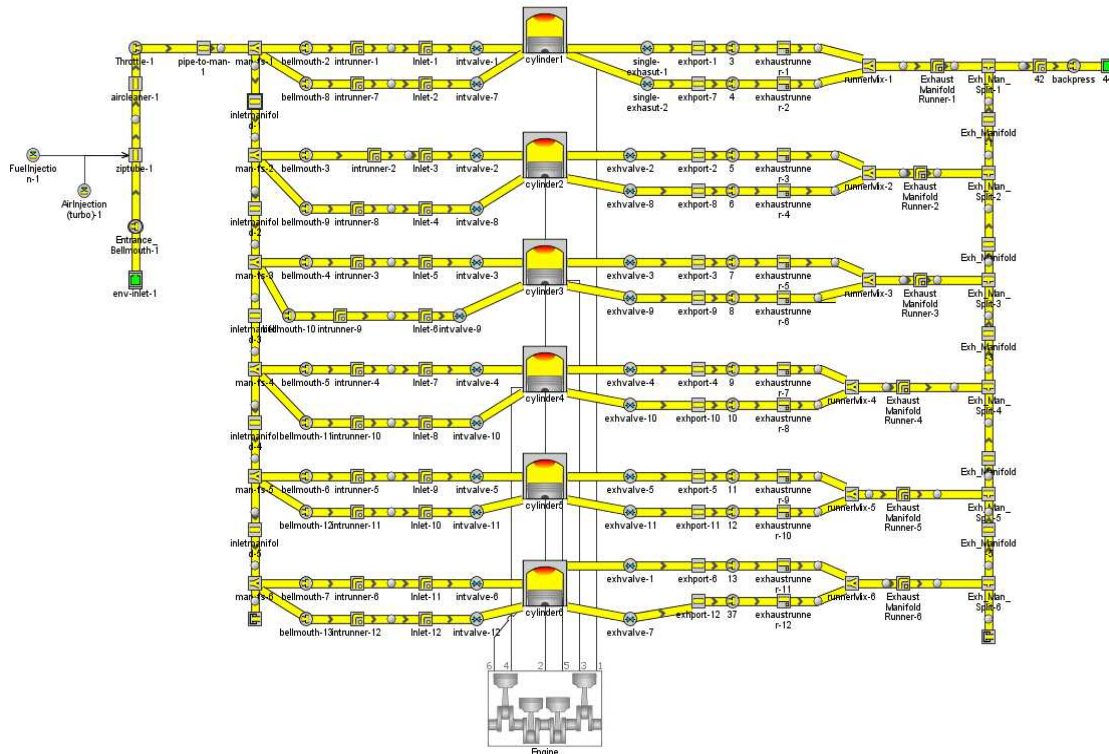


Figure 11. The final six-cylinder model with four ports per cylinder and an air injector.

The finished six-cylinder model shown in Figure 11, after validation, was used for the pressure analysis and analysis of pressure mitigation techniques in Chapter 4- Pressure Analysis and Mitigation Techniques. The model was then modified to correctly portray the effects of cylinder-decommissioning for the purpose of predicting experimental results.

3.3 Defining Individual Components

As shown in Figure 5 and Figure 11, a GT-Power model is an assembly of individual components. Components differ from each other based off of their purpose and the physical engine component that the virtual components are made to model. This section delves into each component of the model and discusses how the components were defined and what assumptions were made.

3.3.1 Defining the Inlet and Exhaust ‘EndEnvironment’ Components

There are two ‘EndEnvironment’ components used in the six-cylinder GT-Power model shown in Figure 11, one for the inlet side of the engine and one for the exhaust side of the engine. These components are used to model the ambient air of Fort Collins, CO in the Engines and Energy Conversion Laboratory of Colorado State University. Table 5 lists the specific attributes and their values for both of the EndEnvironments. The pressure and temperature are set to atmospheric at sea level and the “altitude” attribute is used to modify the temperature and pressure values to the correct elevation.

Table 5. Inlet and Exhaust ‘EndEnvironment’ Attributes

EndEnvironment (Inlet and Exhaust)		
Attribute	Unit	Object Value
Pressure (Absolute)	KPa	101.3
Temperature	K	293
Composition		air
Altitude	m	1525
Reference Altitude	m	0
Altitude Correction For...		PresAndTemp
Relative Humidity (Added to specified fresh air Composition)	fraction	ign
Humidity Species		ign
Apply Humidity to Initial Conditions		yes

3.3.2 Defining the Various ‘OrificeConn’ Components

The ‘OrificeConn’ components in GT-Power are used to link flow components together. An orifice can be used to specify flow restrictions by setting the orifice diameter to be smaller than the diameter of the two mating components. If a flow restriction is not desired, then “def” (default) may be entered for the orifice diameter and the program will use the smaller diameter of the mating components as the orifice diameter. [17] Table 6 displays the possible attributes for an ‘OrificeConn’ component and the specific values selected for those attributes for the ‘Entrance Bellmouth’ component in the model.

Table 6. Entrance Bellmouth (OrificeConn) Component Attributes

Entrance_Bellmouth (OrificeConn)		 Entrance_Bellmouth-1
Attribute	Unit	Object Value
Hole Diameter	mm	39.852
Number of Holes		def (=1.0)
Forward Discharge Coefficient		def
Reverse Discharge Coefficient		def
Hole Thickness	mm	def
Rounded Corner Radius (only if Discharge Coefficient = "def")	mm	ign
Forward End Correction (Length/Diameter)		def
Reverse End Correction (Length/Diameter)		def
Heat Conduction "Flange"		ign
Initial Mass Flow Rate	kg/s	def
Pressure Recovery Choice		PressureRecovery
Laminar Face Friction Multiplier		def

The “Hole Diameter’ in Table 6. Entrance Bellmouth (OrificeConn) Component Attributes was a value found using the optimizer tool in GT-Power to reduce the flow into the environment to create a positive pressure on the intake side of the engine. The pressure that the diameter aligns with is 126.23 KPa, which was a value recorded in the inlet manifold of a Waukesha VGF engine experimentally. The forward and reverse discharge coefficients describe the degree to which the orifice is sharp or rounded. When “def” is set as the value, GT-Power will calculate the correct value of the discharge coefficient based on the flow area ratios in the two directions. The forward and reverse end corrections represent the

amount of virtual mass added into the solution of the momentum equation, but there is no actual change in pipe length or volume. When set to “def” GT-Power calculates this correction automatically. The ‘Heat Conduction “flange”’ controls how heat transfer is calculated through the orifice, and when set to “ign”, GT-Power treats the orifice as a non-conductor; the orifice will be ignored in the heat transfer calculations between the two connected flow components.[17]

Table 7. Back Pressure (OrificeConn) Component Attribute

BackPress (OrificeConn)		
Attribute	Unit	Object Value
Hole Diameter	mm	63.5
Number of Holes		1
Forward Discharge Coefficient		def
Reverse Discharge Coefficient		def
Forward End Correction (Length/Diameter)		def
Reverse End Correction (Length/Diameter)		def
Heat Conduction "Flange"		ign

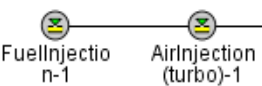
Pressure in the exhaust flow components was regulated using an OrificeConn component, shown in Figure 7. The back pressure in the exhaust manifold of a Waukesha VGF engine was found experimentally and the hole diameter in Table 7 acts as a flow-pinch to increase the average pressure in the exhaust flow components of the model to match the experimental results. The other attributes in the ‘BackPress’ component are the same as the ‘Entrance_Bellmouth’ component shown in Table 6.

3.3.3 Defining the Fuel and Air Injection Components (InjConn)

The fuel and air injector components are used in the model to simulate a carburetor and a turbocharger. The actual component used is an ‘InjConn’ component that allows for an imposed injection rate, which was used because the fuel and air intake rates for a Waukesha VGF engine were found experimentally. Table 8 shows the attributes allowed in the ‘InjConn’ component as well as the values selected for the fuel and air injector.

The mass flow rate for both the fuel and air were found experimentally for a Waukesha VGF engine. The ‘Injector Location’ defines the location of injection into a pipe, and a value of 0.5 was selected so that the injection occurred halfway through a flow pipe; a value arbitrarily picked and assumed to have negligible effect. ‘Injected Fluid Temperature’ was defined as 310K which correlates to 100 degrees Fahrenheit, which was the recorded injection temperature found experimentally. Both of the ‘Fluid Object(s)’ are defined as sub-models in GT-Power and will be covered in more detail in

Table 8. Fuel and Air Injection (InjConn) Component Attributes



InjConn (Fuel and Air Injection Model)		
Attribute	Unit	Object Value
Mass Flow Rate (fuel)	kg/h	55
Mass Flow Rate (Air)	kg/h	1148
Injector Location (Pipes only)		0.5
Injected Fluid Temperature	K	310
Fluid Object (fuel)		methane-vap
Fluid Object (Air)		Air
Vaporized Fluid Fraction		1

section 3.4 Sub-Models. The ‘Vaporized Fluid Fraction’ defines what fraction of the injected liquid is in vapor phase but because only methane and air was used, which are both in vapor state in standard conditions, this value could be set to 1.

3.3.4 Defining the Inlet Pipe Flow Components

The GT-Power model for the six-cylinder Waukesha VGF engine shown in Figure 11 consists mostly of pipe flow components. The major components created are the ziptube, inlet manifold, inlet runners, inlet ports, exhaust ports, exhaust runners, and the exhaust manifold sections. Each one of these components differ from each other for various reasons and assumptions are made in each component. The first component on the intake side of the model is the ziptube, a component that acts as a volume for the injected air and methane to mix in.

The ziptube dimensions are mostly arbitrary as this component is mostly just an extension of the fuel injectors, however, the attributes (but not their values) will be the same for every round pipe. The geometric dimensioning was picked arbitrarily for this component. The ‘Discretization Length’ attribute dictates the size of the sections that a volume is split into for the nodal solving method GT-Power utilizes. Each sub-volume performs their own calculations and the end result will be the same as if several shorter single-volume pipes would have been used.[17] A value of 40mm is large but because this component is not being analyzed, a large value was selected to shorten simulation time.

Table 9. Ziptube (PipeRound) Component Attributes



Ziptube (PipeRound)		
Attribute	Unit	Object Value
Diameter at Inlet End	mm	70
Diameter at Outlet End	mm	70
Length	mm	150
Discretization Length	mm	40
Initial State Name		initial
Surface Finish		Smooth
Radius of Bend	mm	ign
Angle of Bend	deg	ign
Pipe Elevation Change	mm	ign
Number of Identical Pipes		1
Imposed Wall Temperature	K	320
Heat Transfer Multiplier		def (=1.0)
Friction Multiplier		def (=1.0)

For the ‘Roughness of Material’ attribute GT-Power has pre-defined values that can be selected based on what material is used. Table 10 shows all of the pre-defined materials and the associated sand roughness values. For this model, steel, steel with light rust, and steel with heavy rust where the primary materials selected. The methods GT-Power uses for calculating friction losses in pipes can be seen in Section 2.1 Models and Development.

Table 10. Material Roughness Pre-Defined Values for Various Materials

Material	Sand Roughness (mm), ϵ
Drawn tubing, metal	0.0015-0.0025
Smooth plastic, fiberglass	0.0025
Flexible smooth rubber	0.0025
Galvanized metals, smooth finish	0.025
Commercial steel	0.046
Wrought iron	0.046
Asphalted cast iron	0.12
Galvanized metals, normal finish	0.15
Steel pipe with light rust	0.25
Cast iron	0.36
Steel pipe with heavy rust	1

The Inlet was split into five sections with flow splits connecting each section to the next section as well as the inlet runners. Table 11 has all of the object values for an individual inlet manifold section. The diameters and lengths were all measured and the discretization length was selected to be relatively large in favor of faster simulation run time. The inlet manifold is a straight cylinder so the bending attributes could be ignored. An imposed wall temperature was used to once again favor a faster runtime

Table 11. InletManifold (PipeRound) Component Attributes

InletManifold (PipeRound)		
Attribute	Unit	Object Value
Diameter at Inlet End	mm	120.65
Diameter at Outlet End	mm	120.65
Length	mm	50.8
Discretization Length	mm	30
Initial State Name		initial
Roughness from Material		steel
Radius of Bend	mm	ign
Angle of Bend	deg	ign
Pipe Elevation Change	mm	ign
Imposed Wall Temperature	K	300
Heat Transfer Multiplier		def
Friction Multiplier		def

with the assumption that the calculated wall temperature would not be much different and would also have minimal effect on engine operation.

The second portion of the inlet manifold is the flow split. This component connects the various manifold sections to each other as well as the inlet manifold. In order to do this each link needed to be defined based off of angle with respect to (wrt) each axis as well as the characteristic length and expansion diameter for the traveling flow. Characteristic length defines the distance the flow entering the boundary will travel before crossing another boundary or impacting a surface.[17] The expansion diameter is the diameter to which the flow can expand when entering the boundary and is used to determine expansion losses.[17] Table 12 shows the values of the manifold flow split (Man-fs) components of which six were used in conjunction with the ‘InletManifold’ components to define the entire inlet manifold in the model. Volume and surface area were measured and an imposed wall temperature of 350K was used, making the assumption that the value is close to what would be calculated and that the wall temperature has negligible effects on engine performance.

Table 12. Inlet Manifold Flow Split (Man-fs) Component Attributes

Man-fs (FlowSplitGeneral)					
Attribute	Unit	Object Value			
Volume	mm^3	1839124.2			
Surface Area	mm^2	60974.07			
Initial State Name		initial			
Roughness from Material		steel			
Imposed Wall Temperature	K	350			
Link ID Number		1	2	3	4
Angle wrt X-axis (3D)	deg	0	180	70	110
Angle wrt Y-axis (3D)	deg	90	90	90	90
Angle wrt Z-axis (3D)	deg	90	90	20	-20
Characteristic Length	mm	160.7	160.7	101.6	101.6
Expansion Diameter	mm	120.6	120.6	63.5	63.5

Figure 12 is a three-dimensional representation of the Man-fs flow split component. The port location and size are defined by the attributes for ‘Angle wrt ()-axis (3D)’ and ‘Expansion Diameter’ in Table 12. These values were defined to give the closest approximation the manifold design in the Waukesha VGF engine, with the large linear links representing the connections to the manifold segments and the smaller links representing the connections to the inlet runners. The characteristic length and expansion diameter values were obtained through measurements.

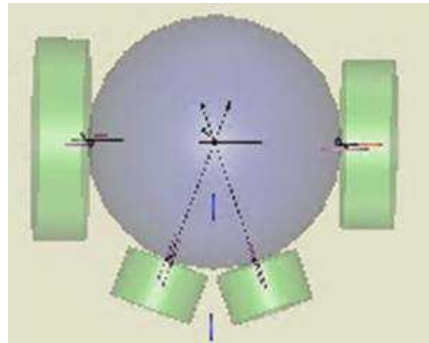


Figure 12. 3D Representation of Man-fs Flow Split

The manifold flow splits connected the various manifold segments to the inlet runners, whose component attributes are shown in Table 13. Once again, the geometric dimensions are based off of measurements of a Waukesha VGF engine. The discretization length was shortened compared to the previous components as this component leads directly to the combustion chamber so more precise calculations were desired. This component has a negative elevation change associated with a bend in the pipe that was found experimentally. The wall temperature was calculated using a sub-model and an initial temperature for the component was designated at 300K; the heat-transfer sub-model is explained with the initial state sub-model in depth in section 3.4 Sub-Models.

The next component in the model is the inlet valve into the combustion chamber and was defined using the attributes shown in Table 14. The valve diameter was found experimentally for a Waukesha VGF engine and the valve lash was assumed to be 0.1mm. There were a pair of inlet valves for every cylinder, totaling in 12 inlet valves; the ‘Cam Timing Angle’ was different for each pair of valves and correlates to the individual cycles of the cylinders. The ‘ValveCamConn’ component type includes the

Table 13. Inlet Runner Component Attributes and Values

Inlet (PipeRound)		
Attribute	Unit	Object Value
Diameter at Inlet End	mm	50.8
Diameter at Outlet End	mm	def
Length	mm	12.7
Discretization Length	mm	6.35
Initial State Name		initial
Radius of Bend	mm	8.89
Angle of Bend	deg	45
Pipe Elevation Change	mm	-6.35
Wall Temperature Solver Object		heat
Initial Wall Temperature	K	300

Table 14. Inlet Valve Component Attributes and Values

Intvalve(ValveCamConn)		
Attribute	Unit	Object Value
Valve Reference Diameter	mm	41.28
Discharge Coefficient Reference Area Definition		constant
Valve Lash	mm	0.1
Cam Timing Angle	Cam Angle	210
Cam Timing Anchor Reference		TDCFiring
Cam Timing Lift Array Reference		Theta=0
Flow Area Multiplier		1
Number of Identical Holes		1
Angle Multiplier		1
Lift Multiplier		1
Swirl Coefficient Multiplier		def
Tumble Coefficient Multiplier		def
Dwell at Maximum Lift	Cam Angle	ign

option to use attribute ‘multipliers’ for things such as angle, lift, flow, swirl, and tumble. These multipliers are multiplied with the attribute properties they correlate to but are set to one (no affect) for the six-cylinder model. In the deactivated-cylinder model these multipliers are used to permanently shut

the valves by changing the lift and flow area multipliers to zero. The inlet and exhaust valves all have the same dimension and attributes, but different cam timing angles.

3.3.5 Defining the Cylinder and Valve Components

The cylinder is completely defined by sub-models that are discussed in section 3.4 Sub-Models.

Table 15 shows the cylinder attributes defined by sub-models, namely the initial state, the wall temperature object, the heat transfer object, and the combustion object.

Table 15. Cylinder (EngCylinder) Component Attributes

Cylinder (EngCylinder)		
Attribute	Unit	Object Value
Initial State Object		cylinderinitial
Wall Temperature defined by Reference Object		twall
Heat Transfer Object		htr
Combustion Object		comb

3.3.6 Defining the Exhaust Pipe Flow Components

The exhaust valve was geometrically identical to the inlet valve in Table 14. Following the exhaust valve is the exhaust port, of which the attributes are shown in Table 16. The diameters and length were measured and a small value was selected for discretization length as the exhaust port is one of the most analyzed components in this report so a high level of accuracy was desired. The roughness was selected to be light-rusted steel as because a buildup of exhaust particles were seen in the exhaust ports of the Waukesha VGF engine, the light rusted steel should provide a close approximation.

The exhaust runner leads from the exhaust port to the exhaust manifold, and is unique in the model because the component is a rectangular pipe (PipeRectangle). Once again the geometric dimensions were measured in a Waukesha VGF engine and a small discretization length was chosen to provide more accurate results in the exhaust flow solver. The material roughness was assumed to be that of steel, which is a good assumption, and sub-models were used to define the wall temperature solver as well as the initial state. All of these attributes can be seen in Table 17.

Table 16. Exhaust Port (PipeRound) Component Attributes

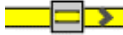
Exhport (PipeRound)		
		exhport-2
Attribute	Unit	Object Value
Diameter at Inlet End	mm	57.404
Diameter at Outlet End	mm	57.404
Length	mm	12.7
Discretization Length	mm	2.54
Initial State Name		initial
Radius of Bend	mm	ign
Angle of Bend	deg	ign
Pipe Elevation Change	mm	ign
Roughness from Material		light_rust_steel
Wall Temperature Solver Object		heat
Initial Wall Temperature	K	350

Table 17. Exhaust Runner (PipeRectangle) Component Attributes

ExhaustRunner (PipeRectangle)		
		exhaustrunner r-1
Attribute	Unit	Object Value
Height at Inlet End	mm	50.8
Width at Inlet End	mm	50.8
Height at Outlet End	mm	50.8
Width at Outlet End	mm	50.8
Length	mm	25.4
Discretization Length	mm	3
Initial State Name		initial
Roughness from Material		steel
Wall Temperature Solver Object		heat
Initial Wall Temperature	K	350

In the Waukesha VGF engine, the two exhaust runners for an individual cylinder combine prior to entering the exhaust manifold; this was mimicked in the model using a ‘FlowSplitGeneral’ component shown in Table 18. The volume was measured and ‘def’ was used to define the surface area, which means GT-Power calculates the surface area using the connecting orifices and assuming a cylindrical flow split.[17] The links were defined as closely to a Waukesha VGF engine as possible with the expansion

diameter's and characteristic length's found through measurements and the angles defined within reasonable values what was seen on the engine. Figure 13 is a three dimensional representation of what the exhaust runner combining flow split looks like to the GT-Power model with the two angular orifices on the left side of the figure representing the two exhaust runners from the cylinder (links one and two) and the orifice on the right representing the connection to the pipe leading to the exhaust manifold. The same heat transfer sub-model was used for this component as in the other flow piping on the exhaust side of the engine. In total there were six "RunnerMix" components used to consolidate the twelve 'ExhaustRunner' runner components.

Table 18. RunnerMix (FlowSplitGeneral) Component Attributes

RunnerMix (FlowSplitGeneral)				
Attribute	Unit	Object Value		
Volume	mm ³	245806.5		
Surface Area	mm ²	def		
Initial State Name		initial		
Roughness from Material		steel		
Wall Temperature Solver Object		Heat		
Initial Wall Temperature	K	400		
Link ID Number		1	2	3
Angle wrt X-axis (3D)	deg	-30	30	180
Angle wrt Y-axis (3D)	deg	90	90	90
Angle wrt Z-axis (3D)	deg	120	60	90
Characteristic Length	mm	63.5	63.5	63.5
Expansion Diameter	mm	76.2	76.2	76.2

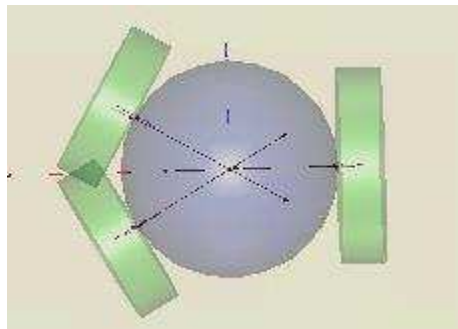


Figure 13. 3D Representation of RunnerMix (FlowSplitGeneral) Component

The component that was varied for analysis of exhaust runner modifications in section 4.3.2 Results of Exhaust Runner Variation is the ‘ExhaustManifoldRunner’ shown in Table 19. This component connects the ‘RunnerMix’ component to the exhaust manifold. The geometric values were measured in a Waukesha VGF engine, major attributes worth noting are that the pipe has an elevation change as the exhaust manifold is slightly raised above the cylinder exhaust ports. A small discretization length was chosen to provide a higher level of detail in the analysis of this component in GT-Power and the material roughness was assumed to be that of steel.

Table 19. Exhaust Manifold Runner (PipeRectangle) Component Attributes

ExhaustManifoldRunner (PipeRectangle)	 Exhaust Manifold Runner-1	
Attribute	Unit	Object Value
Height at Inlet End	mm	76.2
Width at Inlet End	mm	50.8
Height at Outlet End	mm	76.2
Width at Outlet End	mm	50.8
Length	mm	127
Discretization Length	mm	6
Roughness from Material		steel
Radius of Bend Across Height	mm	76.2
Radius of Bend Across Width	mm	ign
Angle of Bend	deg	90
Pipe Elevation Change	mm	50.8
Wall Temperature Solver Object		heat
Initial Wall Temperature	K	400

The exhaust manifold was split into two major components, a round pipe component that modeled the actual manifold, and a flow split that connected the manifold pipes to each other and to the exhaust manifold runners. Table 20 shows the attributes for the flow split component in the exhaust manifold, ‘Exh_Man_Split.’ The manifold split was modeled using a ‘FlowSplitTRight’ component that is shown in Figure 14, where the collinear links are to connect exhaust manifold segments and the perpendicular link is used to connect the exhaust runners to the exhaust manifold. The geometric

Table 20. Exhaust Manifold Flow Split (FlowSplitTRight) Component Attributes

Exh_Man_Split (FlowSplitTRight)		
Attribute	Unit	Object Value
Diameter	mm	88.9
Length	mm	50.8
Surface Area	mm ²	def
Roughness from Material		steel
Wall Temperature Solver Object		heat
Initial Wall Temperature	K	400

properties were measured in a Waukesha VGF engine for the entire model and then split into eleven sub-volumes; six flow splits and five round pipes. The material roughness was assumed to be that of a steel and the “heat” sub-model was used to model the heat transfer to the walls of the exhaust manifold.

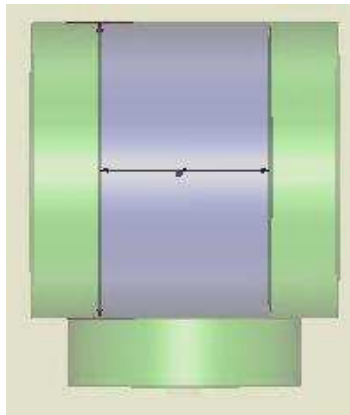
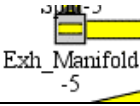


Figure 14. 3D Representation of Exhaust Manifold flow Split

Table 21 shows the attributes for the ‘Exh_Manifold’ component that is used in conjunction with the ‘Exh_Man_Split’ component in the model to simulate the exhaust manifold of a Waukesha VGF engine. As previously mentioned, the geometric attributes were measured and divided into the multiple segments of the exhaust manifold in the model. A small discretization length was chosen to provide a higher level of detail in the analysis of this component. This component was varied in section 4.2.1 Manifold Volume Variation in order to analyze the effect of manifold volume variation on engine performance and pressure wave dynamics in the exhaust ports of the engine. The major attributes varied

in this analysis were the diameters at the inlet and outlet of each section as well as the segment lengths. When these values were varied, it affected every segment, not just one. The material roughness was assumed to be that of steel and the ‘heat’ sub-model was used to model the heat transfer to and from the walls of the pipe. There are a total of five ‘Exh_Manifold’ component segments used to model the entire exhaust manifold of a Waukesha VGF engine.

Table 21. Exhaust Manifold (PipeRound) Component Attributes



Exh_Manifold (PipeRound)		
Attribute	Unit	Object Value
Diameter at Inlet End	mm	88.9
Diameter at Outlet End	mm	def
Length	mm	243.8
Discretization Length	mm	6
Roughness from Material		steel
Wall Temperature Solver Object		heat
Initial Wall Temperature	K	400

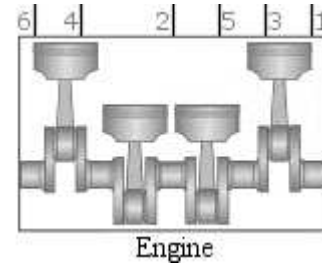
3.3.7 Defining the Engine and Crank Components

The largest component in the GT- Power model is the engine crank train component shown in Table 22. The ‘EngineCrankTrain’ object is used to model the kinematics and rigid dynamics of internal combustion engine crank trains. The rigid-dynamic model translates phased pressure forces acting on each piston to torque at crankpins, which are in turn added to produce total engine torque. The engine type dictates that the engine is 4-stroke, so GT-Power defines an engine cycle as 720 degrees instead of a 360 degree cycle seen in 2-stroke engines. The ‘Speed or Load Specification’ was set to speed which indicates the simulation had a prescribed engine speed (1800 RPM) and the corresponding load variation was then calculated. The values specified as “friction”, “inertia”, “initial”, and “VGF-18” are all sub-models that are used to describe the cylinder geometries, cylinder friction, and engine inertial properties that are integrated into the model. The manifold volumetric efficiency reference was set to “ignore” so that an ambient density was referenced; this attribute is only used to determine output values and is not

used during the simulation. The attributes dealing with percent load were also ignored, as this wasn't of major interest in the simulation and ignoring them was able to save time during simulation.

Table 22. Engine (EngineCrankTrain) Component Attributes

Engine (EngineCrankTrain)							
Attribute	Unit	Object Value					
Engine Type		4-stroke					
Speed or Load Specification		speed					
Engine Speed	RPM	1800					
Engine Friction Object or FMEP		friction					
Start of Cycle (CA at IVC)	deg	-73					
Cylinder Geometry Object		VGf-18					
Crank-Slider Inertia Object		Inertia					
Cylinder Number		1	4	2	6	3	5
Firing Intervals	deg	0	60	60	60	60	60
Reference State for Volumetric Efficiency		initial					
Part Name for Manifold Volumetric Eff. Reference		ign					
RLT for Percent Load Calculation		ign					
100% Load Table Name		ign					
Actuated Nominal Stroke Convention (EngCylGeomUser only)		Dynamic					



3.4 Sub-Models

In order to fully-define the GT-Power model, sub-models were required to define energy processes such as heat transfer, combustion, and friction as well as component geometries and fluid properties. While some of the values could be solved analytically, many had to be solved iteratively using the optimization tool in GT-Power. In addition to this, multiple assumptions were made to simplify the model further.

In order to define the combustion process, a sub-model was created to simulate spark-ignited combustion using a Wiebe function which approximates a “typical” shape of an SI burn rate. The sub-model was called “comb” and the values used for the model are listed in Table 23. Anchor Angle, Duration, and Wiebe Exponent were all solved for iteratively to produce a pressure trace similar to the.

Table 23. Combustion Sub-Model Attributes

Comb (Combustion Sub-Model)		
Attribute	Unit	Object Value
Anchor Angle (def = 50% burn)		10
Duration (def = 10% to 90%)		25
Wiebe Exponent		7
Number of Temperature Zones		two-temp
Fraction of Fuel Burned	fraction	0.97
Air Burning Enhancement Factor	fraction	1
Burned Fuel % at Anchor Angle	%	def
Burned Fuel % at Duration Start	%	def
Burned Fuel % at Duration End	%	def

pressure trace found for a Waukesha VGF-18 engine experimentally. The specific calculations used by GT-Power are shown in section 1.2.3 GT-Power

A sub-model was required to define the geometry of the piston-cylinder assembly. Table 24 shows the sub-model “Waukesha VGF-18” and the attribute values defining the sub-model. Every value in this table was defined by the manufacturer so the only assumption made is that the manufacturing was accurate and that there is negligible deviation from these values experimentally.

The friction in the engine was modeled with the sub-model “EngineFriction” defined in Table 25. Most of the values entered into this sub-model were found experimentally for a Waukesha VGF-18 engine. The ‘Main Bearing Diameter’ and “Connecting Rod Large End Bearing Diameter” were found from manufacturer specification sheets.

Table 24. Engine Cylinder Geometry Sub-Model Attributes

Waukesha VGF-18 (Cylinder Geometry Sub-Model)		
Attribute	Unit	Object Value
Bore	mm	152
Stroke	mm	165.1
Connecting Rod Length	mm	310
Compression Ratio		11.6
TDC Clearance Height	mm	0.380

Table 25. Engine Friction Sub-Model Attributes

EngineFriction (Engine Friction Sub-Model)		
Attribute	Unit	Object Value
Stroke	mm	def
Main Bearing Diameter	mm	67
Connecting Rod Large End Bearing Diameter	mm	121
Oil Temperature	K	352.5
Coolant Temperature	K	308.15
Cylinder Wall Temperature		Cylinder
Engine Speed Upon Entering Friction Transition Band	RPM	def
Reference FMEP	kPa	197
Reference BMEP	kPa	1107
Reference Engine Speed	RPM	[RPM]
Reference Oil Temperature	K	352.0
Reference Coolant Temperature	K	285.4
Reference Cylinder Wall Temperature	K	924.1

Heat transfer in the cylinder was defined in GT-Power using a Woschni correlation without swirl. This method accounts for the changing heat transfer coefficients during the period when the valves are open and heat transfer is increased by inflow velocities through the intake valves and also by backflow through the exhaust valves. This method is recommended in the GT-Power manuals for when swirl data is not available. Table 26 displays the attributes for the heat transfer sub-model “HTR”, where the Head/Bore Area Ratio was calculated and every other attribute was held at the base defined value.

Table 26. In-Cylinder Heat Transfer Sub-Model Attributes

HTR (In-Cylinder Heat Transfer Sub-Model)		
Attribute	Unit	Object Value
Heat Transfer Model		WoschniGT
Overall Convection Multiplier		1
Head/Bore Area Ratio		1.15
Piston/Bore Area Ratio		1
Radiation Multiplier		ign
Convection Temperature Evaluation		quadratic
Low Speed Heat Transfer Enhancement for Woschni* Models		on

The previous sub-model dealt with heat transfer within and out of the cylinder, but in order to fully define the cylinder a separate sub-model was needed to define the wall temperatures of the cylinder head, cylinder wall, and piston. In order to save on computational time, these values were assumed to be constant and the chosen values are shown in Table 27. These values are approximations based on coolant and lube oil temperatures plus offsets.

Table 27. Cylinder Wall Temperature Sub-Model

T_{wall}		
Attribute	Unit	Object Value
Head Temperature	K	550
Piston Temperature	K	590
Cylinder Temperature	K	450

Heat transfer from the flow pipes was solved using a different heat transfer sub-model than for the in-cylinder calculations. Table 28 shows the attributes for the flow-pipe heat transfer sub-model “heat.” This sub-model accounts for convection and radiation from the flow components to the environment. The values entered correlate to an engine in a room-temperature environment with a convection coefficient typical for free convection of air. The emissivity is that of a surface without shine and for conduction from the flow to the environment, the pipes were assumed to have a uniform thickness of about 3mm (1/8 of an inch) and to be made of steel.

Table 28. Flow Pipe Heat Transfer Sub-Model Attributes

Heat (Flow Pipe Heat Transfer Sub-Model)		
Attribute	Unit	Object Value
External Convection Temperature	K	300
External Convection Coefficient	W/(m ² -K)	15
External Radiation Sink Temperature	K	300
Surface Emissivity		0.8
Layer Thickness	mm	3
Layer Material Object		steel

Air and fuel injection had sub-models defining the chemical properties of the gasses they were injecting. Table 29 shows the attributes for fuel injection sub-model “methane” which describes the

chemical properties of the methane. The lower heating value is defined as the enthalpy of the substance minus the enthalpy of its complete combustion products both being evaluated at 298K. The coefficients are used to solve for the enthalpy of the vapor. The following equation is used for calculating the enthalpy in J/kg:

$$h = h_{ref} + \sum_{n=1}^5 a_n(T - T_{ref})^n = h_{ref} + a_1(T - T_{ref}) + \dots + a_5(T - T_{ref})^5$$

Table 29. Methane Sub-Model Attributes

Methane (fuel injection sub-model)		
Attribute	Unit	Object Value
Molecular Weight		ign
Carbon Atoms per Molecule		1
Hydrogen Atoms per Molecule		4
Lower Heating Value	J/kg	5.00E+07
Critical Temperature	K	190.4
Critical Pressure	bar	46
Absolute Entropy at 298K	J/kg-K	11618
(T-Tref) Coefficient, a1		2241
(T-Tref)^2 Coefficient, a2		1.219
(T-Tref)^3 Coefficient, a3		0.00173
(T-Tref)^4 Coefficient, a4		-2.17E-06
(T-Tref)^5 Coefficient, a5		7.90E-10

Oxygen and Nitrogen were injected into the engine using the “Air” sub-model shown in Table 30. Table 31 and Table 32 show the molecular properties defined for Nitrogen and Oxygen. The attributes are defined in the same manner as methane in the above table, with the coefficients used for solving enthalpy and the other attributes defining the molecular structure.

Table 30. Air Injection Sub-Model Attributes

Air (Air Injection Sub-Model)		
Attribute	Unit	Object Value
n2-vap	fraction	0.767
o2-vap	fraction	0.233

Table 31. Oxygen Molecular Properties Sub-Model Attributes

O2 (Oxygen Molecular Properties Sub-Model)		
Attribute	Unit	Object Value
Molecular Weight		ign
Oxygen Atoms per Molecule		2
Lower Heating Value	J/kg	0
Critical Temperature	K	154
Critical Pressure	bar	50.5
Absolute Entropy at 298K	J/kg-K	6411
(T-Tref) Coefficient, a1		918.7
(T-Tref) ² Coefficient, a2		0.174
(T-Tref) ³ Coefficient, a3		-6.83E-05
(T-Tref) ⁴ Coefficient, a4		1.68E-08
(T-Tref) ⁵ Coefficient, a5		-1.68E-12

The final sub-models used define the initial states that GT-Power uses as initial values for simulation. Table 33 shows the attributes for the initial fluid state sub-model “initial.” The values used in this sub-model define the altitude of Colorado, United States where the experimental data was gathered. A resting temperature and pressure were chosen so the simulation begins as though an engine was just being started, this method increases total run-time as the simulation runs until a steady state is achieved.

Table 32. Nitrogen Sub-Model Attributes

N2 (Nitrogen Molecular Properties Sub-Models)		
Attribute	Unit	Object Value
Molecular Weight		ign
Nitrogen Atoms per Molecule		2
Lower Heating Value	J/kg	0
Critical Temperature	K	126
Critical Pressure	bar	33.9
Absolute Entropy at 298K	J/kg-K	6838
(T-Tref) Coefficient, a1		1036
(T-Tref) ² Coefficient, a2		0.058
(T-Tref) ³ Coefficient, a3		5.43E-05
(T-Tref) ⁴ Coefficient, a4		-3.14E-08
(T-Tref) ⁵ Coefficient, a5		4.79E-12

Table 33. Initial Fluid State Sub-Model Attributes

initial		
Attribute	Unit	Object Value
Pressure (Absolute)	kPa	100
Temperature	K	300
Composition		air
Altitude	m	1524
Reference Altitude	m	0
Altitude Correction For...		PresAndTemp

3.5 Six-Cylinder Validation

In order to validate the model, experimental data collected for a Waukesha VGF engine by Kristopher Quillen for completion of his Master’s Thesis at Colorado State University was compared to data collected by running the GT-Power simulation.[20] There were multiple metrics used for validation including combustion, general engine parameters, manifold pressures, fuel flow, and temperature. Table 34 through Table 38 show all of the data used for validation of the model. A T-Test and an F-Test were used as validation metrics, a T-Test examines the difference in means between two samples and an F-Test compares variances.[19] The resulting values representing the confidence level of the predicted results of

Table 34. Six-Cylinder Model Validation at 60% Load with F-Test Values

Data Point	Waukesha VGF-18	GT-Power
Engine Load %	60.00	60.00
General Parameters		
Speed [RPM]	1800	1800
Torque [Nm]	955.1	955.1
Power [bkW]	180.0	180.0
BMEP [kPa]	666.8	667.7
IMEP [kPa]	891.0	902.9
NMEP [kPa]	811.4	829.0
PMEP [kPa]	-79.66	-73.85
FMEP [kPa]	142.4	136.7
Mechanical Efficiency	0.7483	0.7395
Mass Flow A/F	21.55	20.95
	F-test Score	0.993

Table 35. Six-Cylinder Model Validation at 70% Load with F-Test Values

Data Point	Waukesha VGF-18	GT-Power
Engine Load %	70.00	70.00
General Parameters		
Speed [RPM]	1800	1800
Torque [Nm]	1108	1266
Power [bkW]	208.8	238.6
BMEP [kPa]	773.3	800.0
IMEP [kPa]	999.2	985.1
NMEP [kPa]	919.2	903.1
PMEP [kPa]	-79.99	-81.99
FMEP [kPa]	143.4	140.0
Mechanical Efficiency	0.7739	0.8121
Mass Flow A/F	21.57	20.97
	F-test Score	0.944
	T-test Score	0.9502

Table 36. Six-Cylinder Model Validation at 80% Load with T-Test Values

Data Point	Waukesha VGF-18	GT-Power
Engine Load %	80.00	80.00
General Parameters		
Speed [RPM]	1800	1800
Torque [Nm]	1266	1266
Power [bkW]	238.8	238.6
BMEP [kPa]	884.2	885.1
IMEP [kPa]	1109	1026
NMEP [kPa]	1028	944.7
PMEP [kPa]	-81.08	-81.55
FMEP [kPa]	140.9	141.2
Mechanical Efficiency	0.7972	0.8624
Mass Flow A/F	21.64	20.99
	F-test Score	0.956
	T-test Score	0.9551

Table 37. Six-Cylinder Model Validation at 90% Load with T-Test Values

Data Point	Waukesha VGF-18	GT-Power
Engine Load %	90.00	90.00
General Parameters		
Speed [RPM]	1800	1800
Torque [Nm]	1424	1423
Power [bkW]	268.1	268.2
BMEP [kPa]	993.8	994.8
IMEP [kPa]	1219	1133
NMEP [kPa]	1135	1040
PMEP [kPa]	-83.32	-93.11
FMEP [kPa]	138.3	138.7
Mechanical Efficiency	0.8155	0.8776
Mass Flow A/F	21.64	20.95
	F-test Score	0.955
	T-test Score	0.951

Table 38. Six-Cylinder Model Validation at 100% Load with T-Test Values and Total T-Test Value for All Loads

Data Point	Waukesha VGF-18	GT-Power
Engine Load %	100.0	100.0
General Parameters		
Speed [RPM]	1800	1800
Torque [Nm]	1581	1581
Power [bkW]	298.0	298.0
BMEP [kPa]	1104	1105
IMEP [kPa]	1326	1242
NMEP [kPa]	1244	1160
PMEP [kPa]	-81.39	-81.55
FMEP [kPa]	136.7	136.7
Mechanical Efficiency	0.8329	0.8900
Mass Flow A/F	21.66	20.99
	F-test Score	0.955
	T-test Score	0.959
	Total T-Test Score	96.15%
	Total F-Test	96.06%

GT-Power being accurate, with “1” being 100% confident and “0” being not at all confident. The general engine parameters and fuel flow metrics both scored above 95% confidence, indicating that the model was extremely well suited for predicting these values.

Based off of the verification accuracy and the T-Test values shown in the previous table, it is recommended that the values found in this model not be used for exact prediction but rather for understanding general trends. This model is acceptable for testing new components and having a general understanding for engine response to modification.

Chapter 4- Pressure Analysis and Mitigation Techniques

4.1 Objective

One of the objectives of this research was to analyze the exhaust pressure dynamics of an internal combustion engine under various circumstances as well examine various techniques for pressure mitigation in the exhaust system. It is known that exhaust pressure effects volumetric efficiency, in-cylinder pressure, and emissions but it is the aim of this section to create relationships between pressure in the exhaust system of an engine and the engines exhaust hardware dimensions. The focus of hardware variations was on the length and diameter of the exhaust manifold and exhaust runners and how the pressure in the exhaust ports is affected.

4.2 Design and Parametric Variations

The fully-operational engine model was used to simulate the effects of parametric variations (changing hardware dimensions) on the engine operation. This is because the fully-operational model has been verified and validated with very little prediction involved. The fully-operational engine model is more representative of typical engine operation so the results from the simulations using this model are more widely applicable. The single-cylinder model is more specialized making the simulations on this model focused more on pressure mitigation to improve the accuracy of single cylinder engine research.

4.2.1 Manifold Volume Variation

The first component varied and analyzed was the exhaust manifold volume. The exhaust manifold volume is the largest enclosed volume on the exhaust side of the combustion chamber and is where the majority of the pressure is dissipated.[21] While the pressure amplitudes decrease when a pulsation enters the manifold these pressure pulsations travel through the manifold and affect the pressure inside other exhaust ports. It was hypothesized that by increasing the volume of the exhaust manifold a decrease in the total pressure as well as the pressure pulsation transmission would be seen. In order to modify the manifold volume, the GT-Power ability to run multiple cases side-by-side was utilized, as illustrated in

Table 39. The manifold geometry for the Waukesha engine that the model was validated with is in the shape of a cylinder, and this was mimicked in the model. The defined manifold parameters for length and diameter were changed to give differing values for total volume but the ratio between length and diameter was held constant in five of the cases so that the general shape of the manifold remained constant.

Table 39. Exhaust manifold variation input values.

Modified Geometry	OG (Original)	1/2 Manifold Volume	2x Manifold Volume	4x Manifold Volume	8x Manifold Volume	Small Aspect Ratio
Manifold Diameter [m]	0.089	0.075	0.106	0.126	0.150	0.203
Manifold Segment Length [m]	0.244	0.172	0.345	0.488	0.690	0.254
Total Manifold Volume [m³]	0.008	0.004	0.015	0.030	0.061	0.041

4.2.2 Exhaust Runner Modification

The exhaust runner connects the exhaust ports to the exhaust manifold. Pressure waves in the exhaust manifold are extremely important because they directly affect the pressure seen by the exhaust valves.[21] Typically the exhaust runners are sized so that the traveling pressure wave released by the exhaust valve will reflect back from the exhaust manifold in the form of rarefaction waves and cause a low-pressure system outside of the exhaust valve during the exhaust stroke.[22] [23] Runner tuning only works when the engine is run at a constant RPM, but there are currently efforts to create a variable-length runner so that the runner length can be modified during engine operation to have the best results at varying engine speeds.[24]

An analysis of how runner length affects the operation of a full six-cylinder engine was made using GT-Power. The exhaust runners for the Waukesha VGF engine have rectangular cross sections so there were three independent variables that were modified during the simulation; runner width, runner height, and runner length. Several different methods of variation were simulated with length and cross-

Table 40. Exhaust runner variation input values

Modified Geometry	OG (Original)	20x Runner Length	2x Runner Length	10x Runner Length	2x C.S. Area	10x C.S. Area	100x Total Volume
Exhaust Runner Width [m]	0.051	0.051	0.051	0.051	0.076	0.152	0.152
Exhaust Runner Height [m]	0.076	0.076	0.076	0.076	0.102	0.254	0.254
Exhaust Runner Length [m]	0.152	3.048	0.305	1.524	0.152	0.152	1.524
Total Volume [m³]	5.90E-04	1.18E-02	1.18E-03	5.90E-03	1.18E-03	5.90E-03	5.90E-02

sectional area being of the main focus; a test case was simulated with an extremely large total volume 100 times the original volume, shown in Table 40.

4.3 Results of Exhaust Manifold and Runner Variations

The hypothesis that increasing the volume of exhaust system components would decrease the average pressure amplitudes in the exhaust port was shown to be accurate, but the magnitude of the effects were shown to be relatively small. It was seen that for any noticeable change in results to be made, large dimensional variations in either the manifold or runners were required. Another trend was noticed, when the exhaust system component aspect ratio between length and cross-sectional area was held constant and only the total volume changed, there was very little effect on the average pressure amplitude seen at the exhaust ports. Whereas when the aspect ratio between length and cross-sectional area of the components were modified, more drastic changes were observed. These trends are analyzed and presented in the following sections.

4.3.1 Results of Exhaust Manifold Variation

Figure 15 shows the traveling pressure waves seen in the exhaust port of cylinder 1 during normal operation with the original (e.g. OG) manifold design. Prior to the expulsion of exhaust gas from the cylinder the pressure wave has amplitude of 40 kPa, then following the exhaust the peak pressure raises from approximately 250.4 kPa to only 252.7 kPa, which is not a large increase compared to the magnitude of the forward traveling pressure wave, which reaches a peak pressure of just over 266.8 kPa. The figure

shows a rarefaction wave that has an opposite magnitude to the forward traveling wave, which results in deconstructive interference of pressure waves immediately after the expulsion of exhaust gasses, and constructive interference before and after the exhaust event. It can be speculated that the exhaust flow components were designed so that deconstructive interference would occur during exhaust gas expulsion, resulting in lower total pressure amplitudes. Table 41 displays the effects engine manifold variation has on engine performance. It is noted that there is a correlation between engine performance and manifold size, as shown in Figure 16, with engine performance increasing with increasing exhaust manifold volume. This result aligns with the increase in volumetric efficiency with increasing manifold volume as well. However, the “small aspect ratio” case where the geometric ratio between diameter and length was modified showed a sharp decrease in engine performance despite having a total volume approximately five times the original manifold.

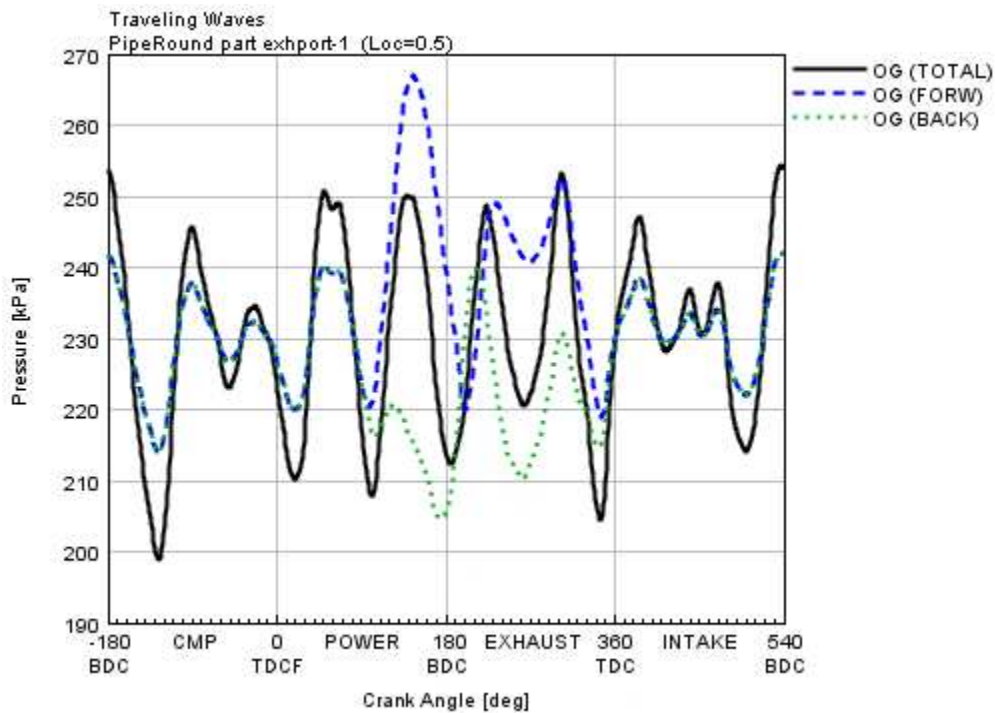


Figure 15. Traveling Pressure Waves in the Exhaust Port of Cylinder 1 for the Original Manifold Design

Table 41. Engine Performance Affected by Exhaust Manifold Variation

Engine Performance Parameters	Units	OG	1/2 Manifold Volume	2x Manifold Volume	4x Manifold Volume	8x Manifold Volume	Small Aspect Ratio
Engine Speed (cycle average)	RPM	1800	1800	1800	1800	1800	1800
Brake Torque	N-m	1580	1569	1601	1607	1615	1590
Brake Power	kW	297.8	295.7	301.8	302.9	304.4	299.6
BSFC - Brake Specific Fuel Consumption, Cyl	g/kW-h	148.2	148.6	148.0	147.9	147.4	148.4
IMEP720 - Net Indicated Mean Effective Pressure	kPa	1287	1279	1302	1306	1312	1294
BMEP - Brake Mean Effective Pressure	kPa	1105	1097	1119	1123	1129	1111
PMEP - Pumping Mean Effective Pressure	kPa	-82.00	-83.59	-80.81	-80.21	-78.32	-82.66
FMEP - Friction Mean Effective Pressure	kPa	182.5	182.4	182.7	182.8	182.8	182.6
Volumetric Efficiency, Air	fraction	0.929	0.925	0.940	0.943	0.944	0.936
Air Flow Rate	kg/h	924.9	920.6	935.7	938.3	939.7	931.8

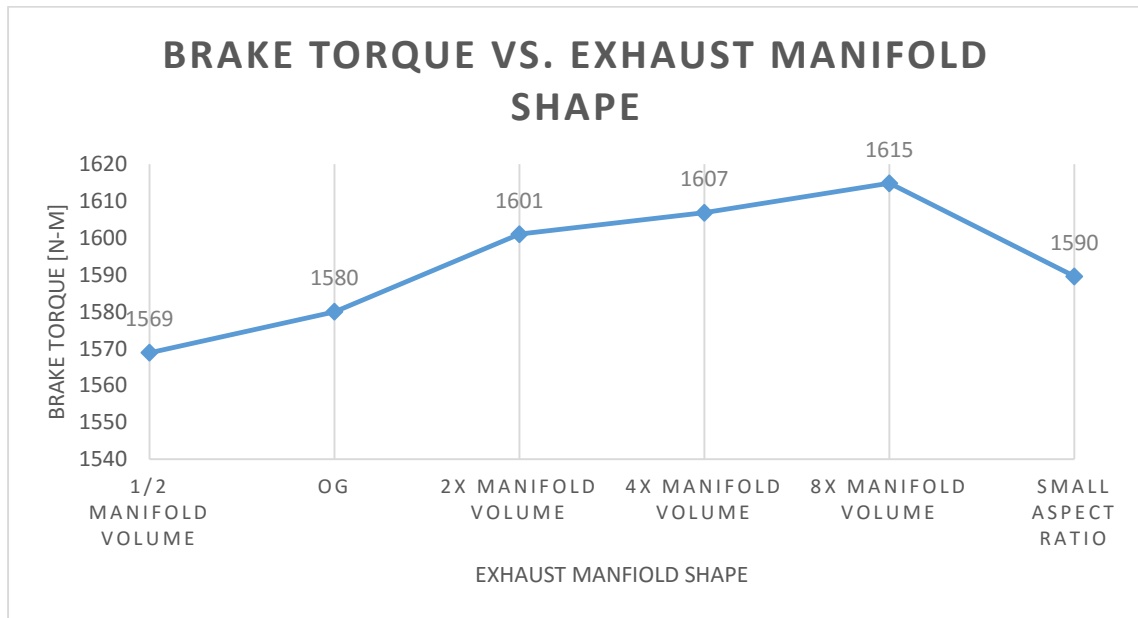


Figure 16. Brake Torque Affected by Exhaust Manifold Geometric Variation

Figure 17 shows the traveling pressure waves in the exhaust port of cylinder 1 but this time the exhaust manifold volume is eight times that of the original volume, with the geometric ratio of length to diameter held constant. The total pressure wave reaches a maximum pressure magnitude of approximately 246 kPa (6 kPa less than the original) and a minimum pressure magnitude of approximately 194 kPa (4 kPa less than the original). The average pressure in the exhaust manifold for this case is 221 kPa which is 7 kPa less than the original. The volumetric efficiency, shown in Table 41, for this case was the highest for any of the manifold volume modification simulations at a value of 0.944, an increase of 0.015 over the original design but only increasing by 0.001 over the manifold four times the original volume.

The next simulation analyzed was case when the length to diameter ratio (e.g. aspect ratio) of the manifold was modified to have shorter length compared to cross-sectional area, the traveling pressure waves for this case are shown in Figure 18. The results of this case displayed a decrease in maximum pressure from approximately 253 kPa in the original manifold to approximately 240 kPa. The forward traveling pressure wave created by the expelling of exhaust gas from the cylinder peaks at a slightly lower

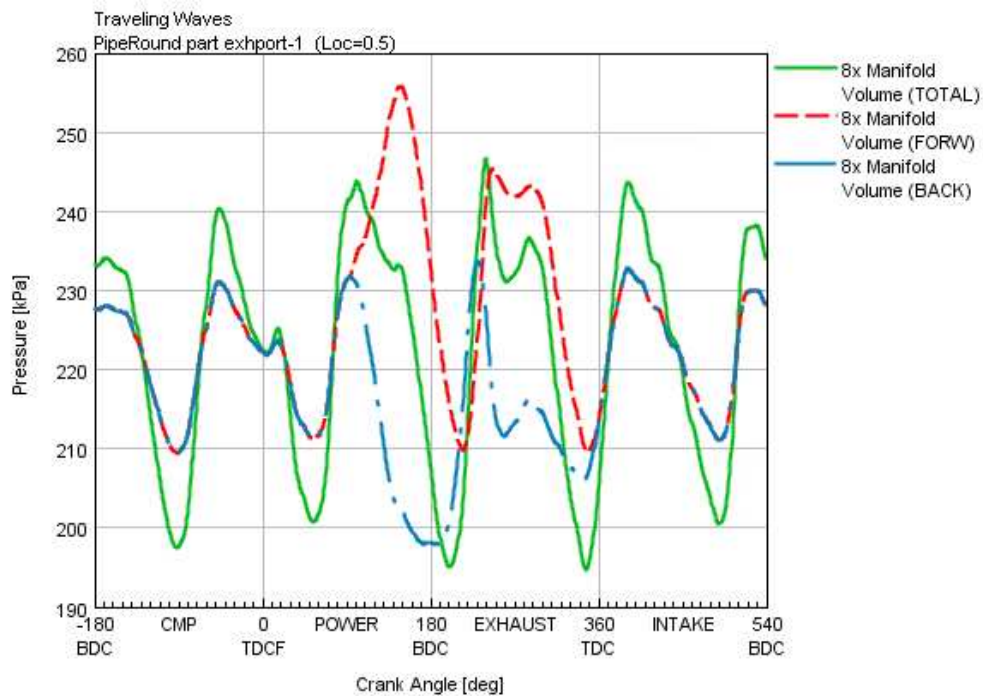


Figure 17. Traveling Pressure Waves in the Exhaust Port with an Exhaust Manifold 8 Times the Original Volume

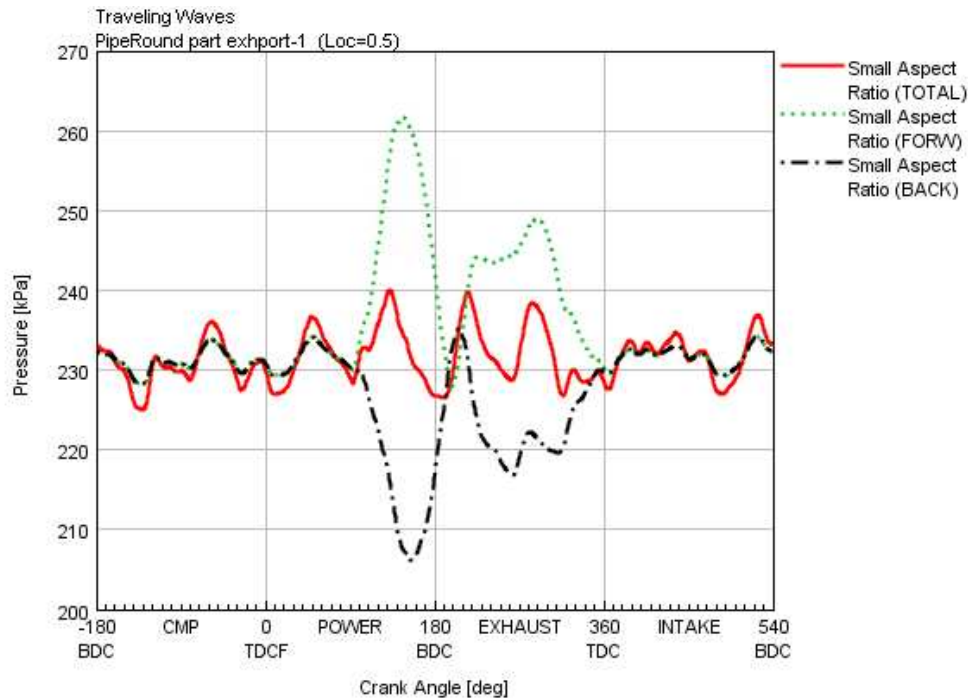


Figure 18. Traveling Pressure Waves in the Exhaust Port of Cylinder 1 for an Exhaust Manifold with a Small Aspect Ratio (Length to C.S. Area)

pressure as well with a magnitude of 262 kPa compared to the 266 kPa of the original design. The average pressure in the exhaust manifold increased from 228 kPa to 231 kPa despite having a volume approximately 5 times larger than the original design. A 10 N-m increase in brake power was also observed. This indicates that exhaust manifold length plays a larger role in exhaust pressure dynamics than diameter or total volume.

4.3.2 Results of Exhaust Runner Variation

Figure 19 is a plot of the total pressure wave seen by the exhaust port of cylinder one during a full cycle for the original exhaust runner design. The maximum total pressure reached during the cycle occurred approximately 40 degrees before the piston reached top dead center (e.g. TDC) after the exhaust stroke and had a value of approximately 254 kPa. The forward traveling pressure wave leaving the cylinder reached a maximum 150 degrees after TDC when combustion occurs and correlates to the expulsion of exhaust gas from the cylinder. The forward traveling pressure wave reached a peak pressure of approximately 266 kPa, roughly 15 kPa higher than the total pressure at that point, but interferes

deconstructively with the backwards traveling pressure caused by a rarefaction wave created when the exhaust runner expands into the exhaust manifold. The total pressure wave reached a minimum 160 degrees before TDC with combustion, when the forward and backwards traveling pressure waves are in sync causing constructive interference, lowering the pressure to approximately 199kPa.

Figure 20 shows the total pressure waves at exhaust port 1 when the exhaust runner length is varied by two times the original length, ten times the original length, and twenty times the original length. The case with an exhaust runner twice the length of the original showed an increase in peak pressure magnitude and reached 258kPa. The two-times runner length case also showed a rise in minimum pressure amplitude from under 200 kPa in the original case to approximately 208kPa, a rise of 8 kPa; this is significant because typically low pressure is ideal for improving volumetric efficiency of an engine. The case for an exhaust runner length ten times the length of the original design resulted in the largest change in peak pressure magnitude, reaching a value of 275 kPa, a net increase of 20 kPa over the original design. The pressure amplitude prior to exhaust gas expulsion from the cylinder was more regular

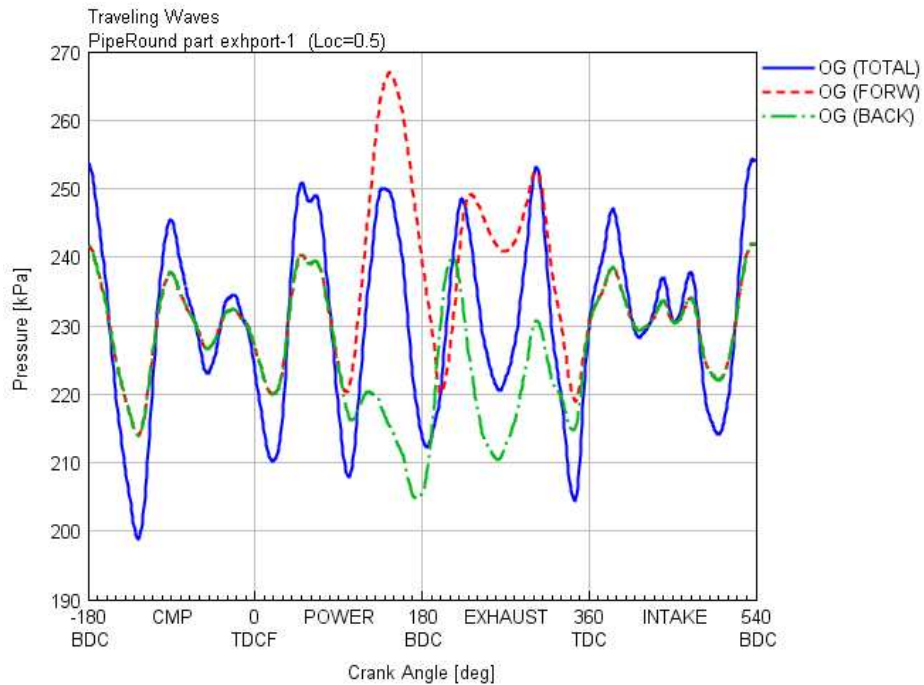


Figure 19. Traveling Pressure Waves in Exhaust Port 1 for the Original Model (OG)

than the original design, and had a lower average pressure of approximately 210 kPa compared to an average of 230 kPa seen in the original design. The minimum pressure reached was approximately 169 kPa, a 30kPa decrease from the original design. The decrease in average pressure at the port as well as total minimum pressure indicates that the ten-times-original-length case should increase volumetric efficiency of the engine. Table 42 shows the engine performance effects of exhaust runner length modification and shows an increase in volumetric efficiency, brake torque, and brake power when the exhaust runner length was increased. When the runner was modified to be twenty times the original length the peak pressure magnitude decreased to approximately 248 kPa, the minimum pressure reduced to approximately 175 kPa and the average pressure reduced to approximately 205 kPa. Table 42 shows that the twenty-time-original-length exhaust runner had the greatest positive effect on engine performance, increasing volumetric efficiency by 0.06, brake power by 30 kW, and IMEP by approximately 110 kPa. The correlation between low pressure on the exhaust side of an engine during the expulsion of exhaust gasses and high engine performance was shown in this simulation.

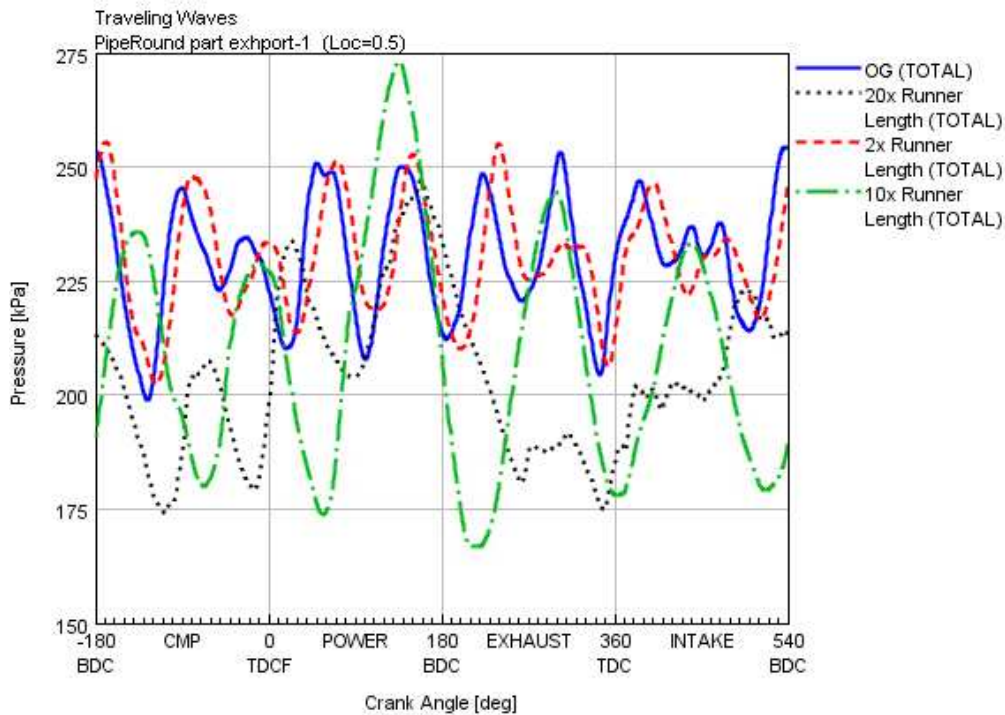


Figure 20. Traveling pressure waves in the exhaust port with varying exhaust runner lengths.

Table 42. Exhaust Runner Length Effect on Engine Performance

Engine Performance Parameters	Units	OG	20x Runner Length	2x Runner Length	10x Runner Length
Engine Speed (cycle average)	RPM	1800	1800	1800	1800
Brake Torque	N-m	1580	1738	1598	1607
Brake Power	kW	297.8	327.6	301.2	303.0
BSFC - Brake Specific Fuel Consumption, Cyl	g/kW-h	148.2	143.4	148.0	146.3
IMEP720 - Net Indicated Mean Effective Pressure	kPa	1287	1399	1300	1306
BMEP - Brake Mean Effective Pressure	kPa	1105	1215	1117	1124
PMEP - Pumping Mean Effective Pressure	kPa	-82.00	-60.35	-80.96	-74.54
FMEP - Friction Mean Effective Pressure	kPa	182.5	183.8	182.7	182.6
Volumetric Efficiency, Air	fraction	0.929	0.989	0.938	0.933
Air Flow Rate	kg/h	924.9	984.6	933.9	928.6

Figure 21 shows the forward traveling pressure waves, the backwards traveling pressure waves, and the total pressure waves seen at the exhaust port of cylinder one for the case with exhaust runner length ten times the original. The figure shows that the forward and backwards traveling pressure waves are interfering constructively to amplify the total pressure wave for almost the entire cycle. The constructive interference results in large pressure amplitudes of approximately 275 kPa at the maximum and 168 kPa at the minimum, which is the largest amplitude of any of the runners simulated. While this runner did show a slight improvement in engine performance, the other two cases showed larger improvements, demonstrating the importance of traveling pressure wave dynamics on engine performance.

When cross-sectional area was varied in the exhaust runner, less of an effect was noticed compared to varying the runner length. Figure 22 shows the total pressure seen in the exhaust port of cylinder one during an engine cycle, it is observed that the peak pressure for when the exhaust runner has a cross-sectional area twice the original size is approximately 3 kPa greater than the original design

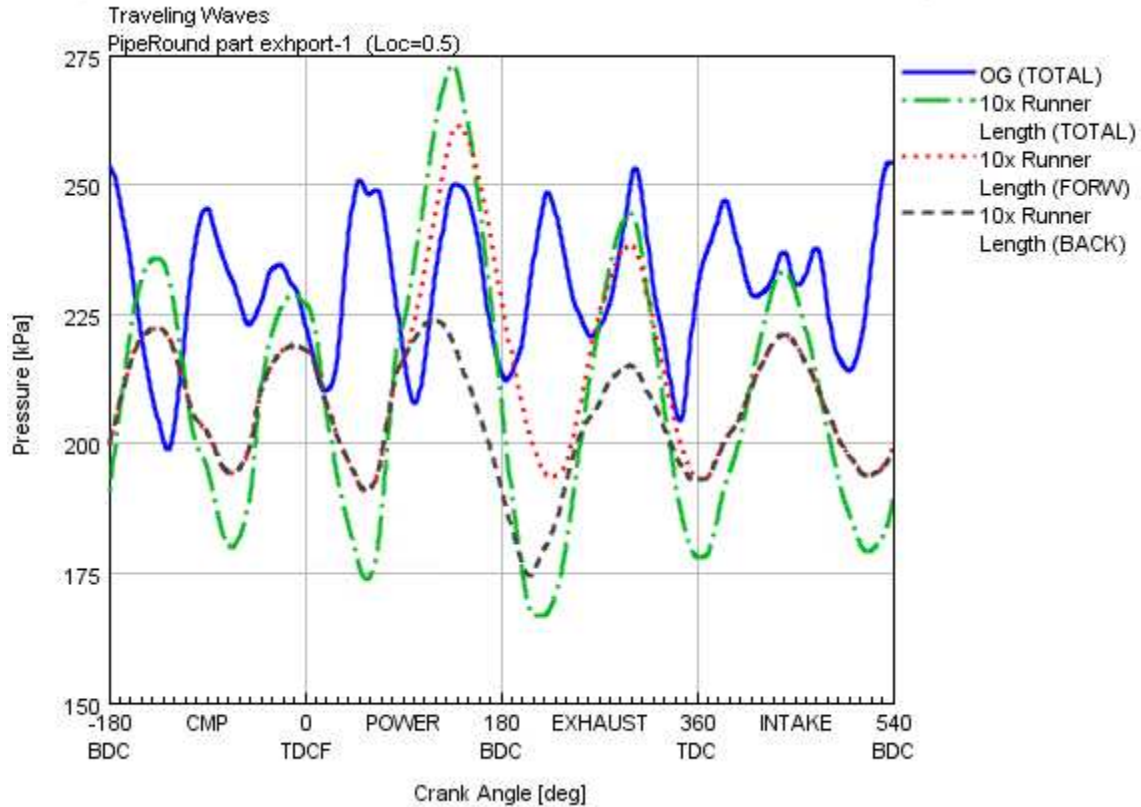


Figure 21. Traveling pressure waves in the exhaust port with an exhaust runner 10x the original length. and reaches a peak pressure magnitude of 257.5 kPa. The case when the exhaust runner cross-sectional area was ten times larger had a dramatic effect on pressure minima and maxima, with a maximum pressure of 244 kPa and a minimum pressure of 219 kPa. However, the average pressure for the ten times cross-sectional area runner case was similar to that of the original case, being about 230 kPa. Table 43 displays the engine performance parameters solved for in GT-Power for the various cases, cross-sectional area had very little effect on engine performance, showing an increase in brake power of only 1.5 kW for the runner with a cross-sectional area twice that of the original runner, and even less of an increase was seen for the ten-time-original-area case. Volumetric efficiency increased slightly with increasing cross-sectional area, but not by a significant amount.

Table 43. Exhaust Runner Cross-Sectional Area Effects on Engine Performance

Engine Performance Parameters	Units	OG	2x C.S. Area	10x C.S. Area
Engine Speed (cycle average)	RPM	1800	1800	1800
Brake Torque	N-m	1580	1588	1587
Brake Power	kW	297.8	299.4	299.1
BSFC - Brake Specific Fuel Consumption, Cyl	g/kW-h	148.2	148.1	148.5
IMEP720 - Net Indicated Mean Effective Pressure	kPa	1287	1293	1292
BMEP - Brake Mean Effective Pressure	kPa	1105	1110	1109
PMEP - Pumping Mean Effective Pressure	kPa	-82.00	-81.67	-82.77
FMEP - Friction Mean Effective Pressure	kPa	182.5	182.6	182.6
Volumetric Efficiency, Air	fraction	0.929	0.934	0.935
Air Flow Rate	kg/h	924.9	929.3	930.5

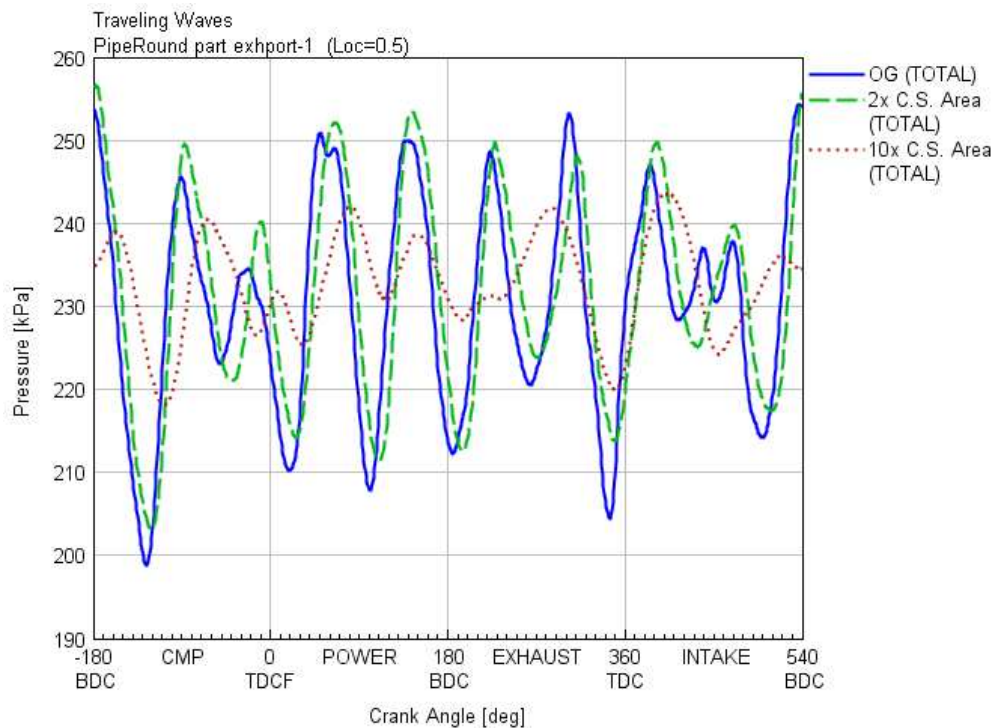


Figure 22. Traveling pressure waves in the exhaust port with an exhaust runner with varying cross sectional areas.

The simulation for the exhaust runner with a cross-sectional area ten times that of the original design was analyzed further because it showed the largest difference from the original design. Figure 23 plots the forward traveling pressure waves (relative to the flow of gas), the backwards traveling pressure waves, and the total pressure waves observed at the exhaust port of cylinder one over an engine cycle. The peak to peak pressure amplitude prior to expulsion of exhaust gas from the cylinder is small with amplitudes of approximately 20 kPa with a peak pressure magnitude of 241 kPa. Prior to the expulsion of exhaust gas the forward and backwards traveling waves are interfering constructively. When the exhaust gas is expelled from the cylinder, the forward traveling pressure wave reaches a peak magnitude of 264 kPa but interferes in a deconstructive manner with the backwards traveling pressure wave that dips to a magnitude of only 211 kPa resulting in a total pressure of only 238 kPa.

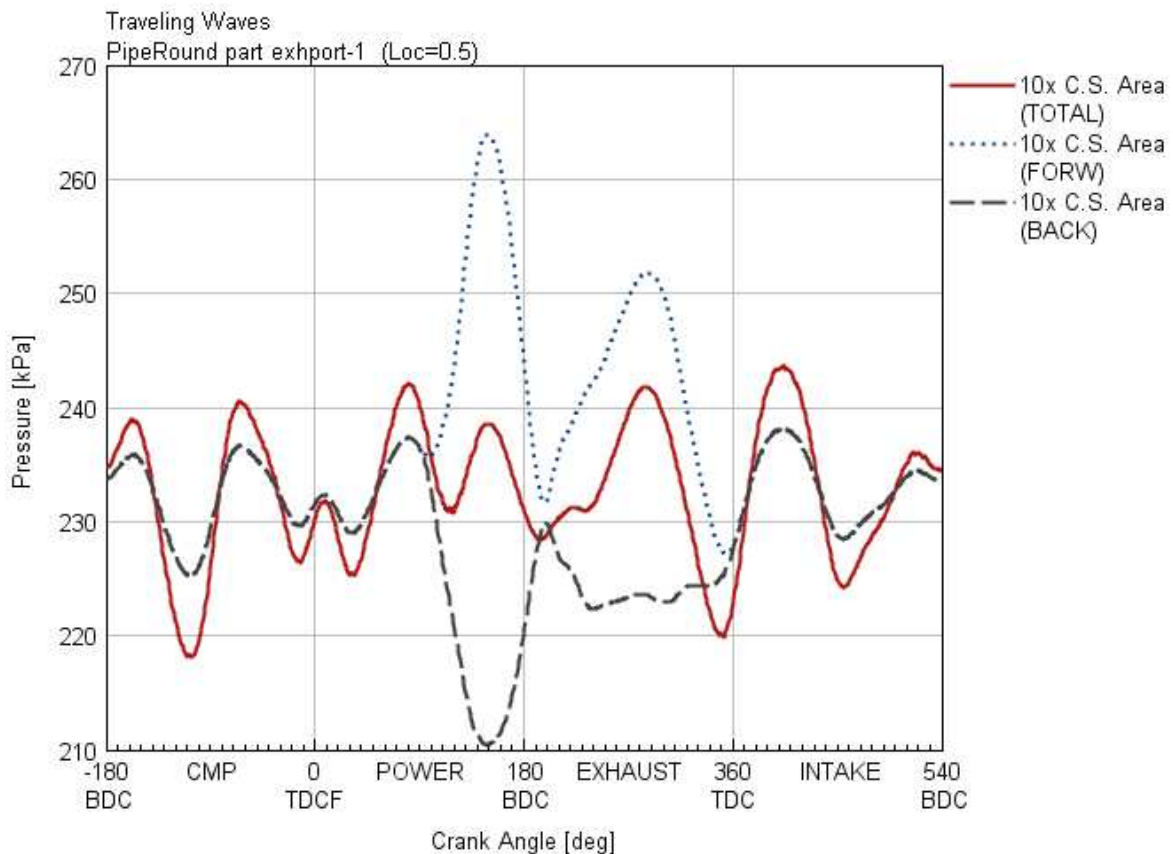


Figure 23. Traveling pressure waves in the exhaust port with an exhaust runner with 10x the original cross-sectional area.

The final case analyzed was for an exhaust runner that had a total volume 100 times the original volume with a cross-sectional area and length ten times the original design. Figure 24 is a plot of the traveling pressure waves observed by the exhaust port in cylinder one for this case. The peak pressure magnitude with the large runner was significantly less than any other case, reaching a magnitude of only 225 kPa. The forward traveling pressure wave reaches a magnitude of 250 kPa with the expulsion of exhaust gas from the cylinder but interferes destructively with a backwards traveling pressure wave that reaches a minimum of 196 kPa. There are no pressure waves occurring with the large exhaust runner before and after the expelling of exhaust gas meaning that the pressure waves from other cylinders are dissipated in the runners and exhaust manifold before they can travel to neighboring cylinders. Table 44 shows the engine performance response to the 100x volume exhaust runner modification, an increase in volumetric efficiency by 0.02 and an increase in brake power of 12.5 kW can be seen. The large exhaust

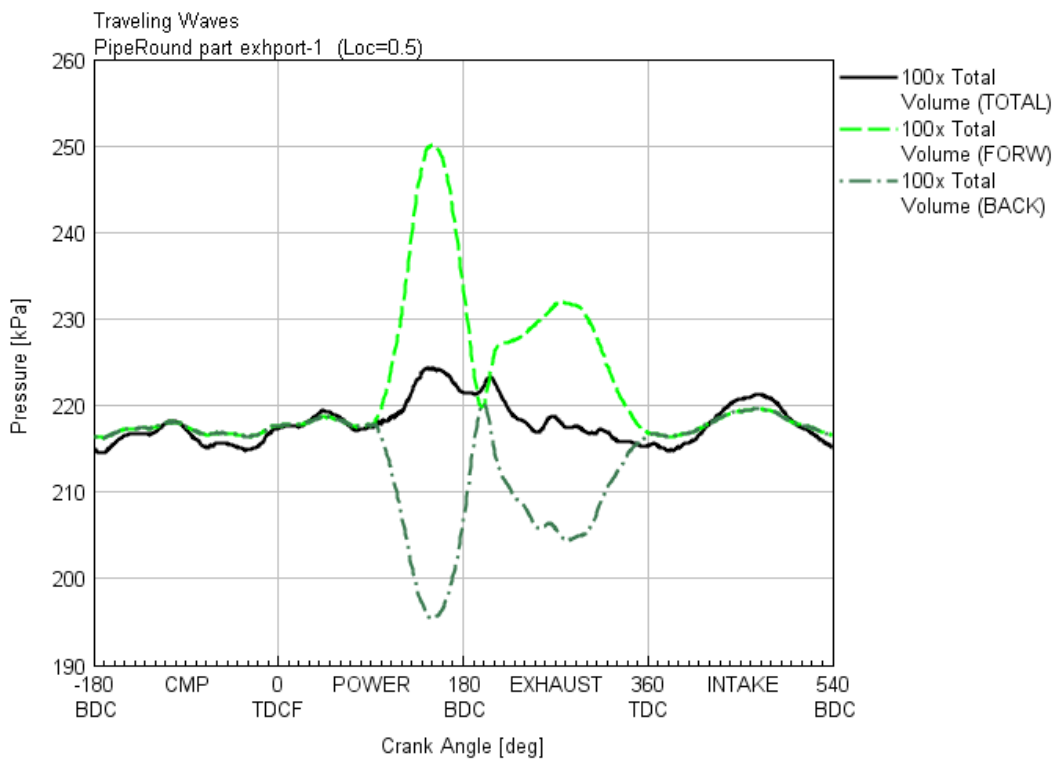


Figure 24. Traveling pressure waves in the exhaust port with an exhaust runner with 10x the original cross-sectional area and 10x the original length.

runner shows the best results for keeping constant and predictable pressure outside the exhaust valve before the expelling of exhaust gasses, but would be very hard to mimic experimentally due to the large volume.

In general, runner modification had little effect on engine performance, with the largest change being with the twenty-times-original-length exhaust runner increasing the brake torque from 1580 N-m to 1738 N-m, a net increase of 150 N-m. This rise in performance is associated with the rise in volumetric efficiency from the original 0.929 to 0.979, a net increase of 0.05 which was also the largest increase for any of the modifications, as seen in Table 42. Figure 25 shows the traveling pressure waves in the exhaust port of cylinder 1 for the twenty-times-original-length exhaust runner. The average pressure in the exhaust port for this case dropped 26 kPa from the original design with a value of 204.4 kPa. The exhaust

Table 44. 100x Runner Volume Effects on Engine Performance

Engine Performance Parameters	Units	OG	100x Total Volume
Engine Speed (cycle average)	RPM	1800	1800
Brake Torque	N-m	1580	1646
Brake Power	kW	297.8	310.3
BSFC - Brake Specific Fuel Consumption, Cyl	g/kW-h	148.2	146.3
IMEP720 - Net Indicated Mean Effective Pressure	kPa	1287	1334
BMEP - Brake Mean Effective Pressure	kPa	1105	1151
PMEP - Pumping Mean Effective Pressure	kPa	-82.00	-73.75
FMEP - Friction Mean Effective Pressure	kPa	182.5	183.1
Volumetric Efficiency, Air	fraction	0.929	0.956
Air Flow Rate	kg/h	924.9	951.2

port had a minimum pressure as low as 175.0 kPa (22 kPa less than the original design) and a maximum pressure reaching 246.2 kPa (6 kPa less than the original design).

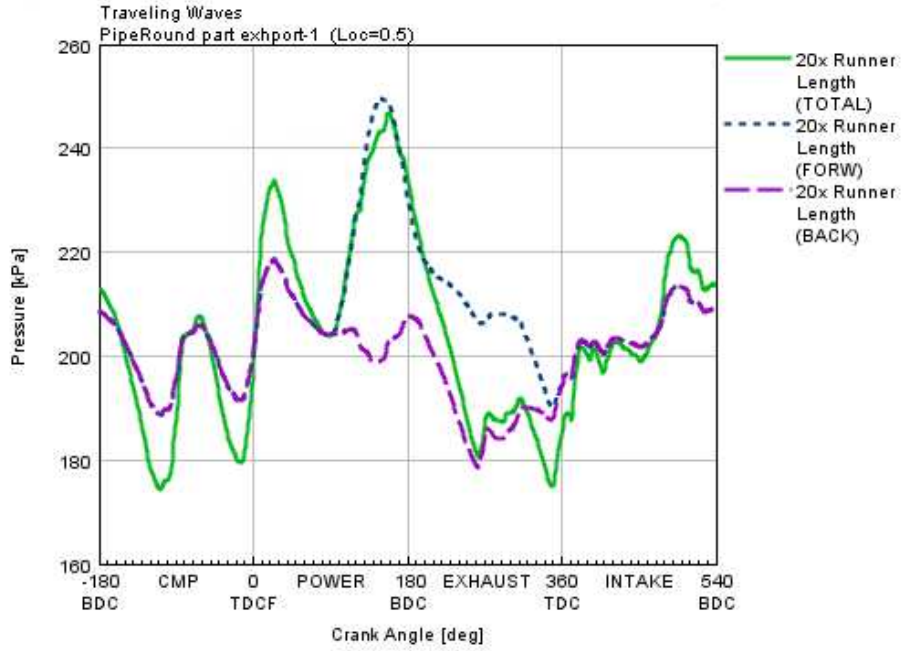


Figure 25. Traveling Pressure Waves in Exhaust Port 1 for an Exhaust Runner 20X the Original Length

Chapter 5- Cylinder Deactivation

There are many reasons for deactivating cylinders and just as many methods for accomplishing it. In industry, common reasons for deactivating cylinders are: to increase engine efficiency at part-load[25], to improve fuel economy by reducing engine pumping losses under certain vehicle operating conditions[4][18][19][28][29], to reduce misfiring at part load in large-bore engines[4], and to reduce power train friction through the absence of actuating forces on the deactivated valves[26]. For research, other reasons can include: the ability to extrapolate experimental data from a deactivated cylinder engine to understand how the experiments would affect a fully-operational engine, to decrease costs and work required to run an experiment by requiring less engine modification, and to decrease the propagation of uncertainties that would arise during modification of multiple cylinders. One of the issues with using deactivated-cylinder engines for research is the instabilities in the exhaust pressure caused by permanently shutting the exhaust valves in the deactivated cylinders. In a fully-operational multi-cylinder engine the average instantaneous pressure in the exhaust manifold is held relatively constant because when one exhaust valve is opening to release exhaust gas, another valve is closing and stopping the release of exhaust gas; this does not occur in deactivated-cylinder engines. The primary focuses of this chapter are the analysis of the pressure wave dynamics in the exhaust manifold of an engine after cylinder deactivation, the analysis of the effects of pressure-mitigation techniques on traveling pressure waves in the exhaust port of an engine after cylinder deactivation, and an analysis on the effects of cylinder deactivation on engine performance.

5.1 Six-cylinder Deactivation Techniques

There are multiple ways of deactivating cylinders in a spark-ignited engine, with each method presenting different benefits. One of the simplest methods involves keeping the intake and exhaust valves closed for particular cylinders, with the pistons still following their strokes. [3][25] If this method is used, the deactivated cylinders still produce frictional power losses in the engine, but have the benefit of

assisting in torsional balancing in the drivetrain as well as simplicity in design.[25] A newer method of cylinder deactivation is using a variable teeth dog clutch in the crank shaft of the engine, allowing the separation of particular crankshaft segments so that the separated cylinders do not rotate with the crankshaft. [25] This method has the benefits of not losing any efficiency to pumping friction losses but requires a high-powered battery to power the solenoids controlling the variable teeth dog clutch as well as creating a very complicated crankshaft that requires a stronger material than before modification.[25] The final method that will be discussed is a method for deactivating cylinders by decoupling the motion of the piston from the rotation of the crankshaft, which is a very similar idea to the previous technique, except the separation occurs in the connecting rod instead of the crankshaft.[3] This method has the same benefits of pumping friction losses in the deactivated cylinders but has the added benefit of simplicity in design and modification.[3]

5.2 The Deactivated-Cylinder Model Method 1: Pressure-Spring Cylinders

It is important to first note the what was held constant during modification. For both cases the exhaust manifold and inlet manifold average pressures were held constant at the same values used in the six-cylinder model. The air-to-fuel ratio and engine rotating speed were also held constant. The first method modeled in GT-Power is the simplest method that removes the ignition source in the engine and blocks the inlet and exhaust stream out of the cylinder, effectively creating an air-pressure-spring inside the cylinder as the deactivated cylinder pistons still move with their normal volume displacement. Experimentally this method has the benefit of being relatively simple to accomplish and easy to simulate. The model is unique in that it simulates the effects of cylinder deactivation in order to predict the effects on the pressure-wave dynamics in the exhaust stream of the engine after deactivation as well as the response of the active cylinder. The largest assumption made during this analysis is that the torsional balancing effects on the crankshaft are minimized by leaving the cylinder closest to the flywheel active, allowing the effects to be ignored.

In order to modify the model to closely simulate actual cylinder deactivation techniques, “EndFlow” components were added to the model on the exhaust side (right side) and intake side (left side) of the combustion chamber, just after the exhaust and intake ports of five of the cylinders simulating how the exhaust manifold would be separated from the cylinder experimentally. Additionally, the typical combustion chamber was replaced by a mechanical piston-cylinders labeled “Deactivated Cylinders” where no combustion occurs. The inlet and exhaust valves for the deactivated cylinders were totally removed from the model. The final modification required was changing the ‘initial state’ sub-model inside the five decommissioned cylinders to contain only air so that no fuel would be present in the cylinder at the start and no fuel could enter the cylinder in sequential cycles. Figure 26 is a representation of the deactivated-cylinder model, with the most noticeable difference between it and the fully-operational model in Figure 11 being the “EndFlow” components and the new piston-cylinder components.

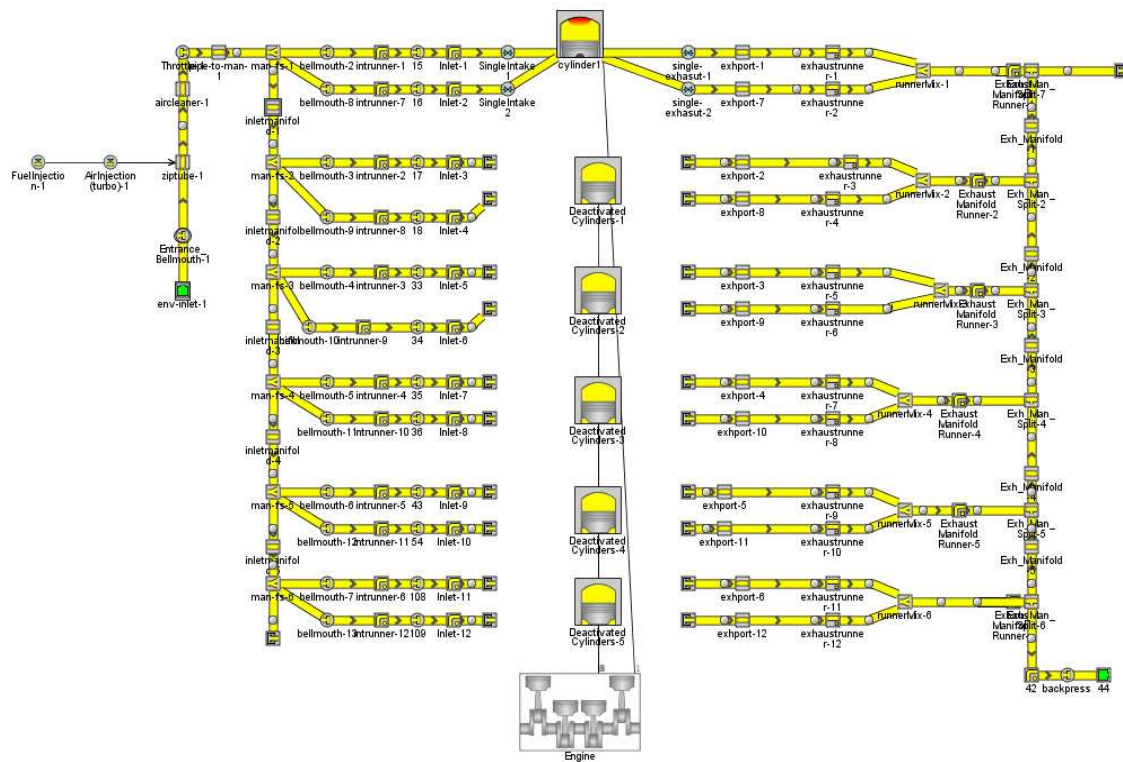


Figure 26. Decommissioned Cylinder GT-Power Model

The deactivated cylinders used a piston-cylinder component in GT-Power called “Deactivated Cylinder.” This component is used to specify the attributes of a piston cylinder volume with no combustion. The attribute values are shown in Table 45. The cylinder geometry is defined the same way as the normal cylinders, shown in Table 24, heat transfer and the initial state are the primary attributes defined for the deactivated cylinders.

Table 45. Deactivated Cylinder Component Attributes

Deactivated Cylinder (PistonCylinder)		
Attribute	Unit	Object Value
Initial State Object		DeadCylinderInitial
Wall Temperature defined by Reference Object		twall
Heat Transfer Object		htr
Initial State Scaling		on

“TWall” and “htr” are defined in section 3.4 Sub-Models but the initial state sub-model “DeadCylinderInitial” was defined specifically for the deactivated cylinders and is described in Table 46. Most attributes describe the ambient air and humidity that is average for Colorado. The major modification is the “Composition” attribute, in which a new species is defined as “air2.” “Air2” is a non-combustible air which only defines the species molecular weight, entropy, and enthalpy and ignores the number of specific atoms per molecule and lower heating value.

Table 46. Deactivated Cylinders Initial Condition Sub-Model Attributes

DeadCylinderInitial (Deactivated Cylinder Initial Condition)		
Attribute	Unit	Object Value
Pressure (Absolute)	kPa	101.3
Temperature	K	310.9
Composition		air2
Altitude	m	1524
Reference Altitude	m	0
Altitude Correction For...		PresAndTemp
Relative Humidity (Added to specified fresh air Composition)	%	32
Humidity Species		h2o-vap

5.3 The Deactivated-Cylinder Model Method 2: Removed Pistons

The second model created to simulate cylinder deactivation is the case when the entire piston is removed in addition to blocking the inlet and exhaust valves for the five deactivated cylinders. Figure 27 shows the GT-Power model that represents this deactivation method. With this method no initial conditions need to be modified. However, the pinch diameters controlling boost pressure in the inlet manifold and back pressure in the exhaust manifold were optimized to produce the same average pressures in the manifolds as for the fully-operational 100% load case. The engine performance characteristics were compared to the fully-operational engine model as well as the deactivated cylinder model with pistons. The same exhaust runner and manifold modifications were completed on this model as in Chapter 4- Pressure Analysis and Mitigation Techniques and the results were analyzed.

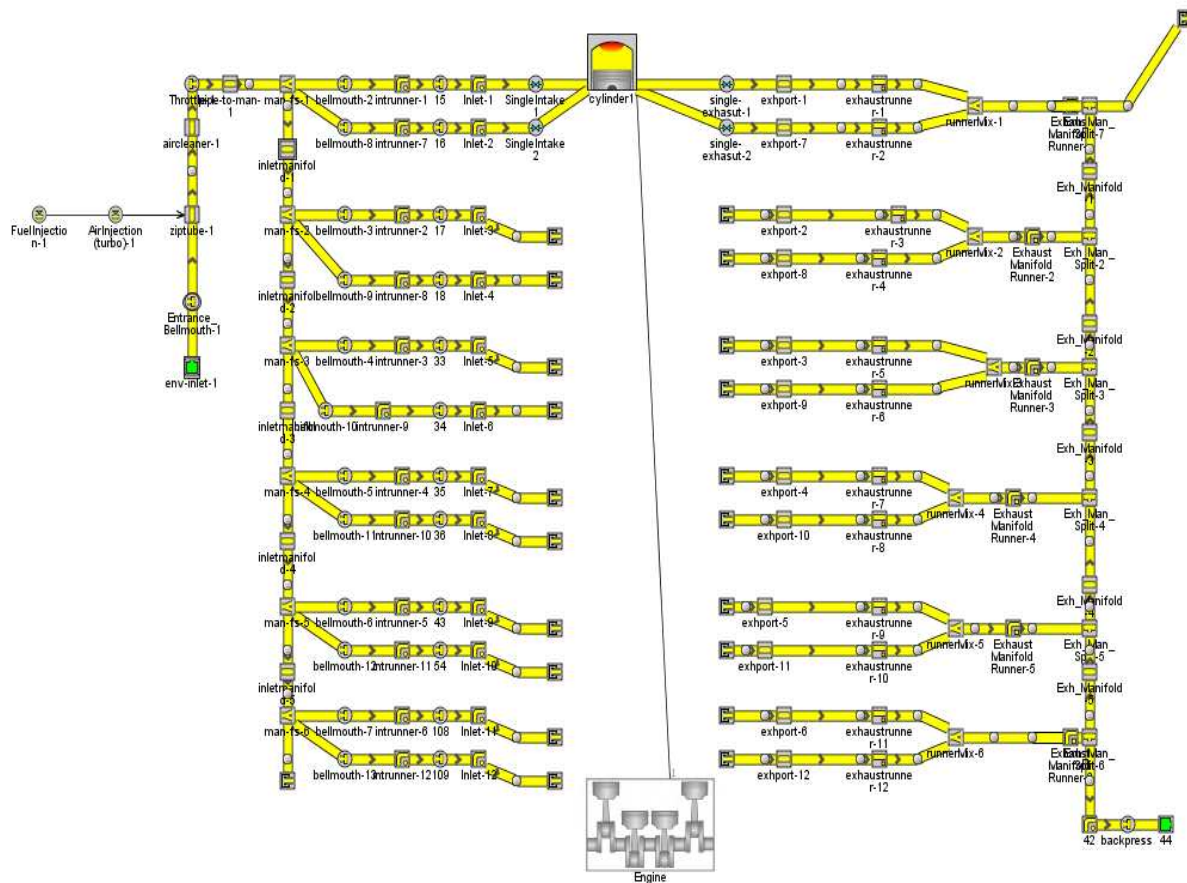


Figure 27. Cylinder Deactivation by Removing Cylinders in GT-Power

5.4 Effects of Cylinder Deactivation on the Exhaust Traveling Pressure Waves

The results of cylinder deactivation with and without pressure-spring cylinders are analyzed in this section. The exhaust flow and traveling pressure waves were identical for the two cases and will be treated as such in the following section. The major components analyzed are the active and deactivated cylinders (for the pressure-spring model) as well as the exhaust ports and exhaust manifold at multiple points in the engine. For the pressure-spring deactivation method, the in-cylinder pressure for two deactivated cylinders and one activated cylinder are shown in Figure 28. The active cylinder reaches a peak pressure of around 6490 KPa, cylinder 3 reaches a peak pressure of around 2685 KPa and cylinder 5 is deviates slightly from cylinder 3, reaching a peak pressure of around 2550 KPa. The two deactivated cylinders acted like pressure-springs since no combustion occurred. The other 3 deactivated cylinders behaved in a very similar way and were left out for simplicity. Combustion occurred in the active cylinder, but reached a lower peak pressure than when every cylinder was active.

The next component observed was the exhaust ports, specifically the pressure in the exhaust ports. Figure 29 displays the pressure vs. crank angle for exhaust ports on each of the cylinders. The

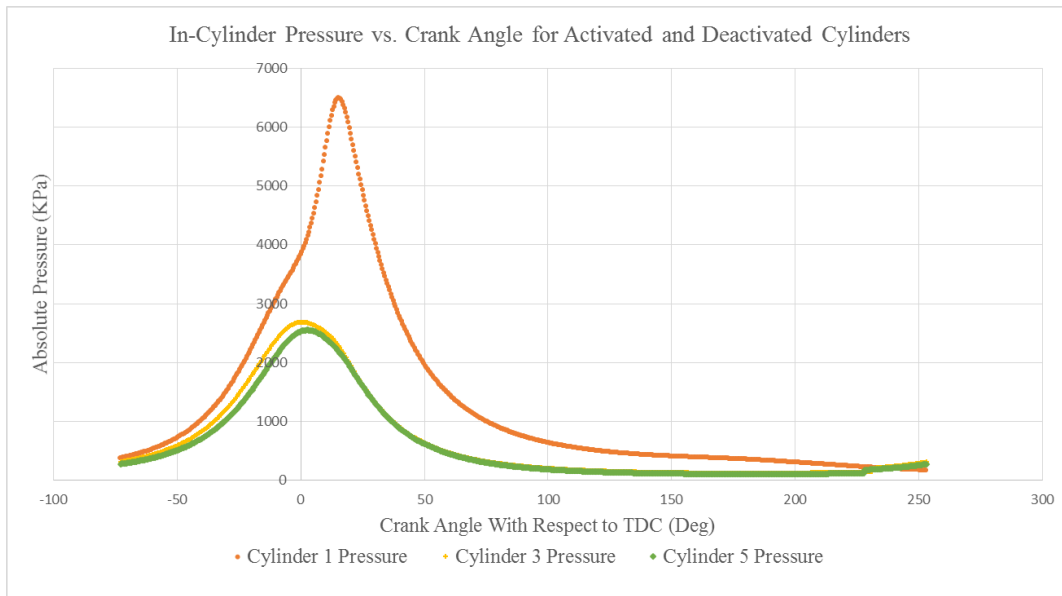


Figure 28. In-Cylinder Pressure vs. Crank Angle for Activated (Cylinder 1) and Deactivated (Cylinders 3 and 5) Cylinders

exhaust port (exhaust port 1) attached to the fully active cylinder displayed the highest pressure rise with a peak pressure amplitude of 145KPa. Every other port reached a peak pressure of around 130KPa. The peak value reached was lower as the distance from the active cylinder increased. This was identical for the two deactivation methods. Figure 30 shows how the traveling pressure wave caused by the expulsion of exhaust gas travels through the manifold and into the successive cylinder runners. There was a slight decrease in peak pressure amplitude from port to port, on the order of approximately 0.4 KPa, as the pressure wave created by the active cylinder's expulsion of exhaust gas traveled through the exhaust manifold and into each runner and then port. Exhaust port 1 also showed the lowest pressure amplitude of 95.5 KPa (13.9 PSI) caused by the rarefaction wave created when the pressure wave expanded into the exhaust manifold. Inversely to peak pressure amplitudes, the minimum pressure amplitudes increased sequentially with distance from the active cylinder, rising by approximately 0.5 KPa with the lowest pressure amplitude being in exhaust port 2 with a value of 95.7 KPa (14 PSI).

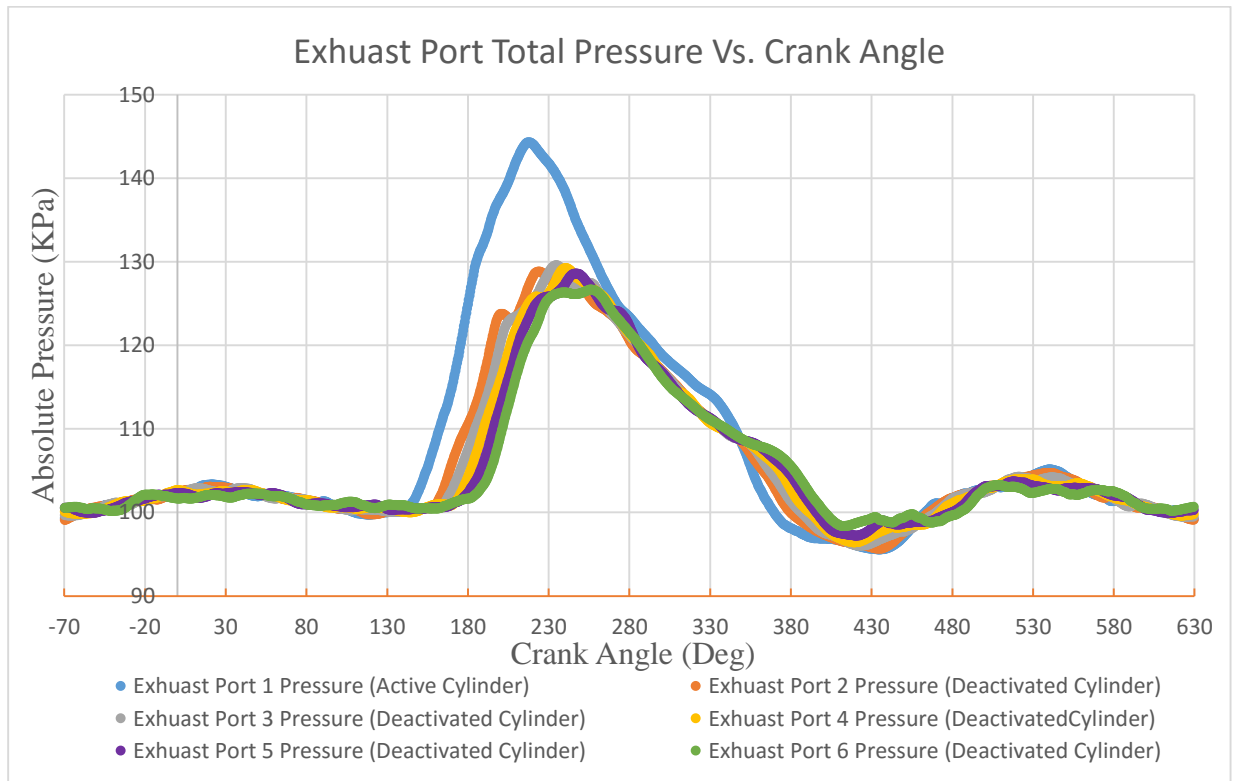


Figure 29. Exhaust Port Pressure Vs. Crank Angle for Deactivated Cylinder Model

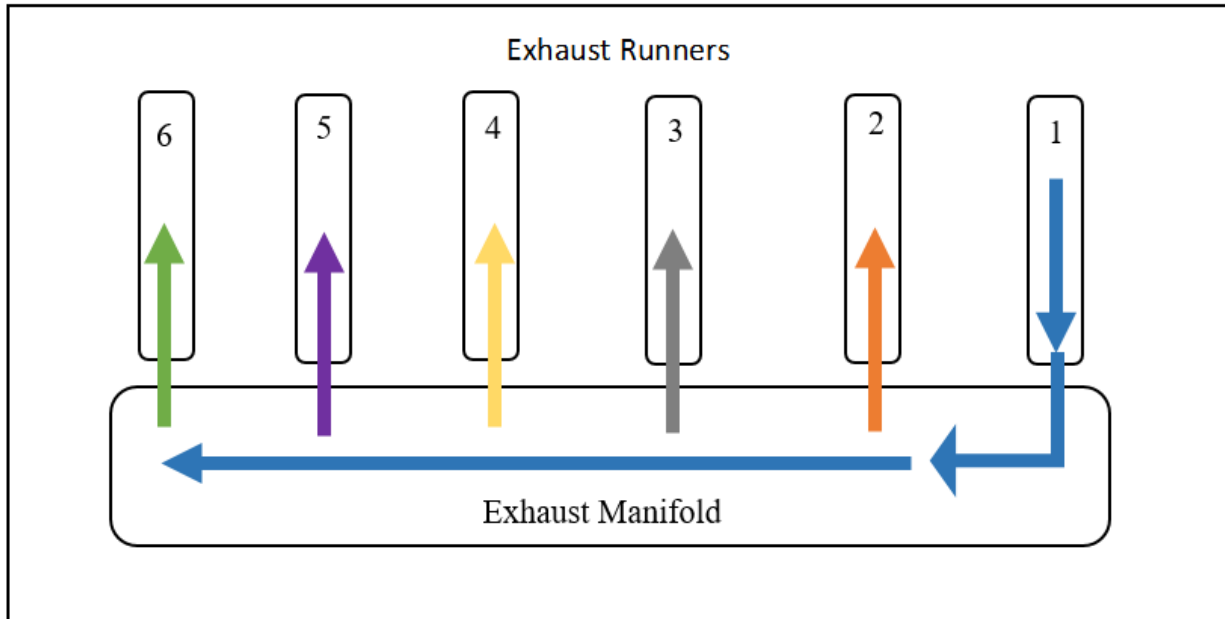


Figure 30. Diagram of Pressure Waves Traveling through the Exhaust Manifold

The next component analyzed was the exhaust manifold, specifically the traveling pressure waves in each of the different manifold segments. Figure 31 shows the total (forward plus backwards) traveling pressure waves through the five manifold segments, which was identical for the two deactivation methods. Prior to the expulsion of exhaust gas out of cylinder one, each segment is nearly uniform with very little deviation of pressure between segments. At the beginning of the exhaust stroke the pressure in each segment begins to increase sequentially with distance from the exhausting cylinder (Cylinder 1). However, at around 20 degrees post exhaust valve opening the sequence switches and the segments farthest from cylinder 1 see a faster increase in pressure which then travels in reverse order through the exhaust manifold so that segment 1 is the last segment to experience the rapid rise in pressure. This phenomenon can be explained by the reflection of the pressure wave at the exhaust exit choke point at the end of the exhaust manifold. Every segment reaches approximately the same peak pressure of 157 KPa with the largest difference being between exhaust manifold segment 1, which reaches a peak pressure of 157.6 KPa, and exhaust manifold segment 5, which reaches a peak pressure of 158.9 KPa.

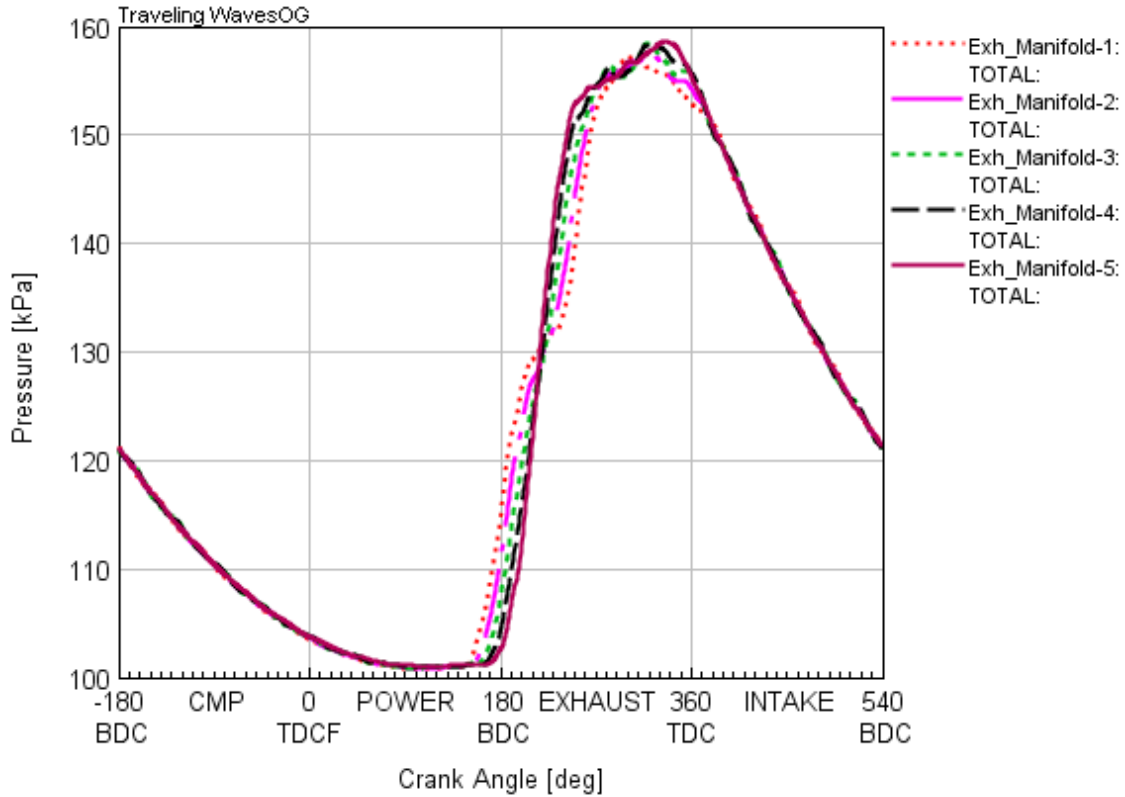


Figure 31. Traveling Pressure Waves in the Five Exhaust Manifold Segments with Five Deactivated Cylinders`

Figure 32 shows the pressure waves traveling in the forward direction, reverse (backwards) direction, and the total pressure recorded in exhaust segment 5. It can be seen that the forward traveling wave and the backwards traveling wave interfere constructively to produce a higher total peak pressure of 158.6 KPa and lower minimum pressure of 102 KPa. There is a 26 degree delay between the time the forward traveling pressure wave reaches the center of the segment and the time the backwards traveling pressure wave reflected from the end of the manifold reaches the center of the segment. Figure 33 shows the same traveling pressure waves as Figure 32 but in the first segment, exhaust manifold segment 1. Again the forward and backwards traveling pressure waves interfere constructively, but now there is a 90 degree delay between pressure waves as well as a greater magnitude pressure peak of the initial forward traveling pressure wave. The total peak pressure of segment 1 is 156.2 KPa, 1.4 KPa less than segment 5.

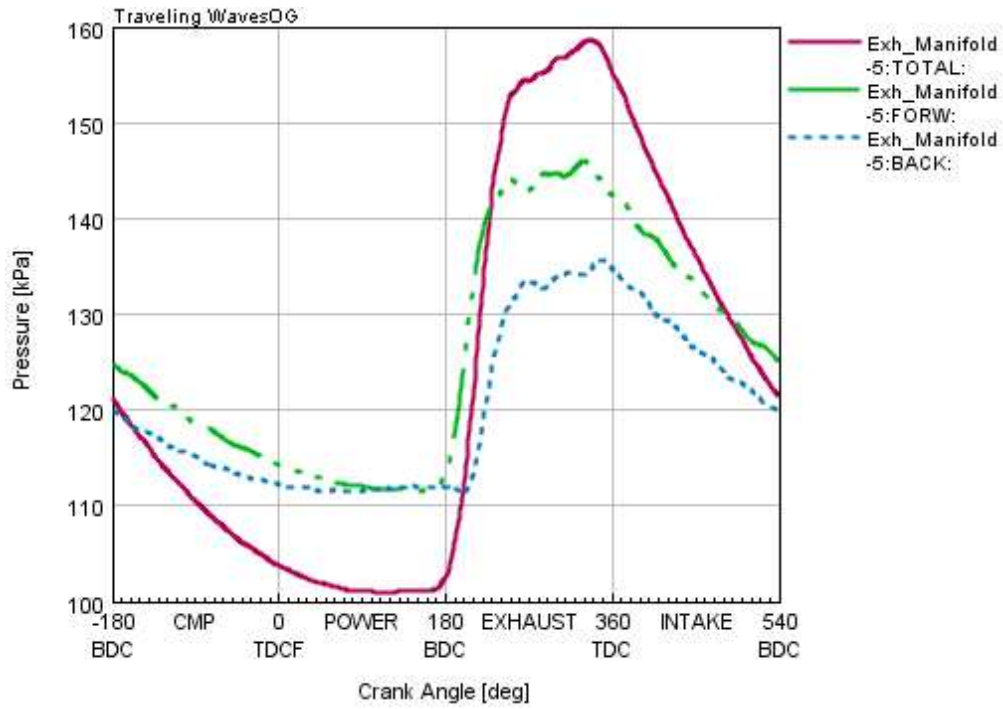


Figure 32. Forwards, Backwards, and Total Traveling Pressure Waves in Exhaust Manifold Segment 5 of the Deactivated Cylinder GT-Power Model

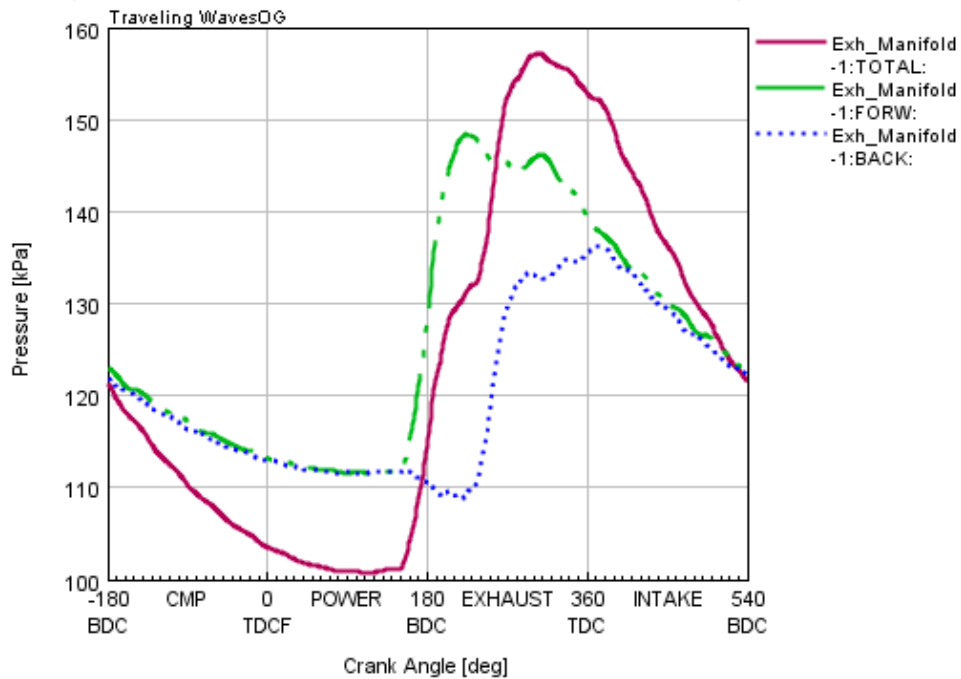


Figure 33. Forwards, Backwards, and Total Traveling Pressure Waves in Exhaust Manifold Segment 1 of the Deactivated Cylinder GT-Power Model

5.5 Effects of Cylinder Deactivation on Engine Performance

Another metric of the models analyzed was the total engine performance for each of the cylinder deactivation methods. Table 47 shows the engine performance for the six-cylinder model as well as the two cylinder deactivation models. For method 1, the friction loss is a large portion of BMEP; to compensate for this increase in frictional effects approximately 50% of the friction power would need to be added to the load as effective brake power. For method 2 the friction portion of brake power is only slightly higher than the baseline 6-cylinder case; only a small correction is needed (3.6% of brake power) to compensate for the added friction.

Table 47. Engine Performance Comparison between Six-Cylinder and Deactivated Cylinder GT-Power Models.

	Units	Six-Cylinder	Cylinder Deactivation Method 1	Cylinder Deactivation Method 2	Percent Change between Six-Cylinder and Method 1	Percent Change between Six-Cylinder and Method 2
Brake Torque	N-m	1763	301.9	260.0	82.87	85.25
Brake Power	kW	332.3	56.91	49.02	82.87	85.25
Mechanical Friction Power	kW	30.88	33.47	6.173	-8.38	80.01
Pumping Power	kW	5.99	0.998	0.998	83.33	83.33
Friction Power	kW	36.87	34.47	7.171	6.52	80.55
Fraction of Brake Power	%	11.10	60.56	14.63	-445.83	-31.85
FMEP	kPa	136.6	766.0	159.4	-460.90	-16.68
MFMEP	kPa	114.4	743.8	137.2	-550.29	-19.92
PMEP	kPa	22.19	22.19	22.19	0.00	0.00
BMEP	kPa	1231	1265	1089	-2.76	11.50

5.6 Effects of Pressure Mitigation Techniques on the Deactivated-Cylinder Models

The same modifications were made to the deactivated-cylinder model with pistons removed as was made for the fully-operational engine model in Chapter 4- Pressure Analysis and Mitigation Techniques. The tables showing the modification metrics are copied in this section convenience. Table 48 shows the modifications made to the exhaust manifold and Table 49 shows the modification made on the exhaust runners. For the fully-operational model it was shown that the manifold design with a small aspect ratio (length to C.S. area) was the best manifold design for mitigating pressure wave amplitudes prior to the expulsion of exhaust gas. The exhaust runner with ten times the original cross section proved to be the most effective, realistic runner design for mitigating pressure waves in exhaust port prior to the expulsion of exhaust gas from the cylinder.

Table 48. Exhaust manifold variation input values.

Modified Geometry	OG (Original)	1/2 Manifold Volume	2x Manifold Volume	4x Manifold Volume	8x Manifold Volume	Small Aspect Ratio
Manifold Diameter [m]	0.089	0.075	0.106	0.126	0.150	0.203
Manifold Segment Length [m]	0.244	0.172	0.345	0.488	0.690	0.254
Total Manifold Volume [m ³]	0.008	0.004	0.015	0.030	0.061	0.041

Table 49. Exhaust runner variation input values

Modified Geometry	OG (Original)	20x Runner Length	2x Runner Length	10x Runner Length	2x C.S. Area	10x C.S. Area	100x Total Volume
Exhaust Runner Width [m]	0.051	0.051	0.051	0.051	0.076	0.152	0.152
Exhaust Runner Height [m]	0.076	0.076	0.076	0.076	0.102	0.254	0.254
Exhaust Runner Length [m]	0.152	3.048	0.305	1.524	0.152	0.152	1.524
Total Volume [m ³]	5.90E-04	1.18E-02	1.18E-03	5.90E-03	1.18E-03	5.90E-03	5.90E-02

Figure 34 shows the traveling pressure waves in the exhaust port of cylinder 1 throughout an engine cycle for the most effective pressure mitigation methods found in Chapter 4, in these figures 'original design' is designated as 'OG'. These methods are the exhaust runner with a cross-section ten times the original, an exhaust runner with a total volume 100 times the original, an exhaust manifold with a total volume five times the original, and a small aspect ratio. Each of these methods showed to still be effective at limiting the pressure wave amplitudes prior to the expulsion of exhaust gas. The exhaust runner 100 times the volume of the original runner showed the best results with an amplitude on the order of 3 kPa and a peak pressure of only 194 kPa after the expulsion of exhaust gas from the cylinder, but is an unrealistic solution due to the size of the component. When the exhaust manifold was modified to have a small aspect ratio, the pre-exhaust pressure amplitude in the exhaust port was on the order of 10 kPa, but only had a change in peak pressure of 13 kPa during the expulsion of exhaust gas, which is significantly less than the original design which showed an increase in peak exhaust pressure in the exhaust port of over 30 kPa with the expulsion of exhaust gas. The ten-times-C.S. area runner showed very similar results as the small aspect ratio manifold but with a slightly lower average pressure in the exhaust port and a slightly greater peak pressure response to the expulsion of exhaust gas from the cylinder. While varying the exhaust runner length showed large changes to the pressure wave response to the expulsion of exhaust gas Figure 35 shows that the pressure wave amplitudes prior to exhaust gas expulsion were actually greater for these cases. The total peak pressure magnitude in the exhaust port of cylinder 1 also increased with each of the cases with a runner twice the length of the original and twenty times the length of the original. The case where the runner was ten times the original length showed a decrease in peak pressure magnitude of approximately 5 kPa, the peak pressure event also occurred 100 degrees earlier in the cycle.

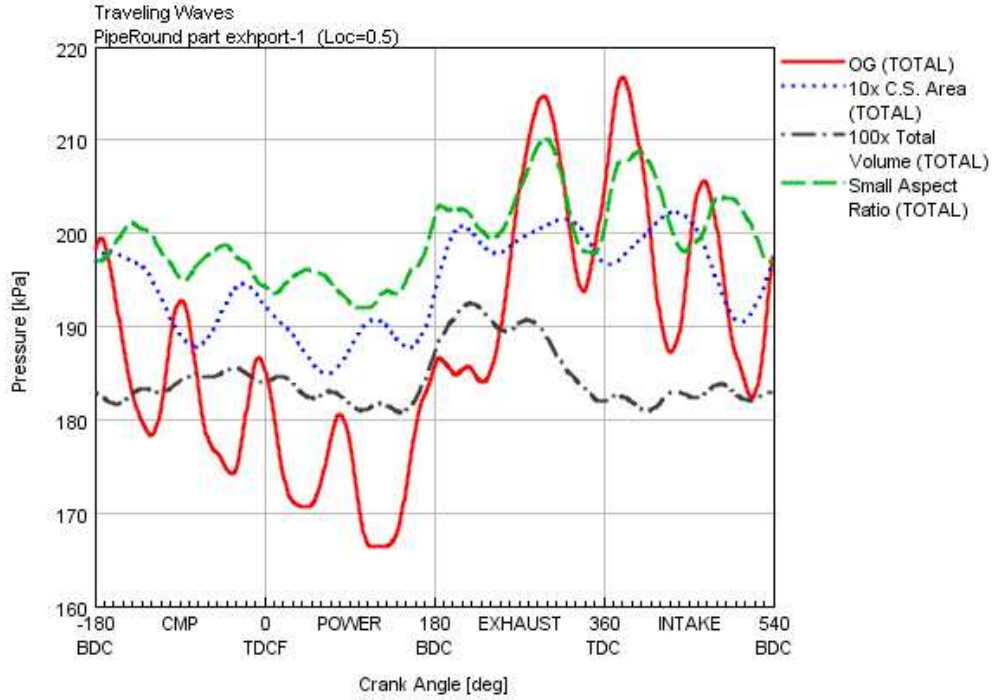


Figure 34. Traveling Pressure Waves in Exhaust Port 1 for Different Exhaust Manifold and Runner Designs

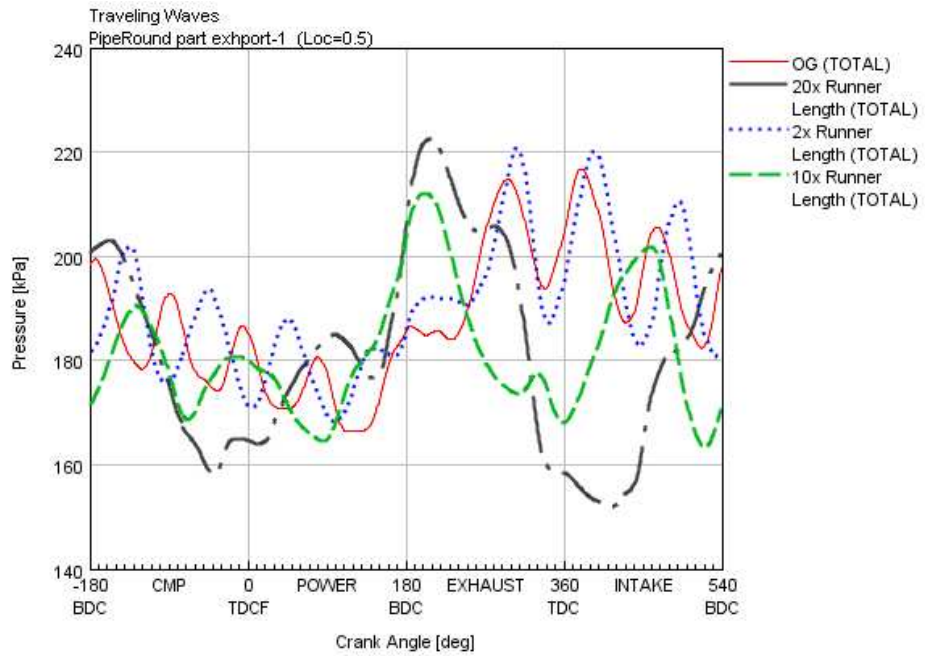


Figure 35. Traveling Pressure Waves in the Exhaust Port of Cylinder 1 with Varying Exhaust Runner Length

Even though exhaust runner length did not have major effects on the pressure waves in the exhaust port of cylinder 1, they did have large effects on engine volumetric efficiency and engine performance. Table 50 shows the effects of exhaust runner length on engine performance. There was a large increase in volumetric efficiency for when the runner was ten times the original size (V.E. of 0.89), and a larger increase in volumetric efficiency for the case when the runner was twenty times the original size (V.E. of 0.96). The brake power and brake torque behaved similarly to volumetric efficiency, increasing from 365 N-m in the original design to 415 N-m when the runner length was increased tenfold and to 437 N-m when the runner length was increased twentyfold.

When the exhaust runner cross-sectional area (e.g. C.S. area) was varied, the case with a C.S. area ten times the original size showed a decrease in pressure wave amplitude in the exhaust port of cylinder 1 prior to the expulsion of exhaust gas. It was observed that the volumetric efficiency and brake torque of the deactivated-cylinder engine increased with increasing cross-sectional area. The case with a

Table 50. Engine Performance Response to Exhaust Runner Length Variation in a Deactivated-Cylinder Engine Model with Removed Pistons

Engine Performance Parameters	Units	OG	20x Runner Length	2x Runner Length	10x Runner Length
Engine Speed (cycle average)	RPM	1800	1800	1800	1800
Brake Torque	N-m	365.8	437.5	378.3	415.0
Brake Power	kW	68.95	82.46	71.30	78.22
BSFC - Brake Specific Fuel Consumption, Cyl	g/kW-h	77.08	93.66	80.67	87.67
IMEP720 - Net Indicated Mean Effective Pressure	kPa	412.9	469.5	422.7	451.4
BMEP - Brake Mean Effective Pressure	kPa	255.7	305.8	264.5	290.1
PMEP - Pumping Mean Effective Pressure	kPa	-75.82	-93.32	-77.27	-71.31
FMEP - Friction Mean Effective Pressure	kPa	157.2	163.7	158.3	161.3
Volumetric Efficiency, Air	fraction	0.7409	0.9580	0.7599	0.8922

total runner volume 100 times the original volume showed the largest increase in engine performance with an increase in brake torque of 33 N-m over the original design. This case has been shown to have the greatest ability to mitigate the pressure wave amplitudes prior to the expulsion of exhaust gas from the cylinder as well as increase the engine performance of the engine. However, this case would be unrealistic to achieve experimentally due to the size of the components.

Table 52 shows the effects of exhaust manifold volume modification on the engine performance of the deactivated-cylinder model. The small aspect ratio case had shown the best capabilities for mitigating the pressure wave amplitudes in the exhaust port of cylinder 1 prior to the expulsion of exhaust gas and also shows an increase in engine performance. For this case the brake torque was increased from 365.8 kPa to 377.4 kPa but the volumetric efficiency decreased slightly from 0.7409 to 0.7389. When the aspect ratio was not modified, there was an increase in engine performance and volumetric efficiency

Table 51. Engine Performance Response to Exhaust Runner Cross-Sectional Area Modification in a Deactivated-Cylinder Engine Model with Removed Pistons

Engine Performance Parameters	Units	OG	2x C.S. Area	10x C.S. Area	100x Total Volume
Engine Speed (cycle average)	RPM	1800	1800	1800	1800
Brake Torque	N-m	365.8	374.8	378.5	398.8
Brake Power	kW	68.95	70.65	71.34	75.17
BSFC - Brake Specific Fuel Consumption, Cyl	g/kW-h	77.08	80.23	80.45	84.90
IMEP720 - Net Indicated Mean Effective Pressure	kPa	412.9	420.1	422.9	438.7
BMEP - Brake Mean Effective Pressure	kPa	255.7	262.0	264.6	278.8
PMEP - Pumping Mean Effective Pressure	kPa	-75.82	-79.89	-76.14	-71.96
FMEP - Friction Mean Effective Pressure	kPa	157.2	158.0	158.3	159.9
Volumetric Efficiency, Air	fraction	0.7409	0.7431	0.7520	0.8260

with increasing manifold volume. When the manifold volume was doubled the brake torque increased by 21 N-m, but when the manifold volume was doubled again there was only a 2 N-m difference in brake power. When the manifold was doubled one more time to a volume eight times the original, the brake power increased by 14 N-m, showing that volume is not the only metric that affects engine performance and that the pressure wave dynamics play an important role.

The pressure mitigation techniques first demonstrated in Chapter 4 were shown to have a similar effect on pressure wave amplitudes for the fully-operational engine model as well as the deactivated-cylinder model with pistons removed. There was a correlation shown between increasing exhaust flow component volume and increasing volumetric efficiency and engine performance. It was also demonstrated that by modifying the geometric ratios between length and cross-sectional it was possible to

Table 52 Engine Performance Response to Exhaust Manifold Volume Modification in a Deactivated-Cylinder Engine Model with Removed Pistons

Engine Performance Parameters	Units	OG	2x Manifold Volume	4x Manifold Volume	8x Manifold Volume	Small Aspect Ratio
Engine Speed (cycle average)	RPM	1800	1800	1800	1800	1800
Brake Torque	N-m	365.8	386.0	388.4	402.5	377.4
Brake Power	kW	68.95	72.76	73.22	75.87	71.13
BSFC - Brake Specific Fuel Consumption, Cyl	g/kW-h	77.08	82.40	82.42	85.57	81.05
IMEP720 - Net Indicated Mean Effective Pressure	kPa	412.9	428.7	430.5	441.6	422.0
BMEP - Brake Mean Effective Pressure	kPa	255.7	269.8	271.6	281.4	263.8
PMEP - Pumping Mean Effective Pressure	kPa	-75.82	-76.43	-70.32	-72.31	-79.19
FMEP - Friction Mean Effective Pressure	kPa	157.2	158.9	159.0	160.2	158.2
Volumetric Efficiency, Air	fraction	0.7409	0.7727	0.7774	0.8312	0.7389

drastically change the pressure wave amplitudes prior to the expulsion of exhaust gas while keeping engine performance relatively unchanged. While increasing the exhaust runner length and manifold volume did show an increase in deactivated-cylinder performance, it wasn't until these sizes were unrealistic that a difference was noticed in the exhaust port pressure wave amplitudes prior to the expulsion of exhaust gas from the active cylinder. For this reason, exhaust runner and exhaust manifold geometric modification is most likely not a valid method for mitigating pressure waves in the exhaust ports of a deactivated-cylinder engine.

Between the two deactivation methods I found that the method did not affect the traveling pressure waves, but had a large effect on engine performance. I would recommend total piston removal for cylinder deactivation due to the decrease in frictional losses. However, an in-depth vibrational analysis and balancing analysis of the crank-train would be beneficial as this was not analyzed in this project.

Chapter 6- Summary and Conclusion

6.1 Summary

A GT-Power model was created to simulate a Waukesha VGF-18 engine and was verified analytically with the use of Chemkin. The results were then validated with experimental data gathered for the Waukesha VGF-18 engine and while the general engine parameters and fuel flow were found to have a predictive confidence level over 90%. Due to the lack of experimental data and comparison points it is recommended that the values presented as results from this model not be used for predicting actual values but rather to predict trends in order to better understand engine response to modification.

Following validation there was a series of geometric modifications done to the exhaust manifold and exhaust runners of the model. The exhaust runner length, width, and height modified and the exhaust manifold length and diameter were modified. The pressure wave dynamics at the exhaust port of cylinder 1 and general engine parameters were analyzed for each of these modifications.

Two cylinder deactivation methods were modeled and analyzed in GT-Power. The first method involved replacing the combustion chambers with purely mechanical piston-cylinders full on non-combustible air and permanently shutting the intake and exhaust valves. The second cylinder deactivation method completely removed the pistons from the model and permanently shut the intake and exhaust valves. A comparison was made on the engine performance of the two models. Using the same pressure mitigation techniques used on the fully-operational engine model, a pressure mitigation analysis was done on the deactivated cylinder model with pistons removed.

6.2 Conclusions

- Pressure mitigation in the fully-operational multi-cylinder engine
 - When the geometric aspect ratio between cross-sectional area and length is held constant in the exhaust manifold, an increase in volumetric efficiency, brake power, brake torque, and brake specific fuel consumption are seen with increasing manifold volume.

- When the geometric aspect ratio between cross-sectional area and length is not held constant in the exhaust manifold there is a large change in the pressure wave dynamics in the exhaust ports of the engines. These changes can result in an increase of constructive pressure wave interference resulting in higher total pressure wave amplitude or an increase in deconstructive interference resulting in lower total pressure amplitudes.
- Exhaust runner cross-sectional area modification was more successful at lowering pressure wave amplitudes in the exhaust port prior to the expulsion of exhaust gas than exhaust runner length modification. However, exhaust runner length had a larger effect on pressure wave maxima and minima in the exhaust port. This method is not feasible due to the instabilities created by having a rapid area change very close to the exhaust valve.
- Cylinder Deactivation Methods
 - Deactivation Method 1 showed a 60% increase in friction percentage of brake power. To compensate for this during experimental modification, approximately 50% of the friction power would need to be added to the load as effective brake power.
 - Deactivation Method 2 showed only a 6% increase in friction percentage of brake power. Only a small correction is needed (3.6% of brake power) to compensate for the added friction.
- Pressure Wave Dynamics and Mitigation in a Deactivated-Cylinder Model with Pistons Removed
 - Pressure waves occur in every port of a deactivated cylinder engine but have the highest magnitude in the active cylinder and decrease in magnitude with distance from the active cylinder.
 - The pressure wave dynamics were identical for the two cylinder deactivation methods.
 - Modifying the cross-sectional area of the exhaust runner and aspect ratio of the exhaust manifold were shown to be most effective at decreasing the pressure wave amplitudes prior to the expulsion of exhaust gas from the active cylinder.

- Modifying the aspect ratio of the manifold was the most successful modification for both mitigating pressure wave amplitudes in the exhaust port prior to the expulsion of exhaust gasses and minimizing the effects on engine performance.

It has been found that cylinder deactivation does have a large effect on the traveling pressure waves in the exhaust system of an engine. The deactivation method that involved the total removal of the pistons in the deactivated cylinders showed less increase in frictional affects compared to the cylinder deactivation method that used the deactivated cylinders as piston-air-springs. For this reason it is recommended that the pistons be totally removed from a deactivated-cylinder engine.

Cylinder deactivation was shown to have a large effect on the traveling pressure waves in the exhaust system of an internal combustion engine. While geometric modification to the exhaust runner and exhaust manifold did show the capability to mitigate the pressure wave amplitudes in the exhaust port prior to the expulsion of exhaust gas, the decrease in amplitude was slight unless the modifications were extreme. Geometric modification of the exhaust runners and exhaust manifold is not recommended as a pressure mitigation technique due to the unrealistic sizes required to make a significant improvement.\

6.3 Future Research Ideas

The following is a list of future research that could be done in conjunction with this work to provide a greater understanding of engine performance and exhaust pressure wave dynamics:

- Experimentally deactivate cylinders of a Waukesha VGF-18 engine and compare results to the modeled predictions.
- Modify a deactivated-cylinder engine's exhaust manifold to attempt to mitigate pressure wave amplitudes in the exhaust port of the active cylinder prior to the expulsion of exhaust gasses.
- Model various pressure reducing techniques in the deactivated-cylinder model including geometric modification of the manifold and runners as well as the use of a Helmholtz resonator.
- Model the heat transfer using a separate program and introduce the correlation into GT-Power to increase the validity of exhaust pressure measurements.

References

- [1] J. C. Livengood and J. V. D. Eppes, “Effect of Changing Manifold Pressure, Exhaust Pressure, and valve timing on the Air Capacity and Output of A Four-Stroke Engine Operated with inlet Valves of Various Diameters and Lifts,” Washington, 1366, 1947.
- [2] M. A. Jemni, G. Kantchev, and M. S. Abid, “Influence of intake manifold design on in-cylinder flow and engine performances in a bus diesel engine converted to LPG gas fuelled, using CFD analyses and experimental investigations,” *Energy*, vol. 36, no. 5, pp. 2701–2715, May 2011.
- [3] A. Boretti and J. Scalco, “Piston and Valve Deactivation for Improved Part Load Performances of Internal Combustion Engines,” *SAE 2011 World Congr. Exhib.*, pp. 2011–01–0368, 2011.
- [4] B. F. Smalley, A. J., Vinyard, S., Evans, “Power Cylinder Deactivation for Reduced Fuel Consumption Under Part Load.pdf,” San Antonio, Texas.
- [5] D. Chalet, A. Mahé, J.-F. Hétet, and J. Migaud, “A new modeling approach of pressure waves at the inlet of internal combustion engines,” *J. Therm. Sci.*, vol. 20, no. 2, pp. 181–188, Mar. 2011.
- [6] G. P. McTaggart-Cowan, W. K. Bushe, P. G. Hill, and S. R. Munshi, “A supercharged heavy-duty diesel single-cylinder research engine for high-pressure direct injection of natural gas,” *Int. J. Engine Res.*, vol. 4, no. 4, pp. 315–330, 2005.
- [7] J. D. Halderman, *Automotive Engine Performance*, 4th ed. Pearson, 2013.
- [8] D. S. Boman, T. F. Nagey, and R. B. Doyle, “Effect of exhaust pressure on the performance of an 18-cylinder air-cooled radial engine with a valve overlap of 40 degrees.pdf,” Cleveland, Ohio, 1220, 1947.
- [9] A. Kirkpatrick, “Intake and Exhaust Flow,” *Colorado State University Engine Web Page*, 1998. [Online]. Available: <http://www.engr.colostate.edu/~allan/fluids/page4/page4f.html>.
- [10] M. Driels, “Dynamics of IC Engine induction systems,” *J. Sound Vib.*, vol. 43, no. April, pp. 499–

- 510, 1975.
- [11] P. M. Morse, R. H. Boden, and H. Schecter, "Acoustic Vibrations and Internal Combustion Engine Performance I. Standing Waves in the Intake Pipe System," *J. Appl. Phys.*, vol. 9, no. 1, p. 16, 1938.
- [12] W. Polifke, C. O. Paschereit, and K. Döbbeling, "Constructive and Destructive Interference of Acoustic and Entropy Waves in a Premixed Combustor with a Choked Exit," *J. Acoust. Vib.*, vol. 6, no. 3, pp. 135–146, 2001.
- [13] J. Zhu, A. Wimmer, E. Schneßl, H. Winter, and F. Chmela, "Parameter based combustion model for large pre-chamber gas engines," *Asme Ices2009*, vol. 132, no. August 2010, pp. 1–9, 2009.
- [14] P. Tribotte, F. Ravet, V. Dugue, P. Obernesser, N. Quechon, J. Benajes, R. Novella, and D. De Lima, "Two Strokes Diesel Engine - Promising Solution to Reduce CO2 Emissions," *Procedia - Soc. Behav. Sci.*, vol. 48, pp. 2295–2314, 2012.
- [15] O. Vitek, J. Macek, and M. Polásek, "New Approach to Turbocharger Optimization Using 1-D Simulation Tools," *SAE Tech. Pap. Ser.*, no. 06P-192, 2006.
- [16] Gamma Technologies, "GT-Power Engine Performance Manual." Gamma Technologies, Inc, Chicago, Illinois, pp. 1–98, 2013.
- [17] Gamma Technologies, "GT-Power Flow Manual." Gamma Technologies, Inc, Chicago, Illinois, pp. 1–110, 2013.
- [18] Gamma Technologies, "GT-Power Mechanical Manual." Gamma Technologies, Inc, Chicago, Illinois, pp. 1–93, 2013.
- [19] D. Montgomery, G. Runger, and N. Hubele, *Engineering Statistics*, Fifth. Hoboken NJ: Wiley, 2011.
- [20] K. Quillen, "ENGINE FRICTION REDUCTION MEASUREMENTS AND PARTICULATE MEASUREMENTS OF A LEAN BURN FOUR STROKE NATURAL GAS INTERNAL COMBUSTION ENGINE," Colorado State University, 2007.

- [21] J. D. Stanitz, "An analysis of the factors that affect the exhaust process of a four-stroke-cycle reciprocating engine," Cleveland, Ohio, 1242, 1947.
- [22] R. S. Benson and W. . A. Woods, "Wave Action in the Exhasut System of a Supercharged Two-Stroke-Engine Model," *Int. J. Mech. Sci.*, vol. 1, pp. 253–281, 1960.
- [23] H. W. Thompson, Michael P, Engleman, "The Two Types of Resonance in Intake Tuning," *A.S.M.E*, p. 10, 1970.
- [24] M. A. Ceviz and M. Akin, "Design of a new SI engine intake manifold with variable length plenum," *Energy Convers. Manag.*, vol. 51, no. 11, pp. 2239–2244, 2010.
- [25] B. Vinodh, "Technology for Cylinder Deactivation Reprinted From : Electronic Engine Controls 2005," *SAE Tech. Pap.*, vol. 2005, no. 724, 2005.
- [26] M. Rebbert, G. Kreusen, and S. Lauer, "A New Cylinder Deactivation by FEV and Mahle," *SAE Tech. Pap. Ser.*, vol. 2174, no. 724, p. 105, 2008.
- [27] Q. Zheng, "Characterization of the Dynamic Response of a Cylinder Deactivation Valvetrain System," *SAE Tech. Pap.*, vol. 0669, no. 724, 2001.
- [28] T. G. Leone and M. Pozar, "Fuel Economy Benefit of Cylinder Deactivation - Sensitivity to Vehicle Application and Operating Constraints," *SAE Tech. Pap. Ser.*, vol. 1645, pp. 10–11, 2001.
- [29] A. Falkowski, M. McElwee, and M. Bonne, "Design and Development of the DaimlerChrysler 5.7L HEMI® Engine Multi-Displacement Cylinder Deactivation System," *SAE Tech. Pap.*, vol. 2106, no. 724, pp. 1–12, 2004.

Appendix A- Waukesha VGF-18 Engine Experimental Data

Baseline								
	60% Load	70% Load	80% Load	90% Load	100% Load	100% Load - mid point	100% Load - final point	100% Load - Average
Data Point	F18BASE 13	F18BAS E11	F18BA SE12	F18BA SE14	F18BA SE15	F18BAS E16	F18BA SE17	Average
General Parameters								
Engine RPM	1796	1801	1800	1795	1794	1794	1794	1794
Torque [ft-lb]	878	1024	1171	1316	1463	1462	1462	1462
Brake Power [BHP]	301	352	403	452	502	502	501	502
BSFC	7963	7692	7502	7335	7313	7304	7388	7335
BMEP	121	141	161	181	201	201	201	201
IMEP [Average / Standard Deviation]	151.5 / 4.63	171.0 / 4.09	190.8 / 5.31	210.8 / 5.26	230.6 / 9.03	231.0 / 8.98	231.1 / 10.07	#DIV/0!
Timing [deg BTDC]	14	14	14	14	14	14	14	14
A/F Stoic. Total	15.65	15.74	15.74	15.72	15.90	15.89	15.93	16
A/F Stoic. Comb.	17.14	17.11	17.11	17.14	17.14	17.14	17.14	17
A/F Urban & Sharpe Total	21.91	22.11	22.34	22.05	22.38	22.31	22.44	22
A/F Urban & Sharpe Comb.	24.74	24.61	24.87	24.73	24.71	24.66	24.71	25
phi	0.71	0.71	0.70	0.71	0.71	0.71	0.71	1
A/F Ratio ECM	20.61	20.62	20.93	20.77	20.91	20.90	20.97	21
AFR4800 Left ECM	NA	NA	NA	NA	NA	NA	NA	NA
AFR4800 Right ECM	NA	NA	NA	NA	NA	NA	NA	NA
Pressures								
Ambient Pressure [psia]	12.06	12.03	12.03	12.06	12.06	12.05	12.05	12
Inlet Air Pressure [”Hg]	5.01	5.00	5.01	5.01	5.01	5.01	5.00	5

Pre Intercooler Pressure [psig]	26.14	27.26	27.58	28.97	30.76	30.72	30.56	31
Intercooler Differential Pressure [“H2O]	6.62	8.18	10.44	11.90	14.11	13.85	14.15	14
Intake Manifold Pressure [psia]	21.43	23.52	26.32	28.72	31.82	31.52	31.82	32
Exhaust Manifold Pressure [psia]	25.59	26.70	28.02	29.59	32.19	31.96	32.27	32
Exhaust Back Pressure [“Hg]	5.01	4.99	4.99	5.00	5.00	5.00	5.01	5
Fuel Manifold Pressure [psig]	26.25	27.39	27.60	28.53	30.36	30.43	30.41	30
Lube Oil Pressure	68.87	67.43	67.39	68.30	68.15	68.76	68.79	69

Temperatures

Ambient Temperature [deg F]	43.969	44.054	41.808	45.46	47.546	47.115	46.138	47
Inlet Air Temperature [deg F]	97.26	100.058	99.799	100.164	100.357	100.209	100.268	100
Pre Intercooler Temperature [deg F]	267.5	279.752	283.027	292	314.5	314.387	315.958	315
Post Intercooler Temperature [deg F]	74.7	77.39	79.41	83	90.013	88.618	87.792	89
Exhaust Turbine Inlet Temp [deg F]	1075.53	1086.32	1101.013	1109.587	1121.849	1123.909	1124.579	1123
Exhaust Stack Temperature [deg F]	808.779	819.401	842.885	847.446	851.261	853.01	851.982	852
Cylinder 1 Exhaust Temp [deg F]	1108.225	1110.879	1104.742	1106.718	1120.279	1120.111	1120.882	1120

Cylinder 2 Exhaust Temp [deg F]	1140.101	1146.054	1150.785	1153.315	1165.413	1166.279	1166.391	1166
Cylinder 3 Exhaust Temp [deg F]	1131.604	1133.653	1135.795	1139.094	1151.121	1151.404	1152.394	1152
Cylinder 4 Exhaust Temp [deg F]	1133.651	1134.242	1135.349	1137.926	1144.131	1145.626	1146.684	1145
Cylinder 5 Exhaust Temp [deg F]	1133.651	1134.242	1135.349	1137.926	1144.131	1145.626	1146.684	1145
Cylinder 6 Exhaust Temp [deg F]	1127.06	1125	1124.557	1133.205	1163.819	1159.68	1160.667	1161
Average Cylinder Exhaust Temp [deg F]	1129.05	1130.717	1131.037	1134.671	1148.171	1148.165	1148.926	1148
Cylinder Exhaust Temp Differential [deg F]	31.907	35.23	45.991	46.607	47.761	46.975	46.539	47
Lube Oil Temperature In [deg F]	174.5	174.6	174.6	175.5	175.5	175.5	175.5	176
Lube Oil Temperature Out [deg F]	158.8	157.5	157.6	157.8	156.8	156.8	156.8	157
Jacket WaterTemp In [deg F]	175	175.201	174.834	173	173	174	174	174
Jacket Water Temp Out [deg F]	180.143	179.286	179.791	179.648	179.238	179.432	179.709	179
Intercooler Water Temp In [deg F]	66.92	67.868	67.81	71.01	74.03	73.02	72.02	73
Intercooler Water Temp Out [deg F]	71.4	73.02	73.02	77.51	81.6	80.59	79.52	81
Oil Cooler Water Temp In [deg F]	55.21	57.28	55.21	59.3	61.31	62.32	61.31	62
Oil Cooler Water Temp Out [deg F]	65.4	65.4	63.39	66.47	67.48	68.49	67.48	68
Dyno Water Temp In [deg F]	103	88.88	89.89	95.77	96.78	98.8	97.79	98

Dyno Water Temp Out [deg F]	121.23	109.786	113.713	121.4	126.6	127.7	126.6	127
Fuel Flow Measurements								
Net (Lower) Heating Value [BTU/scf]	905.4	923	923	908.37	914.98	913.84	915.6	915
Gas Density [lbm/1000scf]	46.324	46.919	46.919	46.247	46.061	46.034	46.009	46
Thermal Efficiency [%]	31.95	33.08	33.91	34.68	34.79	34.83	34.44	35
Fuel Orifice Static Pressure [psig]	51.81	51.45	51.06	50.66	50.22	50.30	50.31	50
Fuel Orifice Differential Pressure [”H2O]	27.14	34.23	42.76	52.32	63.53	62.96	63.75	63
Fuel Orifice Temperature [deg F]	84.99	90.07	90.30	88.05	88.76	86.22	83.88	86
Fuel Flow (SCFH)	2650.50	2937.07	3274.46	3647.83	4016.09	4010.49	4046.39	4024
Fuel Flow (lb/hr)	122.78	137.78	153.61	168.69	184.96	184.61	186.14	185
Data Point	F18BASE13	F18BASE11	F18BASE12	F18BASE14	F18BASE15	F18BASE16	F18BASE17	
Inlet Air Annubar Flow [SCFM]	614	681	779	855	945	934	948	943
Air Flow (lb/hr)	2531	2841	3214	3503	3868	3859	3904	3877
Exhaust Annubar Flow [SCFM]	1273	1628	1974	2218	2500	2492	2500	2497
Jacket Water Flow [gpm]	202	200	199	199	199	199	199	199
Intercooler Water Flow [gpm]	73	73	73	74	73	73	73	73

Oil Cooler Water Flow [gpm]	124	124	123	125	125	125	125	125
Blow-By Parameters								
Blow-by Pressure [”H2O]	-0.56	-0.57	-0.46	-0.52	-0.68	-0.76	-0.44	-1
Blow-by Flow [acfm]	2.84	2.90	3.19	3.20	3.62	3.34	3.51	3
Blow-by Temperature [deg F]	118.50	123.12	124.90	123.60	129.09	123.60	121.60	125
Humidity								
Ambient Relative Humidity [%]	18.25	34.05	37.46	22.98	19.55	22.27	21.68	21
Inlet Air Relative Humidity [%]	14.32	14.02	13.40	19.39	17.82	18.32	18.24	18
Abs. Humidity	0.01	0.01	0.01	0.01	0.01	0.01	0.01	0
Emissions Measured								
FID Total Hydrocarbons [PPM]	1055.33	955.54	944.95	888.23	1185.68	1066.45	1237.34	1163
CL Oxides of Nitrogen [PPM]	75.66	113.61	106.93	143.10	226.42	224.56	223.82	225
PM Oxygen [%]	8.00	7.95	8.08	7.95	8.00	7.93	8.00	8
NDIR Carbon Dioxide [%]	0.00	0.00	0.00	0.00	0.00	0.00	0.00	0
NDIR Carbon Monoxide [PPM]	0.00	0.00	0.00	0.00	0.00	0.00	0.00	0
Calculated Carbon Balance Emissions								
NOx (15% O2,ppm)	42.13	51.74	48.81	66.33	117.13	111.86	111.65	114
% Water	12	17	16	16	16	16	16	16
BS Emissions								

BS THC	2.54	2.33	2.30	2.09	2.74	2.46	2.86	3
BS NOx (Actual/Dry)	0.35	0.47	0.44	0.56	0.94	0.90	0.91	1
BS NO (FTIR)	0.31	0.26	0.24	0.36	0.70	0.66	0.66	1
BS NO2 (FTIR)	0.04	0.21	0.20	0.20	0.24	0.24	0.25	0
BS NOx (FTIR/Actual)	0.35	0.47	0.44	0.56	0.94	0.90	0.91	1
BS CO	1.85	1.29	1.25	1.22	1.22	1.20	1.25	1
BS CO2	466	453	442	430	427	427	430	428
BS CH2O	0.12	0.14	0.13	0.12	0.12	0.12	0.13	0
BS NOx (EPA)	0.52	0.61	0.56	0.75	1.31	1.26	1.26	1
FTIR Analysis								
Carbon Monoxide low	476.56	330.27	322.02	326.12	328.64	324.11	330.96	328
Carbon monoxide high	148.09	111.40	110.18	112.88	112.79	111.55	114.20	113
Carbon dioxide	76546	73549	72525	73277	73043	73133	72692	72956
Nitric oxide	74.05	62.30	57.86	90.16	174.89	166.15	163.30	168
Nitrogen dioxide	7.00	32.39	30.81	32.04	39.84	39.94	40.78	40
Nitrous oxide	<1.004	<1.023	<1.006	<1.038	<1.055 1142.6	<0.982	<0.958	#DIV/ 0!
Methane	1016.13	892.38	900.18	872.12	1	1034.40	1184.62	1121 #DIV/ 0!
Acetylene	<3.646	<3.277	<3.375	<3.866	<3.886	<3.666	<3.663	0!
Ethylene	18.49	17.06	15.03	13.10	14.25	13.10	13.68	14
Ethane	18.86	21.70	18.97	15.67	27.59	22.09	26.15	25
Propylene Formaldehyd e	2.28 28.99	<2.566 32.23	<2.504 30.92	<2.447 28.92	<2.446 31.10	<2.435 30.27	<2.469 31.82	#DIV/ 0! 31 16265
Water	120537	166459	164312	160935	161716	162194	164039	0 #DIV/ 0!
Propane	<2.749	3.10	2.80	<2.942	<3.398	<3.086	<3.411	#DIV/ 0!
Ammonia	3.64	<0.369	<0.351	<0.342	<0.343	<0.336	<0.340	#DIV/ 0!
Acrolein	1.16	<0.654	<0.643	<0.656	<0.707	<0.668	<0.697	#DIV/ 0!
Acetaldehyde	2.54	0.71	0.71	<0.626	<0.669	<0.628	<0.648	#DIV/ 0!

IBTYL	<0.764	<1.039	<1.013	<0.991	<0.990	<0.986	<1.000	#DIV/0!
13BUT	<1.182	<1.607	<1.568	<1.533	<1.532	<1.526	<1.547	#DIV/0!
SF6	<0.017	<0.020	<0.019	<0.017	<0.017	<0.016	<0.017	#DIV/0!
Methanol	<1.502	<1.805	<1.738	<1.705	<1.704	<1.690	<1.718	#DIV/0!
NOx	81.05	94.69	88.67	122.20	214.73	206.09	204.08	208
Total Hydrocarbons	1100.15	979.18	977.09	936.02	1231.34	1110.54	1269.41	1204
Non Methane Hydrocarbons	84.02	86.80	76.90	63.89	88.73	76.14	84.79	83
Data Point	F18BASE13	F18BASE11	F18BASE12	F18BASE14	F18BASE15	F18BASE16	F18BASE17	
Combustion Data								
RPM	1796	1801	1802	1797	1795	1790	1803	1796
Peak Pressure [Avg/Dev]	624.3 / 50.06	729.5 / 61.19	789.5 / 64.96 856.63 /	887.1 / 71.63	1022.9 / 74.62 1178.4 /	1015.9 / 75.98	1021.3 / 75.17	#DIV/0!
Cylinder #1	670 / 55.0831	775.65 / 63.7792	71.109 / 7 753.07 /	989.08 / 75.6952	84.070 / 4 1046.7 /	1179.49 / 85.5743	1183.19 / 86.9003	#DIV/0!
Cylinder #2	606.18 / 51.0028	704.17 / 60.961	61.080 / 8 799.28 /	856.29 / 74.7096	88.199 / 7 1116 /	1027.91 / 89.3906	1045.35 / 86.9678	#DIV/0!
Cylinder #3	632.83 / 59.4167	745.52 / 71.2515	74.298 / 4 749.43 /	918.05 / 82.3684	92.904 / 9 1018.7 /	1104 / 92.0404	1117.01 / 93.1091	#DIV/0!
Cylinder #4	582.43 / 36.5637	682.35 / 57.8191	58.100 / 3 783.52 /	846.45 / 69.7899	89.358 / 7 968 /	998.74 / 86.2606	993.46 / 88.5191	#DIV/0!
Cylinder #5	612.61 / 44.2817	719.96 / 51.1293	58.337 / 795.14 /	901.21 / 64.4387	76.126 / 5 809.42 /	974.9 / 80.3818	978.56 / 80.5617	#DIV/0!
Cylinder #6	642 / 54.0085	749.58 / 62.2156	66.840 / 6	811.39 / 62.7808	17.044 / 9	810.32 / 22.2406	809.96 / 14.9605	#DIV/0!
Peak Cylinder Pressure	624.3	729.5	789.5	887.1	1022.9	1015.9	1021.3	1020

					1178.4			
	670	775.65	856.63	989.08	1	1179.49	1183.19	1180
					1046.7			
	606.18	704.17	753.07	856.29	6	1027.91	1045.35	1040
	632.83	745.52	799.28	918.05	1116	1104	1117.01	1112
					1018.7			
	582.43	682.35	749.43	846.45	1	998.74	993.46	1004
	612.61	719.96	783.52	901.21	968	974.9	978.56	974
	642	749.58	795.14	811.39	809.42	810.32	809.96	810
Average								
Cylinder	441.44676	515.8343	558.26	627.274	723.29	718.3497	722.168	
Pressure	35	969	08037	4256	95265	79	1556	721
	473.76154	548.4673	605.72	699.385	833.26	834.0253	836.641	
	34	748	8882	1751	1702	773	6724	835
	428.63398	497.9233	532.50	605.488	740.17	726.8421	739.174	
	86	821	09037	4657	10943	314	0737	735
	447.47838	527.1622	565.17	649.159	789.13	780.6458	789.845	
	43	475	63081	3805	11678	864	3457	787
	411.84020	482.4943	529.92	598.530	720.33	706.2158	702.482	
	26	121	7035	5349	67491	266	3028	710
	433.18068	509.0885	554.03	637.251	684.47	689.3584	691.946	
	52	982	23052	7023	93642	01	4118	689
	453.96255	530.0331	562.24	573.739	572.34	572.9827	572.728	
	35	01	8886	3712	63708	669	2085	573
Average								
Engine								
Pressure	441	516	558	627	723	718	722	
Peak								
Pressure								
COV [%]	8	8	8	8	7	7	7	7
Cylinder #1	8	8	8	8	7	7	7	7
Cylinder #2	8	9	8	9	8	9	8	8
Cylinder #3	9	10	9	9	8	8	8	8
Cylinder #4	6	8	8	8	9	9	9	9
Cylinder #5	7	7	7	7	8	8	8	8
Cylinder #6	8	8	8	8	2	3	2	2
CA @ Peak		21.3 /	20.7 /	21.0 /	17.9 /	18.3 /	17.9 /	#DIV/
Pr [Avg/Dev]	19.4 / 7.25	3.83	5.83	4.97	3.21	3.68	3.25	0!
	22.05 /	21.8 /	22.17 /	21.54 /	20.38 /	20.27 /	20.39 /	#DIV/
Cylinder #1	4.0065	2.1942	2.956	2.2387	1.7089	1.7315	1.6869	0!
	18.31 /	20.91 /	18.75 /	20.75 /	21.38 /	21.44 /	21.42 /	#DIV/
Cylinder #2	9.2405	5.1538	8.4339	6.1799	2.0872	2.8923	2.5093	0!
	20.86 /	21.92 /	21.91 /	22.31 /	20.78 /	20.94 /	20.89 /	#DIV/
Cylinder #3	6.8654	3.3389	5.2689	2.7135	1.8932	1.8734	1.8117	0!
	12.5 /	19.89 /	17.65 /	19.84 /	21.64 /	21.51 /	21.51 /	#DIV/
Cylinder #4	11.4432	6.9784	9.3306	7.1317	3.1392	3.8446	4.1631	0!
	20.6 /	21.52 /	21.78 /	22.09 /	22.33 /	22.6 /	22.55 /	#DIV/
Cylinder #5	6.2932	2.7318	3.8137	2.2896	3.8906	3.3703	3.1404	0!
	21.95 /	21.98 /	22.23 /	19.27 /	1.19 /	2.75 /	0.89 /	#DIV/
Cylinder #6	5.6232	2.5689	5.1996	9.2951	6.5598	8.3859	6.1982	0!

IMEP [Avg/Dev]	151.5 / 4.63	171.0 / 4.09	190.8 / 5.31 198.75	210.8 / 5.26	230.6 / 9.03 252.29	231.0 / 8.98	231.1 / 10.07	#DIV/ 0!
Cylinder #1	157.55 / 3.8036	176.41 / 3.5957	/ 4.4797 185.58	221.54 / 4.0423	/ 3.6434 237.94	251.56 / 4.4412	253.84 / 4.0005	#DIV/ 0!
Cylinder #2	149.48 / 4.73	167.86 / 4.2144	/ 5.7058 193.85	207.06 / 5.3627	/ 4.5786	236.79 / 5.4957	239.67 / 4.8933	#DIV/ 0!
Cylinder #3	153.17 / 4.9777	173.72 / 4.4168	/ 5.3861 185.13	215.24 / 5.0109	246.2 / 4.9596 235.51	245.22 / 5.3464	247.45 / 5.1737	#DIV/ 0!
Cylinder #4	143.93 / 6.0915	165.13 / 5.0287	/ 6.3971	206.14 / 6.3024	/ 5.4791 227.01	234.24 / 5.8732	235.18 / 6.2872	#DIV/ 0!
Cylinder #5	149.16 / 3.954	168.71 / 3.4599	189.4 / 4.6205 192.35	211.53 / 4.352	/ 5.5822 184.89	228.06 / 5.8531	229.45 / 5.664	#DIV/ 0!
Cylinder #6	155.85 / 4.1988	174.38 / 3.8386	/ 5.2953	203.16 / 6.4781	/ 29.954	189.93 / 26.8695	180.99 / 34.3781	#DIV/ 0!
MFB								
5%_CA	10	8	9	9	8	8	8	8
Cylinder #1	8	7	8	7	5	5	5	5
Cylinder #2	10	9	10	9	7	7	7	7
Cylinder #3	9	8	9	8	6	6	6	6
Cylinder #4	11	9	10	9	8	8	8	8
Cylinder #5	10	8	9	8	9	8	8	8
Cylinder #6	9	8	9	10	15	14	16	15
MFB								
50%_CA	25	23	25	24	24	23	24	24
Cylinder #1	23	21	22	20	18	18	18	18
Cylinder #2	26	24	26	24	21	22	21	21
Cylinder #3	24	22	24	22	19	20	19	20
Cylinder #4	28	25	26	25	22	23	23	23
Cylinder #5	25	23	24	23	23	23	23	23
Cylinder #6	24	22	24	26	36	35	37	36
MFB								
50%_CA	48	45	48	46	46	46	46	46
Cylinder #1	49	47	47	45	42	43	41	42
Cylinder #2	48	45	48	45	41	42	40	41
Cylinder #3	45	42	45	43	40	40	39	39
Cylinder #4	52	46	48	46	41	42	42	42
Cylinder #5	50	46	49	46	46	45	45	45
Cylinder #6	47	45	47	50	67	64	67	66
NMEP	141.02	160.83	181.63	201.66	221.31	221.65	221.88	222
FMEP	20.20	19.93	20.54	20.55	19.95	20.46	20.76	20

Blow-by Flow (SCFM)	2.09	2.11	2.32	2.33	2.62	2.44	2.57	3
---------------------------	------	------	------	------	------	------	------	---

Appendix B- Pressure-Spring Verification Raw Data

Degrees	Temperature	Volume	Pressure	Pressure Calculated	Difference
-74.95	588.15	8.43E-04	187.02	187.02	0.00
-73.99	584.65	8.56E-04	182.96	182.97	0.00
-73.08	580.42	8.73E-04	178.15	178.16	0.00
-72.12	577.31	8.86E-04	174.68	174.68	-0.01
-71.16	573.72	9.00E-04	170.73	170.74	-0.01
-70.20	570.67	9.13E-04	167.43	167.43	-0.01
-69.23	566.63	9.31E-04	163.13	163.14	-0.01
-68.25	563.04	9.47E-04	159.38	159.39	-0.01
-67.29	562.54	9.49E-04	158.85	158.87	-0.01
-66.32	557.54	9.72E-04	153.75	153.76	-0.02
-65.36	552.65	9.95E-04	148.87	148.89	-0.02
-64.40	548.25	1.02E-03	144.58	144.60	-0.02
-63.44	546.36	1.03E-03	142.77	142.79	-0.02
-62.48	541.71	1.05E-03	138.38	138.40	-0.02
-61.52	537.16	1.07E-03	134.17	134.19	-0.02
-60.55	532.70	1.10E-03	130.15	130.17	-0.02
-59.59	528.34	1.12E-03	126.31	126.33	-0.02
-58.63	524.08	1.14E-03	122.62	122.65	-0.02
-57.67	519.91	1.17E-03	119.10	119.12	-0.02
-56.71	515.82	1.19E-03	115.72	115.75	-0.03
-55.75	511.83	1.22E-03	112.49	112.51	-0.03
-54.78	507.93	1.24E-03	109.39	109.41	-0.03
-53.82	504.11	1.27E-03	106.42	106.44	-0.03
-52.86	500.37	1.29E-03	103.57	103.59	-0.03
-51.90	496.72	1.32E-03	100.84	100.86	-0.03
-50.94	493.14	1.35E-03	98.22	98.24	-0.03
-49.98	489.65	1.37E-03	95.70	95.73	-0.03
-49.06	486.23	1.40E-03	93.29	93.32	-0.03
-48.10	482.88	1.42E-03	90.97	91.00	-0.03
-47.14	479.61	1.45E-03	88.75	88.77	-0.03
-46.17	476.42	1.47E-03	86.61	86.64	-0.03
-45.21	473.29	1.50E-03	84.56	84.58	-0.03
-44.25	470.23	1.53E-03	82.58	82.61	-0.03
-43.29	467.24	1.55E-03	80.68	80.71	-0.03

-42.32	464.31	1.58E-03	78.86	78.88	-0.03
--------	--------	----------	-------	-------	-------

Appendix C- Validation Graphs

